The role of microtubule-associated proteins in the generation and regulation of spindle shape

Trupinić, Monika

University of Zagreb

FACULTY OF SCIENCE
DEPARTMENT OF BIOLOGY

Monika Trupinić

The role of microtubule-associated proteins in the generation and regulation of spindle shape

DOCTORAL THESIS

Zagreb, 2023.

University of Zagreb

PRIRODOSLOVNO-MATEMATIČKI FAKULTET
BIOLOŠKI ODSJEK

Monika Trupinić

Uloga proteina vezanih na mikrotubule u stvaranju i regulaciji oblika diobenoga vretena

DOKTORSKI RAD

Zagreb, 2023.

This work was done in laboratory of Iva M. Tolić, PhD, Senior Research Group Leader at Ruđer Bošković Institute, Zagreb, under supervision of Iva M. Tolić, PhD, Senior Research Group Leader. As a part of Postgraduate doctoral programme of Biology, this thesis is submitted for review to Department of Biology at Faculty of Science, University of Zagreb in order to achieve the academic degree Doctor of Biology.

Supervisor biography

Professor Iva M. Tolić was born in Zagreb, Croatia. She graduated Molecular biology at Faculty of Science, University of Zagreb, Croatia in 1996. During graduate studies, Prof Tolić worked as research assistant in the group of Prof Nenad Trinajstić at Ruđer Bošković Institute. Her PhD work was done with Prof Ning Wang at Harvard School of Public Health, Boston, MA, USA. She achieved the academic degree Doctor of biology at University of Zagreb in 2002. After this, she worked as a postdoctoral fellow with Prof Kirstine Berg-Sørensen at Niels Bohr Institute, Copenhagen, Denmark, and later with Prof Francesco Pavone at European Laboratory for Non-Linear Spectroscopy, Florence, Italy. From 2005 to 2014, Prof Tolić worked as a research group leader at Max Planck Institute of Molecular Cell Biology and Genetics in Dresden, Germany. Her research areas are mitosis, mitotic spindle mechanics, microtubules, motor proteins and aneuploidy. Prof Tolić has received 15 research grants including the prestigious projects funded by the European Research Council (ERC) - Consolidator and Synergy grants. She has published more than 90 papers in peer-reviewed journals including Science, Cell, and Nature Cell Biology, cited more than 4400 times, and served as reviewer for these and various other journals. She has been elected to EMBO and Academia Europea membership and received numerous awards such as the Ignaz Lieben Award of the Austrian Academy of Sciences and European Biophysical Societies Association (EBSA) Young Investigators' Medal and Prize. To this date she has mentored 12 PhD and 23 Master theses. As an invited speaker, she has participated in more than 100 conferences and research seminars worldwide. She organized several scientific meetings including the EMBO Conference on Meiosis in 2017 and Mitotic spindle: From living and synthetic systems to theory in 2019 and 2021. Currently, Prof Tolić is a senior research group leader with tenure at Ruđer Bošković Institute in Zagreb.

Acknowledgements

I wish to express my sincere gratitude to my mentor Iva Tolić for giving me an opportunity to become a part of her research group and gain an incredible amount of knowledge and experience during these years. Her guidance and advice helped me countless times during my doctoral study and through the process of writing my thesis. It is hard to put in a few sentences how much I learnt from her, so I will just say it was priceless.

I would also like to thank my committee members Dragomira Majhen, Maja Matulić and Gautam Dey for reading my thesis and providing me with suggestions for improvement.

Many thanks to all my lab colleagues and students in Tolić group for all your support and help during these years; for all discussions, worries and excitement. I had wonderful time with all of you. Special thanks to my lab colleagues and now friends Ivana Ponjavić, Mateja Ćosić, Martina Manenica, Snježana Kodba and Jurica Matković – you made everything more fun. Also, my thanks go to Ivana Šarić for always taking care of us, as well as to prof. Nenad Pavin and his group for all our collaborations and discussions.

I would like to thank all my teachers and professors that partook in my education – you had a big impact on my interest in biology and science in general.

Finally, I would like to thank my family and friends who readily got me through every crisis and showered me with the unconditional support and love. Mom and dad, I genuinely would not be able to pull it off without you. Bruno, my dear brother, this is too cheesy for us, but I still have to thank you too – so thanks. All my friends know who they are (I am not going to name you because you will fight about the order) starting from the kindergarten to this day – I don't know what I did to deserve you, but hopefully you will stick with me forever. And to my little best friend who always loyally studied with me since we were both just kids - you are missed, B <3.

University of Zagreb
Faculty of Science
Department of Biology

Doctoral thesis

The role of microtubule-associated proteins in the generation and regulation of spindle shape

Monika Trupinić

Ruđer Bošković Institute

In the mitotic spindle, a complex micro-structure responsible for the segregation of chromosomes, individual microtubule bundles obtain different shapes depending on the mechanical forces acting on them. In addition to linear forces, rotational forces are present in the spindle, reflected in the left-handed twisted shapes of microtubule bundles that make the spindle chiral. However, it is not known how twist changes throughout mitosis in non-tumor cells, or what are the molecular origins of the twist. This doctoral thesis shows that twist in non-tumor cells is most pronounced at the start of the anaphase, and can be affected by manipulating microtubule-associated proteins, such as motor proteins, but also proteins that crosslink or nucleate microtubule bundles. It also explores how spindles react to the external forces by widening or increasing the twist. To conclude, this thesis uncovers how bending and twisting moments are generated by similar molecular mechanisms and it proposes a physiological role for spindle chirality in allowing the spindle to absorb mechanical load.

(94 pages, 32 figures, 2 tables, 1 supplemental figure, 155 references, original in English)

Keywords: mitotic spindle, chirality, twist, motor proteins, augmin, PRC1, spindle compression

Supervisor: Iva M. Tolić, PhD, Senior Research Group Leader
Reviewers: Dragomira Majhen, PhD, Senior Research Associate
Maja Matulić, PhD, Associate Professor
Gautam Dey, PhD, Research Group Leader

Sveučilište u Zagrebu
Prirodoslovno-matematički fakultet
Biološki odsjek

Doktorski rad

Uloga proteina vezanih na mikrotubule u stvaranju i regulaciji oblika diobenoga vretena

Monika Trupinić

Institut Ruđer Bošković

Unutar diobenog vretena, složene mikro-strukture odgovorne za podijelu kromosoma, pojedinačni svežnjevi mikrotubula poprimaju različite oblike pod djelovanjem mehaničkih sila. U vretenu, osim linearnih sila, prisutne su i rotacijske sile koje se očituju kroz lijevo usmjereni zaokret svežnjeva mikrotubula što čini diobeno vreteno kiralnim. Međutim, nije poznato kako se takav zaokret mijenja kroz različite faze mitoze u netumorskim stanicama, niti koje su njegove molekularne osnove. U ovom doktorskom radu prikazano je kako je zaokret vretena najizraženiji na početku anafaze te podložan promjenama nakon manipulacije proteina vezanih na mikrotubule, kao što su motorni proteini, ali i proteini koji unakrsno vežu mikrotubule ili stvaraju nove. Također, prikazano je kako vretena reagiraju na pritisak vanjskih sila širenjem ili povećanjem zaokreta. Kao zaključak, ova teza prikazuje kako su slični molekularni mehanizmki odgovorni za stvaranje savijanja i zakretanja vretena te predlaže fiziolšku ulogu kiralnosti u očuvanju vretena nakon djelovanja mehaničkih sila.

(94 stranice, 32 slike, 2 tablice, 1 prilog, 155 literaturnih navoda, jezik izvornika engleski)

Ključne riječi: diobeno vreteno, kiralnost, zaokret, motorni proteini, augmin, PRC1, stiskanje

Mentor: prof. dr. sc. Iva M. Tolić, znanstvena savjetnica u trajnom zvanju
Ocjenjivači: dr. sc. Dragomira Majhen, viši znanstveni suradnik
izv. prof. dr. sc. Maja Matulić
dr. sc. Gautam Dey, Research Group Leader

TABLE OF CONTENTS

1. INTRODUCTION

Cell division, a process by which a parent cell divides into two daughter cells, is a fundamental process of every life. Four stages make up the cell cycle in eukaryotic organisms. The two phases of the cell cycle in which the most complex processes are happening are the S phase (S for synthesis), during which DNA is duplicated, and the M phase (M for mitosis), during which duplicated chromosomes are separated into two daughter cells. The S and M phase events are separated by two G (G for gap) phases in the majority of human cells. Interphase is the collective term for G1, S, and G2 phases. Interphase may take up 23 hours of a 24-hour cycle in a typical human cell growing in culture, leaving 1 hour for the M phase. The usual M phase can be divided into mitosis, the division of the nucleus, and cytokinesis, the division of cytoplasm (Lodish et al., 2014). Most eukaryotic cells experience nuclear envelope breakdown (NEBD) at the conclusion of prophase during mitosis which signals the onset of prometaphase, during which mitotic spindle formation takes place, microtubules reorganize, and chromosomes begin to congregate in the metaphase plate. Sister chromatids must be appropriately attached to the opposing spindle poles during metaphase while chromosomes are aligned at the spindle's central plane. The sister chromatids can split during anaphase following correct chromosomal congression and passing the anaphase control checkpoints. Chromosome decondensation, nuclear envelope reemergence, and cytoskeleton reorganization all take place during telophase. In the end, cytokinesis results in cytoplasmic division of the cell (Alberts et al., 2014).

In order to segregate the genetic material during mitosis, the cell forms a mitotic spindle, a complex micro-structure made of microtubules and numerous associated proteins (McIntosh et al., 2012; Pavin and Tolic, 2016; Prosser and Pelletier, 2017). Microtubules are hollow cylindrical polymers made out of tubulin subunits which consist of two non-covalently bound globular proteins named α-tubulin and β-tubulin. One microtubule is made of 13 paralelly organized protofilaments (Akhmanova and Steinmetz, 2008). Microtubules and protofilaments are polar structures with α-tubulins exposed at one end (referred to as the minus (-) end) and the β-tubulin exposed on the other end (referred to as the plus (+) end) (Alberts et al., 2014). We can distinguish between parallel (all microtubules point in the same direction) and antiparallel (microtubules point in opposite directions) fibers based on the orientation of the microtubules within the fiber. Kinetochore fibers (k-fibers) are attached to the kinetochores, which are protein complexes on the

chromosomes, by the (+) ends of their microtubules. K-fibers are the thickest and most stable microtubule bundles in the spindle and, therefore, responsible for the separation of sister chromatids to opposite spindle poles during anaphase (Tolic, 2018). In addition to k-fibers, in human cells we can also discern interpolar and astral microtubules. In the center of the mitotic spindle, interpolar microtubules are arranged into overlapping antiparallel bundles that originate from the opposite spindle poles. On the other hand, astral microtubules are responsible for the spindle location within the cell, as they extend from spindle poles into the cytoplasm and there interact with the cell cortex (Alberts et al., 2014).

It is important to note that mitotic spindle is a mechanical structure that can generate and balance forces within itself (Pavin and Tolic, 2021). Forces in the spindle are crucial for proper spindle functioning in each phase of the mitosis. For example, kinetochore fibers exert forces necessary for the positioning of the chromosomes at the center of the spindle in a metaphase plate (Maiato et al., 2017; Risteski et al., 2021) and for pulling the chromosomes apart during anaphase (Asbury, 2017; Vukusic et al., 2019). On the other hand, overlap bundles balance forces at kinetochores by acting as bridges between sister kinetochore fibers in metaphase and anaphase (Kajtez et al., 2016; Polak et al., 2017; Simunic and Tolic, 2016; Tolic, 2018; Vukusic et al., 2017), and they also regulate pole separation in anaphase (Scholey et al., 2016; Vukusic et al., 2021; Vukusic and Tolic, 2021). All the forces in the spindle arise from the active processes of motor proteins as well as microtubule polymerization and depolymerization (Howard, 2001; Tolic-Norrelykke, 2008). Because of the highly important roles of forces within the spindle, it is crucial to understand them. Direct measurement of the forces in the spindle, although possible (Nicklas, 1983), is challenging because of the small scales.

Forces are also responsible for the shape of a spindle. Due to the mechanical properties of microtubules, which can be thought of as thin and elastic filaments that are inherently straight and curve under forces (Kajtez et al., 2016; Rubinstein et al., 2009), the spindle obtains its characteristic shape. This means that the spindle shape reflects the forces within it, which allows for an indirect measurement of forces by inferring them from the shapes of the microtubule bundles (Kajtez et al., 2016; Tolic et al., 2019), similarly to studies of forces and shapes of individual microtubules *in vitro* (Dogterom and Yurke, 1997; Gittes et al., 1993).

Recently, it was shown that the shape of the mitotic spindle in human HeLa and U2OS cells is chiral as the spindle has a left-handed twist around the pole-to-pole axis (Novak et al.,

2018). Microtubule bundles twist because of the forces and torques that exist within them, as well as the elastic properties of microtubule bundles. The experimentally measured three-dimensional shapes of the microtubule bundles were used to deduce forces and torques in the spindle by comparison with a theoretical model (Novak et al., 2018). Left-handed twist was also observed in anaphase of NuMA- and Eg5-doubly inhibited RPE1 spindles (Neahring et al., 2021).

The spindle twist is potentially generated by motor proteins that, in addition to linear forces, also exert rotational forces on microtubule bundles by switching protofilaments with a bias in a certain direction (Bormuth et al., 2012; Brunnbauer et al., 2012; Bugiel et al., 2015; Can et al., 2014; Mitra et al., 2020; Mitra et al., 2018; Ramaiya et al., 2017; Vale and Toyoshima, 1988; Walker et al., 1990; Yajima and Cross, 2005; Yajima et al., 2008). Until now, only the role of kinesin-5 (Eg5) in the spindle twist has been explored and it was shown that inhibition of Eg5 led to the abolishment of the twist (Novak et al., 2018).

Previous studies have shown that multiple motor proteins can generate rotational forces on microtubules. The first molecular motor discovered to generate torque was the single-headed axonemal dynein, a force-generating protein that powers the movement of cilia and flagella. In *in vitro* gliding motility assays, surface-attached dynein motors rotated the microtubules around their axis in a clockwise motion, when viewed from the minus (-) end of the microtubules, while translocating them in a linear fashion (Vale and Toyoshima, 1988).

The same type of assay was used to show that the minus (-) end directed motor protein kinesin-14 (Ncd) generates torques which rotate microtubules in a clockwise direction as viewed from their minus (-) ends (Walker et al., 1990). Similar results were obtained in an assay with kinesin-14 in which microtubules glide along each other and it was observed that the transport microtubule moved in a helical motion in a clockwise direction (Mitra et al., 2020).

By using a gliding assay, it was shown that the plus (+) end directed kinesin-1 can exert torsional forces which rotate microtubules counterclockwise relative to an observer looking along the microtubule long axis toward the minus (-) end (Yajima and Cross, 2005). In experiments where kinesin-1 motor proteins were coupled with microspheres and placed on the microtubule in a single-molecule conditions, it was shown that the motor was able to generate a torque sufficient to unidirectionally rotate the microsphere, probably with a directly-guided motor head from one binding site to the next without it moving freely through space to its next binding site (Ramaiya et al., 2017).

Counterclockwise rotation direction has also been found for the plus (+) end-directed motor protein kinesin-5 (Eg5), which was observed as a corkscrew motion of a sliding microtubule on surface-attached motors (Yajima et al., 2008).

Heterodimeric kinesin-2, a processive kinesin involved in cargo transport, displays a broad range of pitches along the path on suspended microtubules in laser trap assays, which allow for tracking of kinesin motion on microtubules between two trapped beads in solution (Brunnbauer et al., 2012). They showed that the ability of motor proteins to generate torque is dictated by the structural integrity of the coiled coil in the neck region of the protein, meaning that the motor with a stable neck has reduced propensity to generate torque.

Gliding motility assays, as well as motility assays on freely suspended microtubules, showed a counterclockwise rotation for the plus (+) end-directed motor protein kinesin-8 (Kip3) (Bormuth et al., 2012; Mitra et al., 2018), while another study found that kinesin-8 can switch protofilaments in both directions (Bugiel et al., 2015).

Finally, cytoplasmic dynein, a molecular motor responsible for minus (-) end-directed cargo transport along microtubules, moves in a bidirectional helical trajectory around suspended microtubules, generating torques (Can et al., 2014).

However, the role of motor proteins and their chiral stepping in the generation of spindle twist is unknown. To answer these questions, in this doctoral thesis I will first show how spindle twist changes through different phases of mitosis in human non-tumor RPE1 cells and determine in which phase the twist is most pronounced. Next, I will perform depletions or inhibitions of motor proteins such as kinesin-5 (Eg5), kinesin-8 (Kif18A), kinesin-6 (MKLP1), kinesin-14 (HSET) and dynein, which were selected from the literature (candidate-based approach) based on their chiral stepping ability. For inhibitions or depletions I will use techniques of RNA interference, available small molecule inhibitors of motor proteins and CRISPR knock-out (KO) technology. Also, I will overexpress some of these proteins, more specifically Eg5 and Kif18A, by transfecting the cells with the plasmid carrying the gene for the protein of interest. Additionally, in a same manner I will also test if non-motor proteins such as protein regulator of cytokinesis (PRC1) (Jiang et al., 1998) and protein subunits of the augmin complex (HAUS6 and HAUS8) have a role in generation of twisted shapes of microtubule bundles. PRC1 is the main crosslinking protein of antiparallel microtubules within bridging fibers (Kajtez et al., 2016; Polak et al., 2017) and is responsible for the stronger bridges and more curved shape of the spindle (Jagric et al.,

2021; Kajtez et al., 2016) which led me to hypothesize that it can also affect spindle twist. Augmin complex is responsible for the microtubule nucleation from the lateral surface of the pre-existing microtubules (David et al., 2019; Uehara et al., 2009). Augmin is important for the nucleation of the bridging fibers and, consequentially, the maintenance of the spindle shape (Stimac et al., 2022). To determine the efficiency of protein depletion, I will use an immunofluorescent staining of cells to determine that specific protein of interest is not localized on the mitotic spindle in comparison to the control cells.

Next, I will show if roundness of spindles affect their twist by comparing spindles in RPE1 cells with spindles in HeLa cells, which we observed to be generally more round, and also by comparing differently perturbed spindles inside the RPE1 group. Also, I will show how spindles react to external forces by performing compression experiments on them to see whether they will keep their shape or they will change, and determine how extreme the change would be and what causes it.

Main method to uncover and eventually analyze spindle twist will be confocal microscopy which allows me to image the entire mitotic spindle in multiple z-planes and provides me with the information of the spindle shape in x-, y- and z-plane. I will image all spindles for analysis by using the live RPE1 cells dyed with the color that allows for the visualization of spindle microtubule bundles. I will perform analysis of spindle twist on the images that I put through the computational processing of rotating the spindle from horizontal orientation to end-on (pole-to-pole) orientation which allows for the best visualization of spindle twist. First, I will determine twist visually by following the movement of bundles in the spindle, and then I will calculate it by using the newly developed method of optical flow (Trupinic et al., 2022).

Additionally, I will mention analysis of the spindle twist in a unicellular eukaryote amoeba *Naegleria gruberi* from the images provided from our colleagues from the University of Massachusetts (Velle et al., 2022). Mitotic spindles in amoeba have a distinctively different shape when compared to human cells, for example, they are much smaller and do not have centrosomes, so this will present us with the interesting information on the spindle twist across different species. In order to analyze amoeba spindles, because of the differences in spindle shape mentioned above, in a collaboration with the theoretical physicist from Faculty of Science, University of Zagreb, we developed a new method of twist calculation which is based on the manual traces of microtubule

bundles from which we acquire the geometric information characteristic for each bundle (Ivec et al., 2021).

The main objective of my doctoral thesis is to determine how spindle twist is generated in non-tumor human RPE1 cells, which motor and non-motor proteins are involved in generation and maintenance of spindle twist, and how twist changes in different phases of mitosis and during different protein perturbations. Additionally, based on the compression experiments I will try to propose a physiological role of spindle chirality. Finally, I will discuss if spindle twist is unique for human cells or it also exists in different species, such as amoebas. With this I will try to give an explanation for the existence and importance of spindle chirality in cells.

2. OVERVIEWS OF RESEARCH

2.1. Cell cycle

The ability of cells to duplicate genetic material and equally transfer it into newly formed daughter cells is considered the most important process in sustaining the life of every living eukaryote. This process, also called the cell cycle, can roughly be divided into interphase and M phase (Figure 1). Interphase consists of G1, S and G2 phases, while M phase consists of nuclear division (mitosis) and cytoplasmic division (cytokinesis) (Alberts et al., 2014). In human cells during the G1 phase of interphase, that lasts approximately 15 hours, cells expand in size and produce all proteins and RNAs necessary for DNA replication. After they pass the G1 checkpoint and enter the next phase in cell cycle, cells are irreversibly driven to continue with the division (Meraldi et al., 2004). Next phase is S phase, that lasts approximately 6 hours, during which each chromosome's genetic material duplicates to create two identical sister chromatids through the process of semiconservative replication. The last phase of interphase is G2 phase which lasts approximately 2 hours, during which cells continue to grow and produce proteins. Finally, cells enter M phase during which duplicated genetic material is divided and followed with the division of cytoplasm. Human cells spend the least amount of time in M phase, only ~1 hour of 24 hour cell cycle (Lodish et al., 2014).

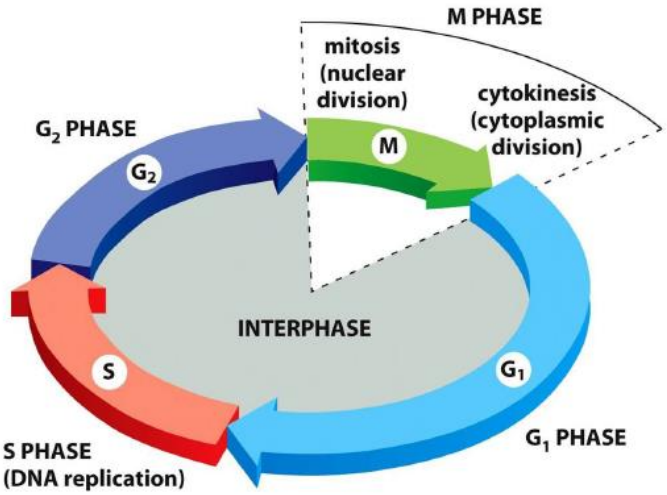

Figure 1. Overview of main phases of the cell cycle in animal cells. Cell cycle consists of interphase and M phase. S phase of the interphase is period of DNA replication followed by G2 phase of protein synthesis and cell growth. Start of mitosis is marked with the breakdown of nuclear envelope (NEBD), followed by mitosis, and finished with cytokinesis. After M phase, cell cycle continues with G1 phase of protein synthesis. Taken from (Alberts et al., 2014).

Main function of mitosis is to ensure that each daughter cell has a same number of chromosomes as the parental cell. However, sometimes errors can occur which results in aneuploidy, a condition characterized by a wrong number of chromosomes in the cell. Aneuploidy is common in cancers and often is a cause of miscarriages and genetic disorders, such as Down syndrome (Knouse et al., 2017; Santaguida and Amon, 2015; Webster and Schuh, 2017). For that reason, cell division has to be very precise, otherwise some loss or gain in DNA material can be either lethal to the cell, or can cause severe complications. Healthy cells achieve division accuracy and fidelity by implementing control checkpoint pathways. They delay the start of the subsequent phase in the cell cycle until all apparent faults have been fixed in prior steps (Meraldi et al., 2004).

The primary regulators of cell cycle progression are highly conserved heterodimeric protein serine-threonine kinases that contain a regulatory subunit (cyclin) and a catalytic subunit (cyclin-dependent kinase, CDK). They control key checkpoints: transition from G1 phase to S phase (G1 checkpoint), progression through the S phase (S checkpoint), and transition from G2 to M phase (G2 checkpoint) (Figure 2). This regulation, involved in entry of different stages of cell cycle, is achieved by phosphorylation of various proteins at specific regulatory sites (Hochegger et al., 2008). The G1 cell cycle checkpoint stops the transition from the G1 phase to S phase if environmental circumstances are adverse for cell division, such as the presence of DNA damage or a lack of growth factors. Before cells enter the M phase, the S phase checkpoint controls the DNA replication and repair, and ensures the fidelity of DNA replication. The G2 checkpoint prevents cells from entering mitosis while DNA is damaged, providing an opportunity for repair and stopping the proliferation of damaged cells (Panda et al., 2019). Additionally, during mitosis, cells have the spindle assembly checkpoint (SAC) which controls if kinetochores are properly attached to the spindle and, therefore, can block cell cycle progression if errors occur (Figure 2) (Nezi and Musacchio, 2009).

Although many eukaryotic species share conserved proteins and the fundamentals of the cell cycle, the process can vary greatly between species, leading to the existence of numerous analogue principles that perform the same function by various ways (McIntosh et al., 2012). Due to the fact that this research involves human RPE1 cell lines, focus will be on mitotic mechanisms in human model systems.

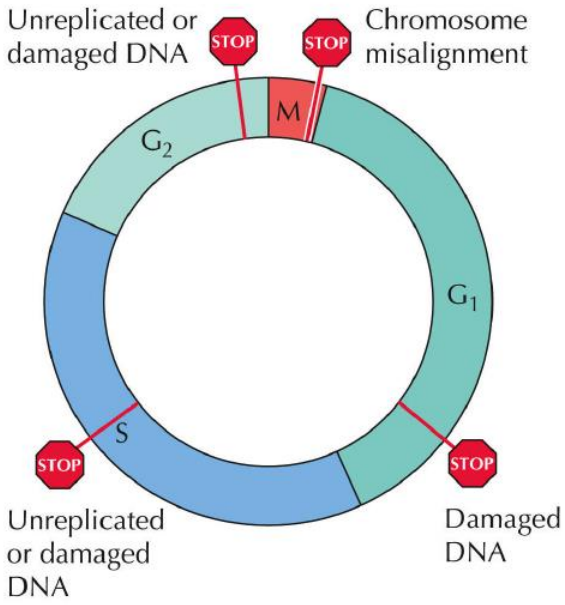

Figure 2. Four control points or checkpoints in the cell cycle. The G1 checkpoint at the G1/S transition, the S checkpoint during S phase, the G2 checkpoint at the G2/M transition, and spindle assembly checkpoint (SAC) during M phase. Taken from (Cooper and Hausman, 2003).

2.2. M phase

In order for duplicated genetic material from S phase to divide, cell needs to go through extensive changes during M phase. Firstly, cell will equally divide genetic material during the process called mitosis or nuclear division. Secondly, cell will divide cytoplasm and organelles into two daughter cells during the process called cytokinesis or cytoplasm division. Just like the cell cycle, the M phase is a continuous process, as there is no microscopically visual event when mitosis ends and cytokinesis starts (Lodish et al., 2014).

2.2.1. Mitosis

For easier description, mitosis, a continuous process, has been divided into five stages: prophase, prometaphase, metaphase, anaphase and telophase (Lodish et al., 2014) (Figure 3).

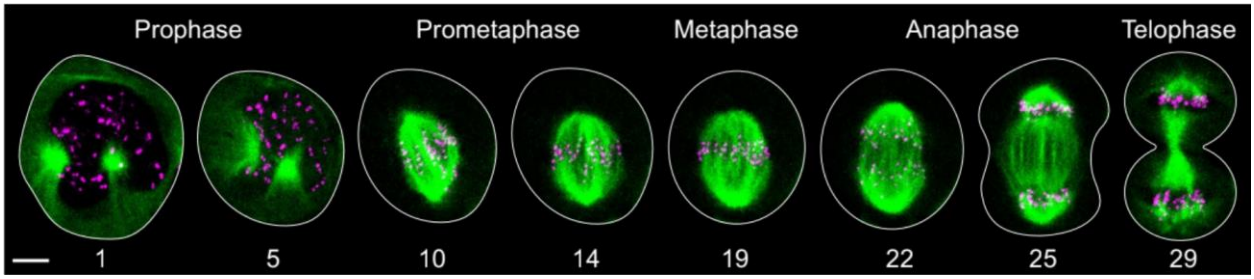

Figure 3. Stages of mitosis in human cell. Microtubules are shown in green and kinetochores in magenta, in U2OS cells expressing CENP-A-GFP and mCherry-α-tubulin. The white line marks the cell outline; time is given in minutes; scale bar represents 5 μm. Taken from (Tolic, 2018).

During prophase, previously duplicated microtubule organizing centers (MTOCs; in animal cells called centrosomes) start to separate, with the help of a motor protein kinesin-5 (Eg5), in order to become two spindle poles of a bipolar mitotic spindle. This pathway of centrosome separation is called prophase pathway, as centrosomes can also separate in prometaphase (prometaphase pathway) (Kaseda et al., 2012). Centrosomes, at this stage, are outside of the still intact nuclear envelope as they begin to nucleate microtubules to form mitotic asters, structures consisting of centrosome and its radial arrays of microtubules converged at the centrosome (Mogilner and Craig, 2010). Additionally, the dynamics of growing microtubules increase at their plus (+) ends. Furthermore, in prophase, proteins called condensins regulate condensation of replicated DNA in the nucleus. DNA becomes condensed into compact structures, chromosomes, while its length is reduced by more than 1000-fold (McIntosh et al., 2012). Now, duplicated DNA forms two equal halves of the chromosome called sister chromatids which are connected at the central region on sites called centromeres. On centromeres, begins an assembly of protein complexes that represent sites for microtubule attachments – kinetochores (Musacchio and Desai, 2017). Just before the next phase of mitosis, the spindle undergoes internal disruptions of order of membrane system - endocytosis and exocytosis stop, and actin microfilaments rearrange to give rise to rounded cell (McIntosh et al., 2012).

Prometaphase begins with the nuclear envelope breakdown (NEBD) which allows microtubules to search and capture chromosomes by associating with their kinetochores (Kirschner and Mitchison, 1986). This first interaction between chromosomes and growing microtubules marks the beginning of assembly of mitotic spindle. When sister chromatids are captured to opposite spindle poles they are said to be bi-oriented and they can begin a process of chromosome congression which will eventually align sister chromatids in equatorial plane of a metaphase spindle (Maiato et al., 2017) (Figure 3). Some cells can separate their centrosomes in this phase thereby taking the prometaphase pathway of centrosome separation (Kaseda et al., 2012).

Metaphase is evident when all chromosomes are fully condensed, attached to the microtubules and aligned at the central metaphase plate (Figure 3). Microtubules exert forces on kinetochores in order to pull them towards the opposite spindle poles and to generate the tension which will indicate whether sister chromatids have achieved appropriate bi-orientation. The cell monitors the attachments of microtubules to the chromosomes to ensure that sister chromatids are properly aligned at the metaphase plate (Musacchio and Salmon, 2007). This process is the foundation of spindle assembly checkpoint (SAC). If one of sister kinetochores is not properly attached to microtubules, the transition to anaphase is inhibited. Metaphase is known as a biophysical steady state which means that despite large fluctuations, average amount and position of spindle components is constant over time (Dumont and Mitchison, 2009b).

Anaphase begins only if SAC checkpoint is successfully passed and all the conditions are fulfilled - anaphase-promoting complex/cyclosome (APC/C) is activated and protein complexes in centromeric region are broken which leads to chromosome separation and pulling to the opposite poles by the forces exerted by microtubule depolymerization (anaphase A) (Asbury, 2017). Additionally, spindle poles are moving apart from each other, elongating the spindle extensively, mediated by sliding of antiparallel microtubules in overlap region of the spindle (anaphase B) (Scholey et al., 2016; Vukusic and Tolic, 2021).

The last stage of mitosis is telophase during which sister chromatids reach the opposite poles and the nuclear envelope starts to re-form. Also, chromosomes are beginning to decondense and the invagination of the cell membrane becomes apparent (Figure 3). Eventually, at the place of membrane invagination, contractile ring will divide cell cytoplasm during cytokinesis which will end with the cutting of the microtubule and membrane intercellular bridge connecting the 2

daughter cells. This process is known as cytokinetic abscission and it marks the end of the M phase of cell cycle (Lodish et al., 2014).

2.3. Mitotic spindle

The mitotic spindle is a precisely constructed micro-structure made out of microtubules and numerous associated proteins (McIntosh et al., 2012; Pavin and Tolic, 2016; Prosser and Pelletier, 2017). In most cell types, the mitotic spindle formation starts when microtubules nucleate from microtubule-organizing centers (MTOCs) or centrosomes (MTOCs in animal cells), also referred to as spindle poles (Luders and Stearns, 2007). Together with the cell-division cycle, the centrosome replication cycle takes place. Newly born cells have a pair of centrioles that made up centrosome, one engaged orthogonally to the other. As centrioles disengage in the early G1 phase, this arrangement is gone and the two wander apart in G1 phase. They are now only connected by a loose fibrous attachment. In G1/S, procentrioles (daughter centrioles) are assembled perpendicular to each mother, and throughout G2, they lengthen until they are about the same size as their mothers. The fibrous tether among centrosomes resolves permitting centrosomes to disjoin and separate to opposite sides of the cell as the spindle poles (Fu et al., 2015).

We describe four different groups of microtubule bundles that build mitotic spindle: kinetochore fibers, overlap bundles, polar bundles and astral microtubule bundles (Figure 4) (Mastronarde et al., 1993; Musacchio and Desai, 2017; Tolic, 2018). Kinetochore fibers (k-fibers), which are consisting of parallel microtubules, extend from the spindle poles and attach to the kinetochores, protein complexes on the chromosomes, with their plus (+) ends. Their main function is exerting pulling forces on sister chromatids during metaphase, and during anaphase they pull separated sister chromatids to different poles of the spindle. They also silence the SAC if sister kinetochores are properly attached to microtubules and kinetochores are under sufficient tension, which allows cells to enter anaphase (Dumont et al., 2012). Microtubule bundles that do not associate with the kinetochores, meet at the spindle center and form antiparallel bundles, known as interpolar or overlap bundles (Brinkley and Cartwright, 1971). Their primary functions are to keep spindle pole apart through sliding between their antiparallel bundles by the action of molecular motors, to regulate spindle length and to generate a force that moves poles apart during anaphase B (Kajtez et al., 2016; Vukusic et al., 2017). Other non-kinetochore microtubule bundles

are polar bundles that end before their plus (+) ends reach the spindle equator (McIntosh and Landis, 1971) and astral bundles whose plus (+) ends extend toward the cell cortex (Dumont and Mitchison, 2009b). For fast mitotic spindle assembly and formation of complex structures, the presence of microtubule-associated proteins (MAPs) is important, which will be described in detail further in the text.

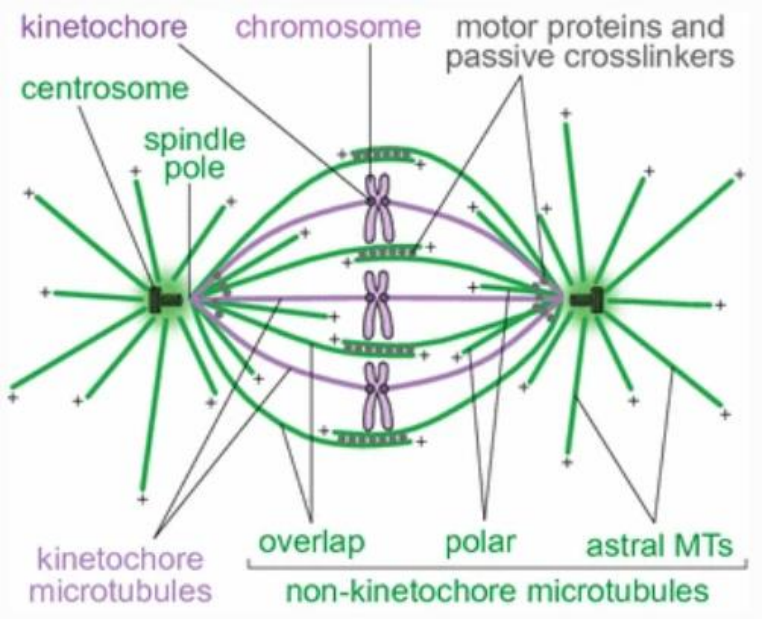

Figure 4. Scheme of the mitotic spindle. Redrawn and modified from (Alberts et al., 2014). Taken from (Tolic, 2018).

2.3.1. Microtubules

Among cytoskeletal filaments, microtubules are the largest with diameter size of approximately 25 nm. In comparison, actin filaments are ~7 nm and intermediate filaments are ~10 nm in diameter size (Alberts et al., 2014). Microtubules are dynamic and polar polymers whose protofilaments are composed of αβ-tubulin heterodimers connected by non-covalent bonds and arranged in a head-to-tail configuration (Figure 5a) (Downing and Nogales, 1998). Each microtubule is made up of 13 parallel, laterally connected protofilaments that create a hollow, cylinder-shaped structure (Figure 5b). All of the protofilaments within a microtubule have the same polarity because the subunits are orientated in the same direction throughout the whole protofilament, giving the

microtubule as a whole an overall polarity (Akhmanova and Steinmetz, 2008). Conventionally, the plus (+) end of microtubules is referred to as having exposed β-subunits, while the minus (-) end has exposed α-subunits (Figure 5b). The plus (+) end of a microtubule experiences substantially higher rates of growth and shrinkage due to structural variations between subunits on the two ends of the microtubules (Akhmanova and Steinmetz, 2008).

Both subunits of tubulin heterodimers can bind one molecule of guanosine triphosphate (GTP). After incorporation into a microtubule, GTP bound to α-tubulin will never be exchanged or hydrolyzed, while β-tubulin-bound GTP can undergo hydrolysis to produce guanosine diphosphate (GDP). Moreover, GDP does not exchange while β-tubulin remains in the polymer. This means that each protofilament in a growing microtubule is composed mostly of GDP-bound β-tubulin subunits while only at the growing tip it is capped by one or two terminal heterodimers containing GTP-bound β-tubulin subunits – GTP cap (Figure 5c) (Mitchison and Kirschner, 1984). This difference in the free energy of GTP/GDP-bound polymers is the cause of microtubule dynamic instability. The presence of unhydrolyzed GTP at the plus (+) end of microtubules promotes further growth because GTP dissociates four times slower than GDP and causes GTP cap at plus (+) end to stabilize microtubules. Sporadic switching to rapid shrinkage is referred to as microtubule catastrophe (loss of GTP cap), while microtubule rescue refers to the switching back to growth (Figure 5c). When necessary, the cell can quickly restructure the microtubular cytoskeleton thanks to its dynamic instability (Howard and Hyman, 2009).

Microtubules provide a variety of purposes. They give the cells structural support, act as key components of cilia and flagella, and provide tracks for motor proteins to move organelles. Not least of all, they serve as the primary structural and functional component of the mitotic spindle during cell division.

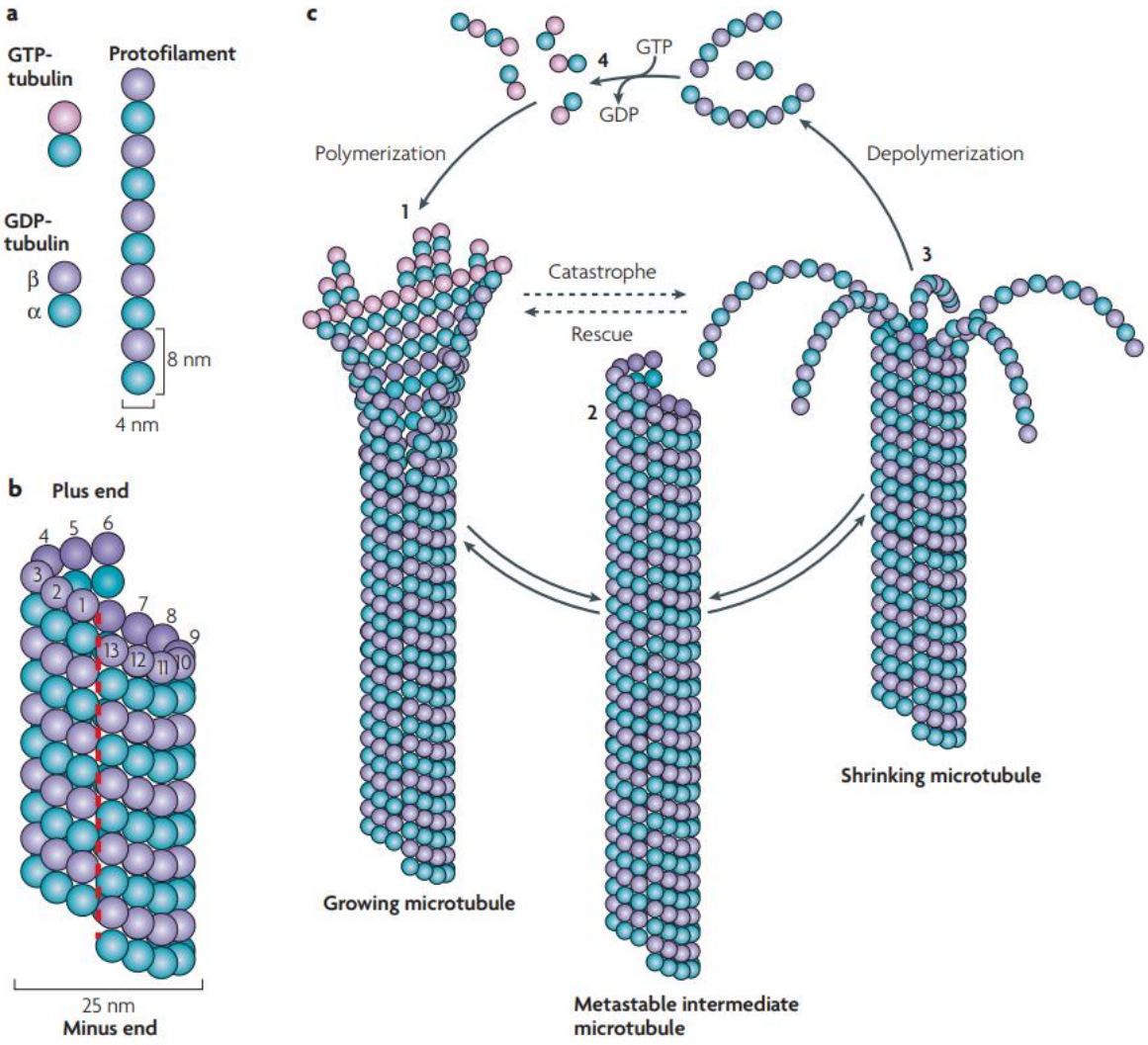

Figure 5. Microtubule structure and dynamic instability. a) To create protofilaments, tubulin heterodimers are aligned in a polar head-to-tail form. **b)** The microtubule cylinder typically consists of 13 parallel protofilaments. **c)** Growth and shrinkage of microtubules is driven by the binding, hydrolysis and exchange of a GTP on the β-tubulin subunit. Once tubulin is incorporated into the microtubule, its GTP is hydrolysed into GDP. The GDP-bound microtubule can stochastically switch to a shrinking state, realeasing GDP-tubulin. The cycle is completed by exchanging the GDP of the disassembly products with GTP, enabling the tubulin to start a new cycle. Taken from (Akhmanova and Steinmetz, 2008).

2.3.2. Centrosomes

Centrosomes are microtubule-organizing centers (MTOCs) of animal cells which nucleate microtubules in orientation with their minus (-) ends close to the centrosome while their plus (+) ends radiate away from the centrosome (McIntosh et al., 2012). The interphase radial array of microtubules is produced with the centrosomes close to the nucleus (Lodish et al., 2014). Centrosomes are made up of two orthogonal centrioles, which are highly stable cylindrical structures, surrounded by pericentriolar material (PCM) (Figure 6) (Wiese and Zheng, 2006). In PCM, we can find more than 50 copies of γ-tubulin ring complex (γTuRC) which represent essential core of the microtubule nucleating machinery. Every γTuRC contains about 13 copies of the γ-isoform of tubulin and several associated proteins. This complex defines the position of microtubule nucleation, their polar orientation, and the fiber into which tubulin assembles (McIntosh et al., 2012). Duplication of centrosomes occurs during the G2 phase of interphase. Centrioles disengage in the early G1 phase and the two wander apart. Assembly of a daughter centrioles perpendicular to each mother begins in G1/S. Before mitosis, the mother centrioles begin to accumulate more PCM and are able to nucleate increased microtubules in preparation for spindle assembly. Once duplicated, centrosomes separate usually in prophase of mitosis and these will become two spindle poles of mitotic spindle (Godinho and Pellman, 2014).

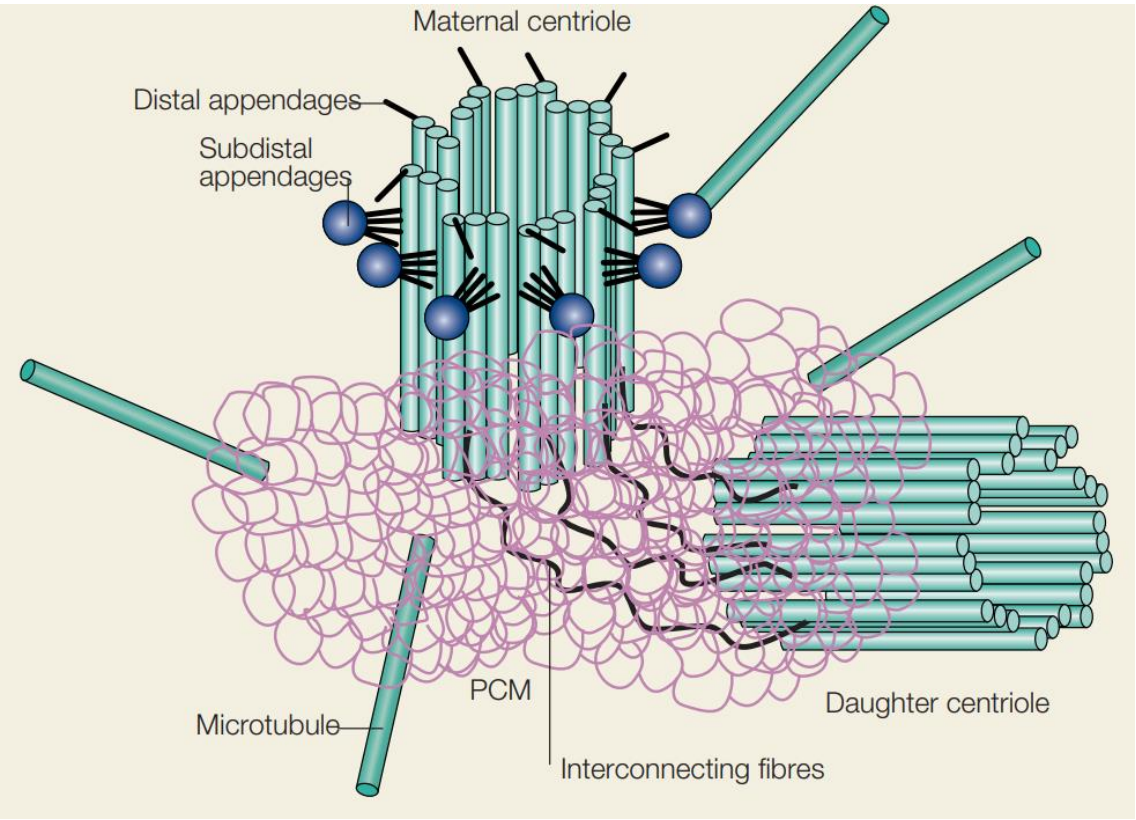

Figure 6. Scheme of the centrosome. The centrosome is composed of two centrioles, connected by interconnecting fibres and surrounded by the pericentriolar material (PCM). Microtubules are nucleated from the PCM. Taken from (Stearns, 2004).

2.3.3. Kinetochores

Kinetochores are large protein complexes formed on centromeric regions of chromosomes during prophase. They are responsible for specific and tight interactions between chromosomes and microtubules. One chromosome with two sister chromatids will contain two sister kinetochores on opposite sides of the centromeric regions. They contains two main regions: the inner one is tightly associated with the centromeric DNA and appears like a discrete heterochromatin domain, while the outer one is highly dynamic and is the site of interaction with the growing microtubules (Figure 7) (Cheeseman and Desai, 2008). If one of sister kinetochores does not properly attach to a microtubule, the transition to anaphase is inhibited. The main protein involved in this process is Mad2, which activates by attaching to the kinetochores that are not attached to microtubules.

Activated, it inhibits Cdc20 activity. Since Cdc20 is an activator of anaphase-promoting complex/cyclosome (APC/C) that is required to initiate anaphase, transition to anaphase will be inhibited as long as Mad2 protein is present (Marques et al., 2015). The checkpoint is held active by any unattached centromere; only when all centromeres are attached will anaphase commence. The Cdc20 is an important target of the SAC, which consists of several different proteins, including Mad2. The two main targets of the APC/C are the S/M cyclins and the protein securin. S/M cyclins activate cyclin-dependent kinases (Cdks), which have a vast array of downstream effects that work to guide the cell through mitosis. They must be degraded for cells to exit mitosis. Securin is a protein that inhibits separase, which in turn inhibits cohesin, a protein that holds sister chromatids together. Therefore, in order for anaphase to progress, securin must be inhibited so that cohesin can be cleaved by separase. These processes are dependent on both the APC/C and Cdc20: When Cdks phosphorylate the APC/C, Cdc20 can bind and activate it, allowing both the degradation of Cdks and the cleavage of cohesin (Yu, 2007).

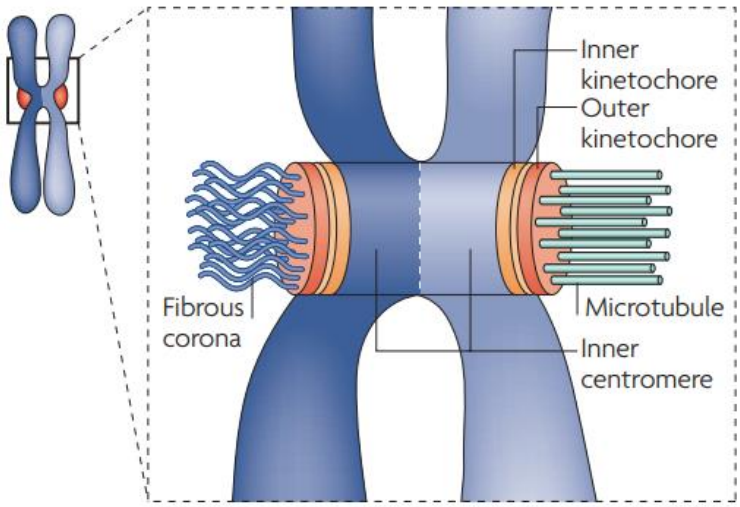

Figure 7. A scheme of a mitotic chromosome with paired sister kinetochores. The chromatid on the right is attached to microtubules and the chromatid on the left is unattached. The inner kinetochore, the outer kinetochore, the inner centromere and the fibrous corona, which is detectable on the unattached kinetochore, are highlighted. Taken from (Cheeseman and Desai, 2008).

2.3.4. Microtubule-associated proteins (MAPs)

The spindle's dynamic characteristics and stability, in addition to the previously mentioned fundamental construction blocks, strongly depend on microtubule-associated proteins (MAPs). MAPs are roughly divided into four groups (Figure 8). The first group consists of crosslinking side-binding proteins that stabilize and align microtubules in specific structures. The second group of plus (+) end tracking proteins (+TIPs) either regulate microtubule growth at plus (+) end or link plus (+) ends to the other cellular structures. The third group consists of enzymes that regulate microtubule destabilization, and the fourth of motor proteins that move along microtubules powered by chemical energy (Lodish et al., 2014).

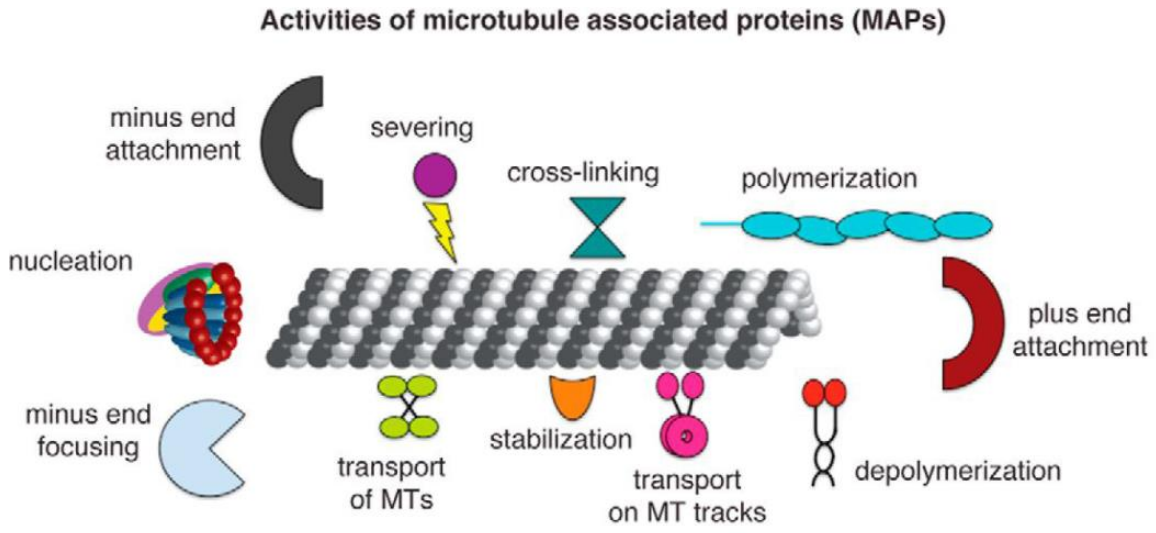

Figure 8. Organization of the microtubule cytoskeleton by MAPs. Representative classes of MAP activities are depicted schematically. Taken from (Alfaro-Aco and Petry, 2015).

From the group of crosslinking MAPs, the most interesting protein concerning this doctoral thesis is protein regulator of cytokinesis 1 (PRC1). PRC1 protein is a key regulator of cytokinesis (Jiang et al., 1998), but also the main crosslinking protein of antiparallel microtubules within bridging fibers (Kajtez et al., 2016; Polak et al., 2017). PRC1 protein is expressed at relatively high levels during S and G2/M phases of the cell cycle before dropping dramatically after mitotic exit and entrance into G1 phase and it was shown to be a substrate of several cyclin-dependent kinases (Cdks) (Jiang et al., 1998). Its role in spindle's midzone microtubule formation is made possible

through its collaboration with the motor protein kinesin-4 (Bechstedt and Brouhard, 2013). PRC1 is normally inhibited until anaphase onset by Cdk1 mediated phosphorylation, preventing its dimerization. Upon anaphase onset and removal of inhibitory Cdk1 phosphorylation, PRC1 dimers form and specifically recognize antiparallel microtubule overlaps, found at the spindle midzone which they bind, allowing microtubule sliding, crosslinking of microtubule filaments, and assembly of central-spindle-mediating proteins, including but not limited to kinesin-4 (Fededa and Gerlich, 2012). PRC1 dimers recruit kinesin-4 to regions of antiparallel microtubule overlap where this plus (+) end-directed motor protein inhibits microtubule dynamics, helps to form length-dependent end tags that help stabilize and regulate spindle microtubule assembly within cytokinesis (Subramanian et al., 2013).

Microtubule plus (+) end tracking proteins, often known as +TIPs, are a group of structurally unrelated factors that growing microtubules accumulate at their plus (+) ends. The most conserved +TIPs are end-binding proteins (EBs) (Tirnauer and Bierer, 2000). EBs have a precise N-terminal domain which is accountable for microtubule binding. The C-terminus however, sustains an α-helical coiled region which regulates parallel dimerization of EB monomers and comprises an acidic tail along with an EB homology domain (EBH). The EBH domain allow the EB proteins to physically interrelate with an array of +TIPs in order to recruit them to microtubule ends. Structural studies suggest that the EBs probably act by enhancing lateral interactions between individual protofilaments and may affect microtubule lattice structure (Sandblad et al., 2006).

Group of microtubule polymerases and depolymerases regulate microtubule dynamics. They achieve this by selectively binding to αβ-tubulin dimers in defined conformations that will favor the process to be catalyzed (Brouhard and Rice, 2014). Microtubule depolymerases destabilize microtubules by promoting catastrophe to regulate microtubule's stability and length; one of the best characterized depolymerases is the kinesin-13 (MCAK) (Kline-Smith and Walczak, 2002). During mitosis, it plays an important role for chromosome segregation at kinetochores (Rogers et al., 2004) and during anaphase (Maney et al., 2001). Microtubule polymerases oppose depolymerases and promote growth or rescue depolymerizing microtubules (Al-Bassam and Chang, 2011). One of the best-studied microtubule stabilizing agents is the microtubule polymerase XMAP215, which enhances microtubule growth rates up to 10-fold (Brouhard et al., 2008). In the cell, microtubule polymerases and depolymerases do not act individually on

microtubules, but work in a coordinated fashion, and interacting with other MAPs, to construct cell cycle-specific and local microtubule structures (Niethammer et al., 2007).

Associated with spindles, we also find complexes, such as augmin which consists of multiple proteins, and cannot be grouped into any of the mentioned groups of proteins. Augmin complex consists of eight polypeptides that can bind to existing microtubules, at which point it recruits γTuRC that nucleate assembly of new microtubules. This is a centrosome-independent microtubule formation in dividing cells (Hsia et al., 2014). It is believed that this complex is not essential for spindle formation, but in its absence, levels of spindle microtubules are greatly reduced (Goshima et al., 2008). Augmin consists of eight subunits named HAUS1–8, composed mostly of α-helices (Uehara et al., 2009). Functional analysis of different subunits, indicated the importance of augmin in mitosis, evidenced by loss of HAUS proteins causing chromosome misalignment, multi-polar spindle asters, and cytokinesis failure (Goshima et al., 2007; Lawo et al., 2009; Uehara et al., 2009). Current models suggest that augmin binds to pre-existing microtubules within the spindle and recruits the γTuRC via the neural precursor cell expressed developmentally down-regulated protein 1 (NEDD1) (Wieczorek et al., 2020). This allows for the nucleation of shallow angled, daughter microtubules within the spindle to maintain spindle polarity. Augmin-nucleated microtubules grow at an angle of 0-30° relative to the pre-existing microtubule (Kamasaki et al., 2013) and show a directional bias towards kinetochores (David et al., 2019).

The next big group of proteins, which are important for this thesis, are motor proteins. Motor proteins are a class of proteins that bind to and catalyze the hydrolysis of adenosine triphosphate (ATP) into adenosine diphosphate (ADP) and a free phosphate ion. These enzymes are generally referred to as ATPases (Barton and Goldstein, 1996). To perform mechanical work, they tie the chemical energy released by ATP hydrolysis to reversible conformational changes in one or more of their motor domains. Motor proteins switch between their bound and unbound states as a result of this mechanochemically induced cycling, which enables them to walk along microtubules (Lodish et al., 2014). Most of them have one or more motor domains that bind and hydrolyze ATP which allows them to move along microtubules, sometimes even on multiple tracks. Additionally, they may possess some non-motor domains that are class-specific, such as binding domains that bind their cargo molecules, dimerization domains, and often domains that influence structural changes (Gatlin and Bloom, 2010). They always move in a single direction

along the microtubules, which is due to the intrinsic polarity of the microtubules mentioned above. Therefore, it is believed that some of these proteins walk toward the plus (+) and some toward the minus (-) end of microtubules (Lodish et al., 2014).

Big superfamily of motor proteins are kinesins. Kinesins can be classified into 14 groups in total (Table 1). Most of them move toward the plus (+) end of the microtubules with some exceptions, for example kinesin-14 (HSET, Ndc) that walks toward the minus (-) end, while some are non-motile, like kinesin-13 that was already mentioned above as microtubule depolymerase (Cross and McAinsh, 2014). Some kinesins, like kinesin-5, due to orientation of its motor domains, preferentially binds to antiparallel microtubules and then slides them by walking to their plus (+) ends. This process is important for establishing the mitotic spindle bipolarity by centrosome separation (Waitzman and Rice, 2014). Large group of kinesins can bind chromosome arms along with microtubules, so therefore, they are called chromokinesins. In this group, for example, are kinesin-10 and kinesin-4. Chromokinesins are involved in generation of polar ejection forces (force production on chromosomes) (Rieder and Salmon, 1994), and to a different degree in some other processes including chromosome segregation, spindle organization and cytokinesis (Mazumdar and Misteli, 2005).

Other than kinesins, motor protein's group also include dyneins. Dyneins are a family of minus (-) end-directed microtubule motors, which we can classify into two major branches: axonemal dyneins and cytoplasmic dyneins (Alberts et al., 2014). Axonemal dynein is responsible for the rapid sliding movements of microtubules that drive the cilia and flagella. On the other hand, the main role of cytoplasmic dynein is focusing microtubules into a united pole of a mitotic spindle by binding one microtubule as a cargo and transporting it toward the minus (-) end of another microtubule, thereby clustering the minus (-) ends of microtubules together (Civelekoglu-Scholey and Scholey, 2010). It can also bind different cargoes and transport them to minus (-) ends of microtubules, located mainly at spindle poles.

A lot of motor proteins have the preference to step sideways while walking on microtubules and in a way rotate around microtubules. This feature has a direct impact on the subject of this thesis.

Table 1. Proposed kinesin family nomenclature and features. Taken from (Miki et al., 2005).

Standardized name	Previous nomenclature	Founding member(s)[a]	Representative family members	Reported function/structural features	Member no.[b]
Kinesin-1	N-1 [2,16], KIN N-Conventional [5], KHC [20], Kinesin-I [19]	LpKHC **P** [21,22], DmKHC **N** [108]	KIF5B, KHC, NKin, DdK3, DdK5	Vesicle transport, conventional	3/1/1/4/3
Kinesin-2	N-4 [2,16], KIN N-Hetero [5], KRP85/95 [20], Kinesin-II [19]	MmKIF3A **N** [7], StrPuKRP85/95 **P** [30]	KIF3A/3B, KIF17, Krp85/95, Osm3, Fla10	Vesicle-intraflagellar transport/ heterotrimeric	4/3/3/0/0
Kinesin-3	N-3 [2,16], KIN N-Monomeric [5], Unc104/KIF1 [20], Unc104 [19]	CeUnc104 **N** [36], MmKIF1B **P** [38]	KIF1A, KIF1B, KIF13A, UNC104, DdUnc104	Organelle transport/monomeric	8/4/2/0/1
Kinesin-4	N-5 [2,16], KIN N-Chromo [5], Chromokinesin /KIF4 [20], Chromokinesin [19]	MmKIF4 [45]	KIF4A, KIF21A/B, Chromokinesin	Organelle transport, chromosome movement	5/3/2/3/1
Kinesin-5	N-2 [2,16], KIN N-Bipolar [5] BimC [19,20]	AnBimC **N** [57], SchPoCut7 **P** [109]	KIF11, Eg5, BimC, CIN8, KIP1, Cut7	Spindle formation/homotetrameric, bipolar	1/1/1/4
Kinesin-6	N-6 [2,16], MKLP1 [20], MKLP [19]	CgCHO1 [61]	KIF20, KIF23, Rab6Kinesin, CHO1, MKLP1	Cytokinesis, spindle polarity	5/2/1/0/1
Kinesin-7	N-7 [2,16], CENP-E [19,20]	ScKip2 **N** [110], HsCENP-E **P** [111]	KIF10, CENP-E, CMET, CANA, KIP2	Kinetochore microtubule capture	1/2/0/14/2
Kinesin-8	N-8 [2,16], KIP3 [19,20]	DmKLP67A [67]	KIF18B, KIF19A, KLP67A, KIP3	Nuclear migration, mitochondrial transport	3/2/1/2/0
Kinesin-9		CrKLP1 [72]	KIF6, KIF9, KRP3, CrKLP1	Unclear	2/0/0/0/0
Kinesin-10		DmNod N [112] **P** [113]	KIF22, KID, Nod	Chromosome segregation/helix–hairpin–helix DNA-binding motif	1/1/0/1/0
Kinesin-11	N-11 [2,16]	ScSmy1 **N** [74], **P** [75]	KIF26A, KIF26B, VAB8, SMY1	Signal transduction/divergent catalytic core	2/1/1/2/0
Kinesin-12		XlXklp2 [114]	KIF12, KIF15, HKLP2, KLP54D, Xklp2, PAKRPd	Organelle transport/homologous tail	2/1/0/6/0
Kinesin-13	M [2,16], KIN I [5], MCAK/KIF2 [20], I-Type [19]	MmKIF2A **N** [7], CgMCAK **P** [115]	KIF2A, MCAK, XKCM1, PfKinI	Microtubule depolymerizing/central motor	4/3/2/1/1
Kinesin-14A	C-1 [2,16], KIN C-Mitotic [5], C-I [19]	ScKAR3 **N** [87], DmNCD **P** [116]	KIFC1, CHO2, Ncd, Kar3, KatA	Chromosome segregation/ C-terminal motor,	1/1/4/4/1
Kinesin-14B	N-1 [2,16], KIN C-Neuronal [5], C-II [19]	AtKCBP [117]	KIFC2, KIFC3, KatD, KCBP, KIF25	Organelle transport/C-terminal motor	3/0/1/16/0
Orphans			CeKLP10, CeKLP18, DdK9	Ungrouped	0/0/2/2/1
					Total: 45/25/19/60/10

[a]Code: **N**, founding member deduced from nucleotide sequence; **P**, founding member deduced from protein sequence.
[b]Numbers of members in Human/*Drosophila*/*Caenorhabditis elegans*/*Arabidopsis*/*Dictyostelium* genomes.

2.4. Chirality

Recent work from my group showed that the shape of the mitotic spindle in human cells is chiral, as the spindle has a left-handed twist around the pole-to-pole axis (Novak et al., 2018).

Chirality is a property of asymmetry in which an object can be chiral if it is distinguishable from its mirror image; that is, if it cannot be superimposed onto it (Prelog, 1976). In mathematics, chirality is the property of a figure that is not identical to its mirror image. The word chirality is derived from the Greek χειρ (*kheir*), "hand", a familiar chiral object. Human hands are the best example on how to easily visualize chirality: hand and its image in a plane mirror (which is same as the opposite hand) cannot be brought to coincide with itself, that is, no matter how the two hands

are oriented, it is impossible for all the major features of both hands to coincide across all axes (Figure 9) (Kelvin, 1894). This difference in symmetry becomes obvious if someone attempts to place a left-handed glove on a right hand.

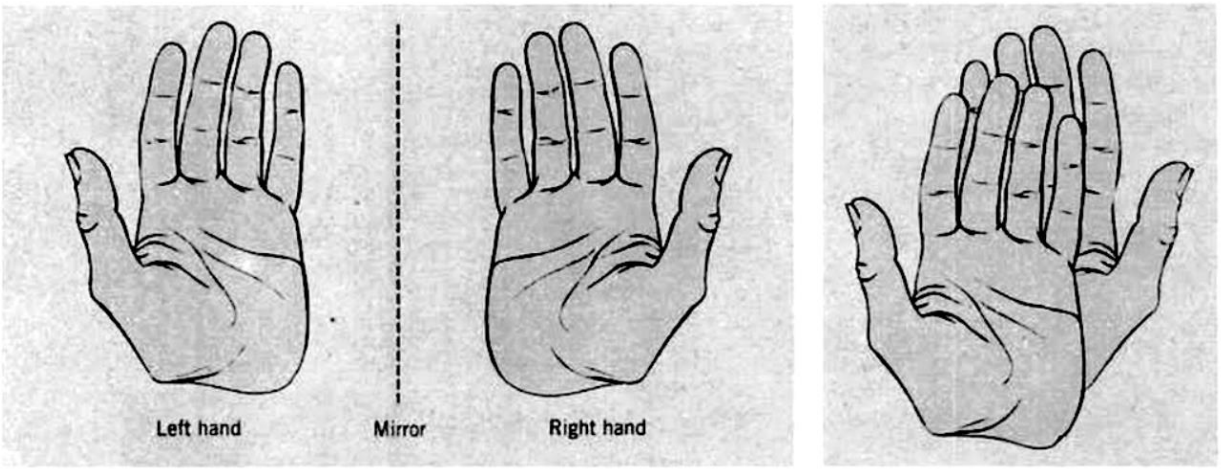

Figure 9. Chirality of human hands. On the left: the mirror image of a left hand is a right hand. On the right: left and right hands are not superposable. Taken from (Solomons and Fryhle, 2003).

Chirality is present everywhere in the nature. In chemistry, chirality usually refers to molecules: two mirror images of a chiral molecule are called enantiomers or optical isomers. Pairs of enantiomers are often designated as right-, left-handed or, if they have no bias, achiral (Solomons and Fryhle, 2003). In physics, chirality may be found in the spin of a particle, where the handedness of the object is determined by the direction in which the particle spins; depending on the linear and rotational motion, the particle can either be defined by left-handedness or right-handedness (*Quantum Diaries*, 19 June 2016). In biology, macroscopic examples of chirality are found in the plant kingdom, the animal kingdom and all other groups of organism. Simple examples are the coiling direction of any climber plant (Burnham et al., 2019), which can grow to form either a left- or right-handed helix, organisms such as gastropods exhibit chirality in their coiled shells (Schilthuizen and Davison, 2005), species of flowers with individuals that either have the style points to the right or the style pointed to the left (Helme and Linder, 1992), etc. Additional examples of helical structures in plants are *lefty* mutants in *Arabidopsis thaliana* that have cortical microtubule arrays that form right-handed helices, causing clockwise bending of flower petals and

leaf petioles when viewed from above (Thitamadee et al., 2002), whereas *spiral* mutants exhibit counterclockwise bending (Furutani et al., 2000). On a molecular level, chirality in biology is important because biological systems show extreme stereospecificity in synthesis, uptake, sensing and metabolic processing. A living system usually deals with two enantiomers of the same compound in drastically different ways, or e.g. they significantly differ in their taste, smell and other biological actions (Solomons and Fryhle, 2003). Also, for artificial compounds, including medicines, in case of chiral drugs, the two enantiomers sometimes show remarkable difference in effect of their biological actions (Sanganyado et al., 2017). For example, penicillamine, the (S)-isomer is used in the treatment of primary chronic arthritis, whereas the (R)-isomer has no therapeutic effect, as well as being highly toxic (Solomons and Fryhle, 2003). In molecular biology, we find chirality as a common property of amino acids and carbohydrates. The protein-making amino acids, which are translated through the ribosome from genetic coding, occur in the L-form. However, D-amino acids are also found in nature. Also, the monosaccharides are commonly found in D-configuration. DNA double helix is chiral, and B-form of DNA shows a right-handed turn (Solomons and Fryhle, 2003).

2.4.1. Chirality of the mitotic spindle

Chirality of the mitotic spindle is evident from the finding that microtubule bundles in human spindles follow a left-handed helical path, which was shown in recent study from my group (Novak et al., 2018). Super-resolution microscopy (STED) images of the spindle suggest that microtubules are arranged into bundles exhibiting a variety of shapes, which run almost through the whole spindle (Figure 10a). While the outer bundles have a shape resembling the letter C, bundles that look like the letter S are found in the inner part of the spindle. In order to obtain three-dimensional (3D) contours of microtubule bundles, vertically oriented spindles were used and imaged by confocal microscopy (Figure 10b). If spindles were imaged while in horizontal orientation (Figure 10c) their z-stacks were rearranged to obtain the slices perpendicular to the spindle axis, similar to the z-stacks of vertical spindles.

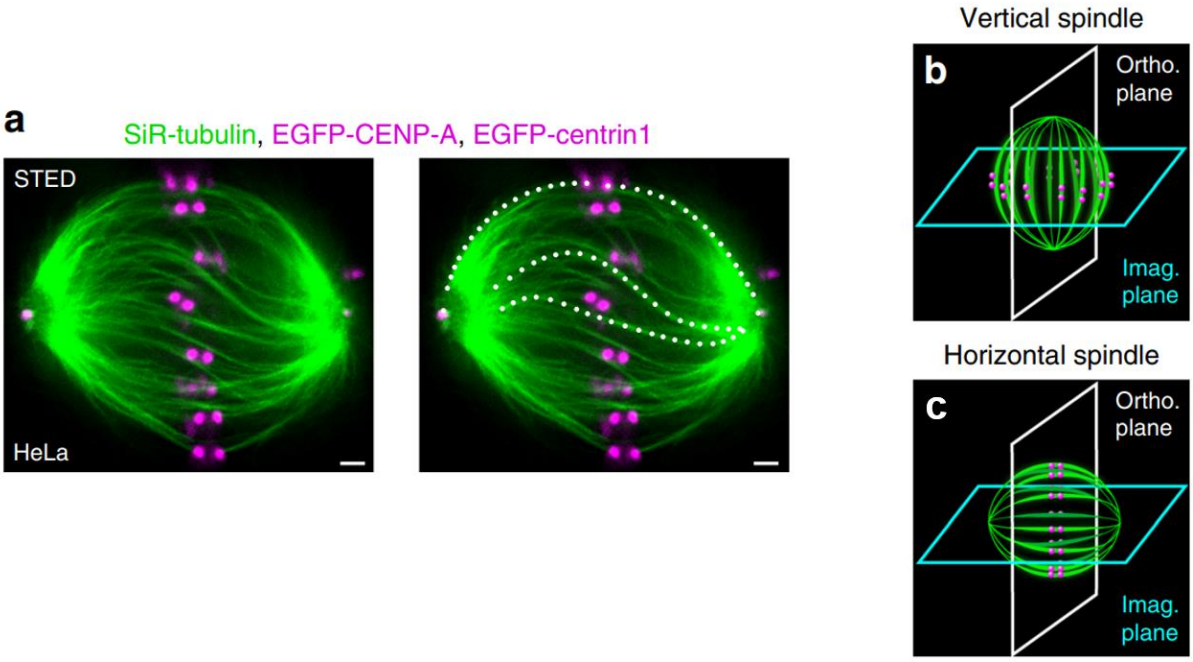

Figure 10. Shapes of microtubule bundles inside the mitotic spindle and possible orientations of mitotic spindles during imaging. a) STED image of metaphase spindle in a live HeLa cell expressing EGFP-CENP-A and EGFP-centrin1 (both shown in magenta); microtubules (SiR-tubulin dye) are shown in green; right panel shows traces of microtubule bundles superimposed on the image. **b)** Imaging scheme of a vertically oriented spindle. **c)** Imaging scheme of a horizontally oriented spindle. Scale bars, 1 μm. Taken from (Novak et al., 2018).

When imaged in this manner and viewed end-on along the spindle axis, the bundles that have a planar shape would form an aster-like arrangement. Arrows connecting bottom and top end of each bundle (traced upwards) rotate clockwise, implying that bundles follow a left-handed helical path along the spindle axis (Figure 11a). The helicity of bundles, defined as the average change in angle with height, where negative numbers denote left-handed helicity, was −2.5±0.2 °/μm in vertically orientated HeLa cells (n=10). This concludes that the mitotic spindle is a chiral object with left-handed helicity of the microtubule bundles. Similar was also shown for horizontally oriented HeLa spindles, live and fixed, as well as U2OS spindles in the same conditions (Figure 11b) (Novak et al., 2018).

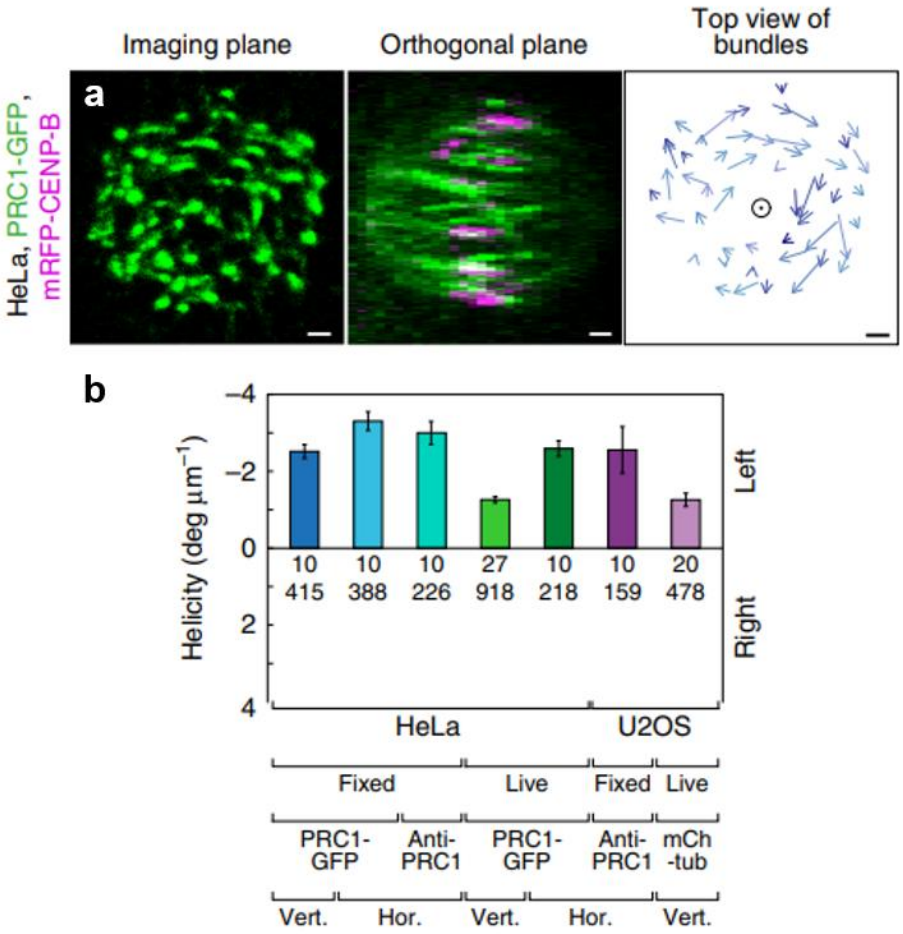

Figure 11. Chirality of the mitotic spindle. a) On the left, imaging plane of a vertical spindle in a fixed HeLa cell expressing PRC1-GFP and mRFP-CENP-B (only PRC1-GFP is shown); in the middle, orthogonal plane of the same spindle; on the right, arrows connecting starting and ending points of PRC1-GFP bundles traced upwards. **b)** Spindle helicity averaged over bundles for different conditions (vertical and horizontal spindles, fixed and live cells) and cell lines as indicated. Numbers represent the number of cells (top) and bundles (bottom). Scale bars, 1 µm; error bars, s.e.m. Taken from (Novak et al., 2018).

To investigate the mechanism as to how the chirality is generated in the spindle, in (Novak et al., 2018) they proposed a hypothesis. It is known that motor proteins can rotate microtubules as they walk on the microtubule lattice, as is the case for kinesin-5 (Eg5) (Yajima et al., 2008). The importance of Eg5 activity for spindle chirality was confirmed in the experiment during which Eg5 activity was inhibited with a drug S-trityl-L-cysteine (STLC). STLC caused the bundle traces

to change from a left-handed rotation to a more random distribution (Figure 12a) (Novak et al., 2018), which indicates an important role of Eg5 motor protein in the maintenance of the spindle chirality. This confirms the hypothesis that perturbation of motor proteins can alter spindle chirality (Figures 12b and 12c), and that chirality relies on forces generated within microtubule bundles by proteins that walk along and rotate the microtubule lattice.

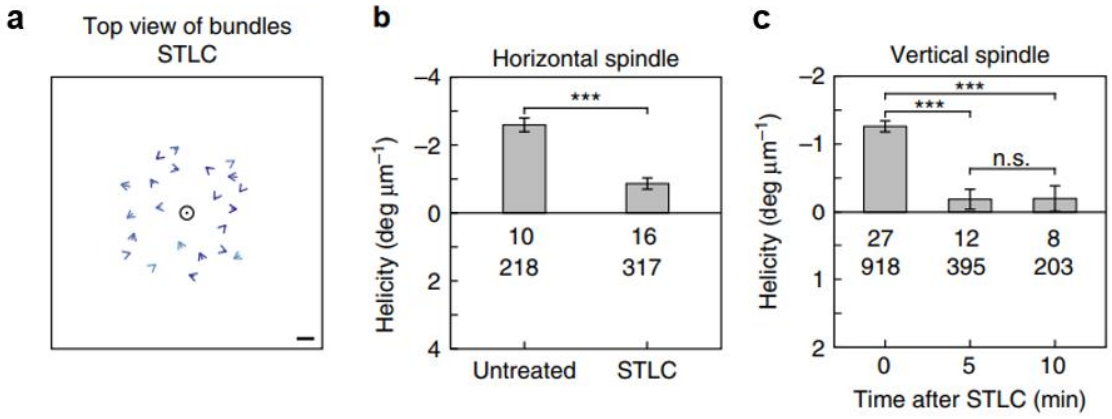

Figure 12. Kinesin-5 (Eg5) inactivation by STLC reduces spindle chirality. a) Arrows connecting starting and ending points of bundles traced upwards. **b)** Helicity of horizontal spindles before and after STLC treatment. **c)** Helicity of vertical spindles before treatment was different from zero, but not at 5 and 10 min. Numbers represent the number of cells (top) and bundles (bottom); ***$p < 0.001$, n.s. not significant; Scale bars, 1 µm; error bars, s.e.m. Taken from (Novak et al., 2018).

Furthermore, recently it was also observed that spindles lacking nuclear mitotic apparatus protein (NuMA), which is a crosslinker, and the kinesin-5 activity in RPE1 cells have strong left-handed twist during anaphase (Figure 13) (Neahring et al., 2021). As evident, this study shows an opposing result when it comes to the inhibition of Eg5 activity, but with the absence of one additional protein, which indicates that likely more than one molecular player is responsible for spindle chirality.

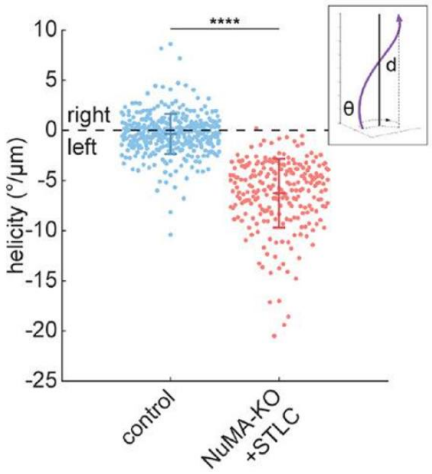

Figure 13. Chirality of spindles in RPE1 cells lacking NuMA and Eg5 activity. Helicity of individual interpolar microtubule bundles, measured in degrees rotated (θ) around the pole-to-pole axis per µm traversed (d) along the pole-to-pole axis for each bundle. Schematic illustration of the helicity measurement shown in inset. ****, $p < 0.00005$; error bars mean ± s.d. Taken from (Neahring et al., 2021).

2.4.1.1. Protein candidates for generation and maintenance of spindle chirality

The spindle chirality is potentially generated by motor proteins that, in addition to linear forces, also exert rotational forces on microtubule bundles by switching protofilaments with a bias in a certain direction. This movement and force production of motor proteins was detected in previous studies by *in vitro* assays such as gliding and bead assays (Bormuth et al., 2012; Brunnbauer et al., 2012; Bugiel et al., 2015; Can et al., 2014; Maruyama et al., 2021; Mitra et al., 2020; Mitra et al., 2018; Ramaiya et al., 2017; Vale and Toyoshima, 1988; Walker et al., 1990; Yajima and Cross, 2005; Yajima et al., 2008).

The principle of a gliding assay involves the adsorption of purified motor proteins to a coverslip on which the drug-stabilized microtubules are added, along with the ATP. Microtubules move or 'glide' on the surface of the coverslip and by knowing the orientation of the microtubules, the direction of the force production can be determined (Figure 14a) (Shim et al., 2017). Similar approach is used in bead assay where latex beads are coated with motor proteins and added onto

the immobilized microtubules along which they will be translocated in an ATP-dependent fashion (Figure 14c) (Vale, 1987).

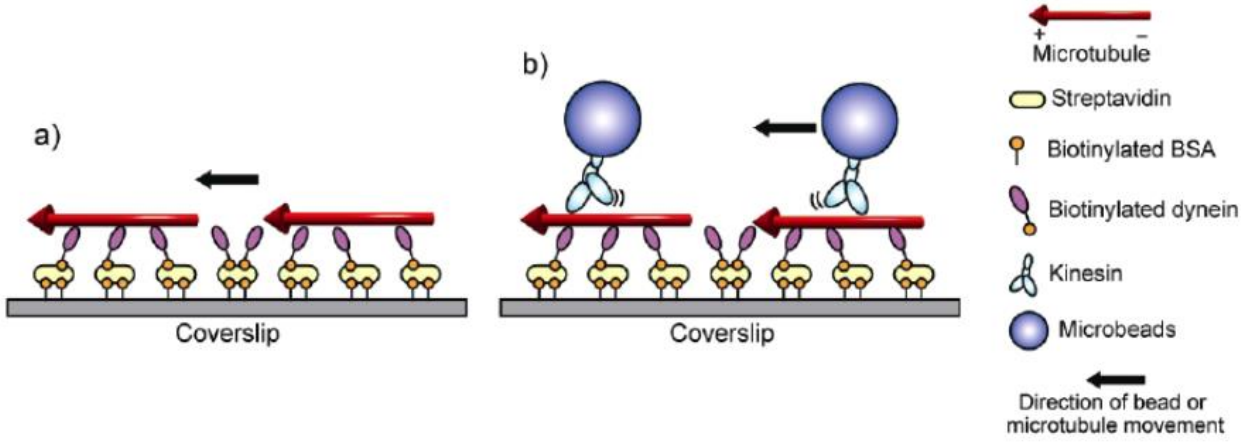

Figure 14. Schematics of *in vitro* assays for motor protein systems. a) Microtubule gliding assay. **b)** Motor protein-coated bead assay on immobilized microtubules. Taken from (Yokokawa et al., 2008)

The first molecular motor discovered to generate torque was the single-headed axonemal dynein, protein that powers the movement of cilia and flagella. In *in vitro* gliding motility assays, surface-attached dynein motors rotated the microtubules around their axis in a clockwise motion, when viewed from the minus (-) end of the microtubules while translocating them in a linear fashion (Vale and Toyoshima, 1988). Also with the gliding assay, similar microtubule rotation was observed for the minus (-) end-directed motor kinesin-14 (HSET/Ncd) which rotates microtubules in a clockwise direction as viewed from their minus (-) ends (Figure 15) (Mitra et al., 2020; Walker et al., 1990). Kinesin-14 has a terminal tail domain that enables the motor to crosslink and slide antiparallel microtubules, which makes this protein an antagonist to kinesin-5 (Eg5) (Fink et al., 2009).

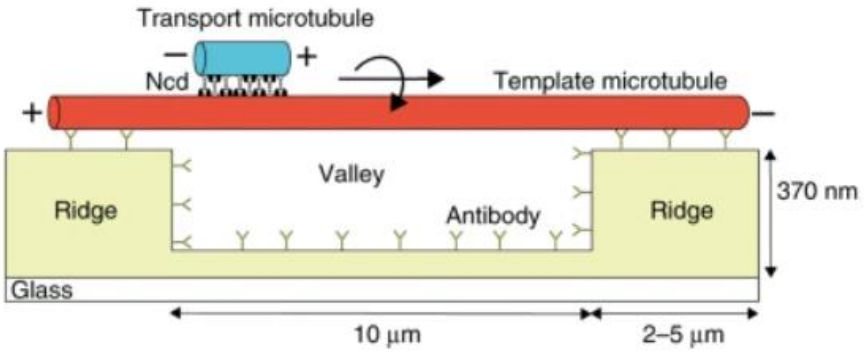

Figure 15. 3D sliding of transport microtubules driven by kinesin-14 (HSET/Ncd) on suspended template microtubules. Schematic representation of a suspended template microtubule immobilized on optically transparent polymer ridges. Transport microtubules are capable of freely accessing the 3D lattice of the template microtubule between the ridges (in the region referred to as valley), as they slide along them driven by Ncd motors. Taken from (Mitra et al., 2020).

Counterclockwise rotation was found for the plus (+) end-directed motor kinesin-5 (Eg5) (Yajima et al., 2008). Eg5 exerts torsional forces which rotate microtubules counterclockwise relative to an observer looking along the microtubule long axis toward the microtubule minus (-) end (Figure 16). For recollection, Eg5 is a bipolar homotetramer with two motor domains that are capable of binding and crosslinking microtubules, and then sliding them by walking to their plus (+) ends (Waitzman and Rice, 2014). Its role is crucial during prometaphase and metaphase in producing and maintaining a mitotic bipolar spindle architecture (Sawin et al., 1992).

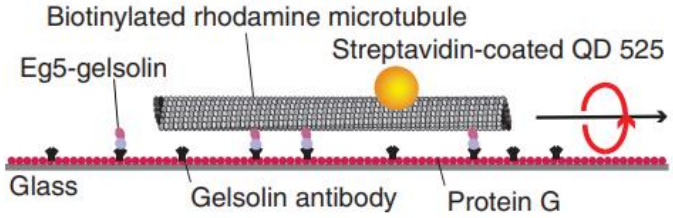

Figure 16. Observation of corkscrew motion of a sliding microtubule driven by kinesin-5 (Eg5). Scheme of the *in vitro* microtubule sliding assay during 3D measurement. Labeled microtubule-attached quantum dot slides in the direction indicated by the arrow, driven Eg5 anchored to the surface. Taken from (Yajima et al., 2008).

Similar counterclockwise rotation was also observed for the plus (+) end-directed motor protein kinesin-8 (Kif18A/Kip3) (Bormuth et al., 2012). Same assay setup as for Eg5, showed counterclockwise rotation when looking from the trailing microtubule plus (+) end in the direction toward the leading minus (-) end. This was also confirmed in the study that used bead assay in which kinesin-8 sidestepped to neighboring microtubule protofilaments with a bias to the left (Figure 17) (Mitra et al., 2018). Additionally, one other study verified sidestepping of kinesin-8 motors, but suggested that protofilament switching occurred intrinsically unbiased toward both directions (Bugiel et al., 2015). Generally, kinesin-8 is a molecular motor known to regulate microtubule dynamics at plus (+) end of kinetochore microtubules by acting as a depolymerase (Mayr et al., 2007). Therefore, it has been shown to play an important role in chromosome alignment during mitosis.

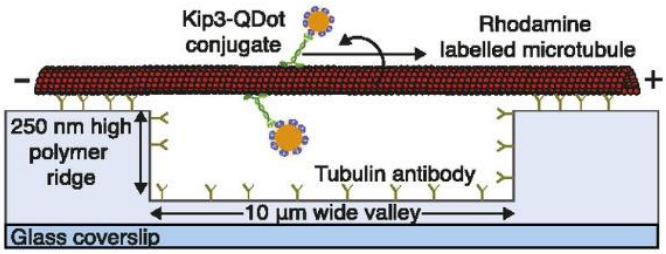

Figure 17. Observation of kinesin-8 (Kif18A/Kip3) motors movement with helical trajectories on freely suspended microtubules. Schematic representation of a freely suspended microtubule immobilized on optically transparent polymer ridges. Single, labeled kinesin-8 motors are capable of accessing the entire 3D lattice of the microtubule between two ridges. Taken from (Mitra et al., 2018).

Cytoplasmic dynein, a molecular motor with the minus (-) end-directed movement along microtubules, moves in a bidirectional helical trajectory around microtubules generating torques (Can et al., 2014). This study demonstrates that dynein generates torque during cargo transport, but unlike other motors that produce torque in a specific direction, dynein generates torque in either direction, resulting in bidirectional helical motility (Figure 18). Dynein has a net preference to move along a right-handed helical path, suggesting that the heads tend to bind to the closest tubulin binding site in the forward direction when taking sideways steps. This bidirectional helical motility

may allow dynein to avoid roadblocks in dense cytoplasmic environments during cargo transport, but the molecular basis of the switches in helical directionality remains unclear.

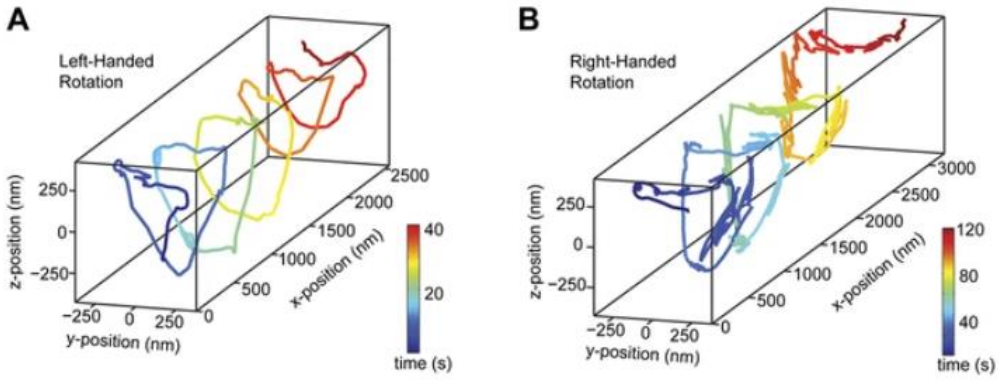

Figure 18. Dynein moves in both left- and right-handed helical paths along microtubule. Representative 3D trace of a cargo bead-driven by dynein motors shows left- **(A)** and right-handed **(B)** helical motion. Taken from (Can et al., 2014).

Kinesin-6 (MKLP1) was also found to rotate around microtubules in a study in which it exhibits persistently left-handed helical trajectories around the microtubule axis, indicating torque generation (Maruyama et al., 2021). In mitosis, MKLP1 forms heterotetrameric centralspindlin complex, with its partner CYK4 (Mishima et al., 2002), which has microtubule bundling properties and is essential for spindle midzone stabilization (Glotzer, 2009). Centralspindlin plays crucial roles in animal cytokinesis both as a key organizer of the post-anaphase microtubule structures and as an important hub for cytokinesis signaling (Mishima, 2016).

Kinesin-1 and kinesin-2 motor proteins were also shown to exhibit rotational movements (Brunnbauer et al., 2012; Ramaiya et al., 2017; Yajima and Cross, 2005), but as they are mostly vesicle transporters, they will not be further explored in this thesis.

Other than by motor proteins, spindle shape can be influenced by variety other spindle-associated proteins, such as microtubule crosslinkers and nucleators. Crosslinker of interest, concerning spindle chirality, is PRC1. As PRC1 is the main crosslinking protein of antiparallel microtubules within bridging fibers (Kajtez et al., 2016; Polak et al., 2017), its absence results in thinner bridging

fibers and spindles that have a less curved and more diamond-like shape (Figure 19) (Jagric et al., 2021; Kajtez et al., 2016), which potentially can have an effect on the spindle twist.

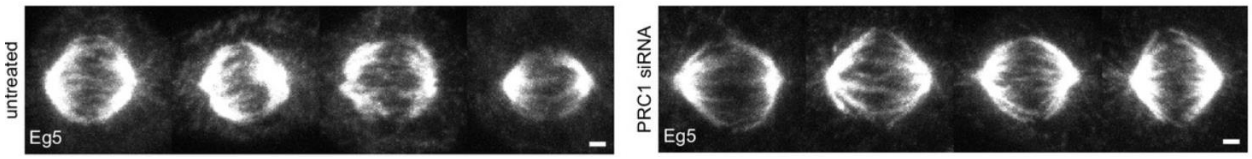

Figure 19. Reduction of bridging fibers, by depletion of PRC1, straightens the spindle contour. Metaphase spindles in fixed U2OS cells immunostained for Eg5 in untreated (left) and PRC1 siRNA-treated cells (right). Scale bar 2 µm. Taken from (Jagric et al., 2021).

The augmin-mediated nucleation of microtubules along the wall of pre-existing microtubules could be an important determinant of the spindle chirality, knowing that the augmin is important for the nucleation of the bridging fibers and, consequentially, the maintenance of the spindle shape (Figure 20) (Stimac et al., 2022). Additionally, augmin nucleates microtubules in a specific way at the angle of 0-30° relative to the pre-existing microtubule (Kamasaki et al., 2013), which naturally, provokes questions whether this geometry could influence spindle chirality.

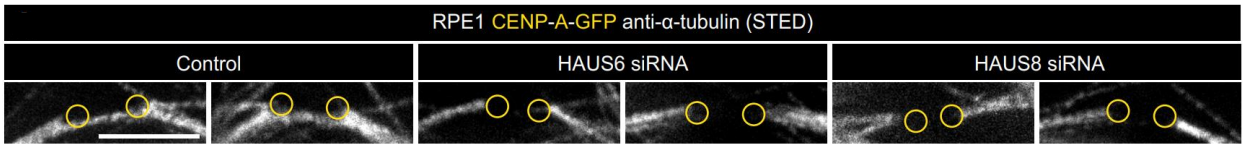

Figure 20. Augmin is crucial for the nucleation of bridging microtubules. The insets of kinetochore pairs in RPE1 cells immunostained for α-tubulin (gray, STED) in control cells (left) and after HAUS6 (middle) or HAUS8 (right) depletion. The insets demonstrate kinetochore pairs with bridging fibers affected by HAUS6 or HAUS8 depletion compared to bridging fibers in control cells. The positions of kinetochores are marked with yellow circles. Taken from (Stimac et al., 2022).

3. MATERIALS AND METHODS

3.1. Cell lines

The cell lines used are: **1.** human hTERT-RPE1 (retinal pigmented epithelium, female) permanently transfected and stabilized using CENP-A-GFP (protein of kinetochore complex) and centrin1-GFP (protein of a centrosome complex), which were a gift from Alexey Khodjakov (Wadsworth Center, New York State Department of Health, Albany, NY) (Magidson et al., 2011), **2.** human hTERT-RPE1 inducible CRISPR/Cas9/ DYNC1H1 knock-out (KO) which were a gift from Iain Cheeseman (Massachusetts Institute of Technology, Cambridge, MA, USA) (McKinley and Cheeseman, 2017). Cells were grown in flasks in Dulbecco's modified Eagle's medium (DMEM; Capricorn Scientific GmbH, Germany) supplemented with 10% fetal bovine serum (FBS; Sigma-Aldrich, MO, USA) and 10000 U/ml penicillin/streptomycin solution (Capricorn Scientific GmbH, Germany). CRISPR/Cas9 knockout of DYNC1H1 in RPE1 cell line was induced with doxycycline hyclate (D9891-1G, Sigma-Aldrich, MO, USA) at the final concentration of 1 μg/mL at 24 hour intervals for 4 consecutive days, with imaging and analysis on the fifth day. The cells were kept at 37 °C and 5% CO2 in a Galaxy 170S CO2 humidified incubator (Eppendorf, Hamburg, Germany) and regularly passaged at the confluence of 70-80%. All used cell lines were confirmed to be mycoplasma free by monthly checks using MycoAlert Mycoplasma Detection Kit (Lonza) and regular checks during imaging experiments with DNA labelling stains.

3.2. Sample preparation

To visualize microtubules in all RPE1 cells, silicon rhodamine (SiR)-tubulin (λ_{Abs} 652 nm, λ_{Em} 674 nm) (Spirochrome AG, Stein am Rhein, Switzerland) dye was added to the dish at the final concentration of 100 nM, 2-3 hours prior to imaging. To visualize microtubules in U2OS cells, SPY650-tubulin (λ_{Abs} 652 nm, λ_{Em} 674 nm) (Spirochrome AG, Stein am Rhein, Switzerland) dye was added to the dish at the final concentration of 100 nM, 2-3 hours prior to imaging. Additionally, to visualize chromosomes and determine phase of the mitosis of the spindles in experiments on RPE1 inducible DYNC1H1 knockout cells, and in all spindle compression

experiments, 50 μL of NucBlue Live Ready Probes Reagent (Hoechst 33342) (Invitrogen by Thermo Fischer Scientific, MA, USA) dye was added to the dishes, 1 min before imaging.

For the inhibition of Eg5, cells were treated with (+)-S-Trityl-L-cysteine (STLC, Sigma-Aldrich, MO, USA) at the final concentration of 40 μM right before the imaging so that cells are not yet collapsed into a monopol during imaging. STLC-treated cells were imaged before spindle shortening (up to 5 min in STLC) and after shortening (10-20 min in STLC). For the inhibition of dynein, cells were treated with dynarrestin (HY-121802/CS-0083323, MedChemExpress, NJ, USA) at the final concentration of 50 μM, 1 hour prior to imaging, and were imaged up to 2 hours after the addition of the drug. This time period allowed the spindles to shorten, which was used to confirm that the inhibition experiment worked (Hoing et al., 2018).

Lipofectamine RNAiMAX reagent (Invitrogen by Thermo Fisher Scientific, MA, USA) was used for RNAi treatments following manufacturer's instructions. Transfections with siRNA were always performed 48 hours prior to imaging at the final concentration of 100 nM. For depletion of endogenous Kif18A, cells were transfected with Kif18A Silencer Select siRNA (4390824, Ambion, Thermo Fisher Scientific, MA, USA). For depletion of endogenous PRC1, cells were transfected with ON-TARGETplus SMARTpool Human PRC1 (L-C19491-00-0010, Dharmacon, CO, USA). For depletions of endogenous HAUS6 and HAUS8, cells were transfected with ON-TARGETplus SMARTpool Human HAUS6 (L-018372-01-0005, Dharmacon, CO, USA) and ON-TARGETplus SMARTpool Human HAUS8 (L-031247-01-0005, Dharmacon, CO, USA), respectively. For the depletion of endogenous HSET, cells were transfected with ON-TARGETplus SMART pool Human KIFC1 (L-004958-00, Dharmacon, CO, USA). For the depletion of endogenous MKLP1, cells were transfected with siRNA (sc-35936; Santa Cruz Biotechnology, TX, USA). In mock experiments cells were transfected with equal amount of ON-TARGETplus Control Pool Non-Targeting pool (D-001810-10-05, Dharmacon, CO, USA) or Silencer Select Negative Control #1 siRNA (4390843, Ambion, Thermo Fisher Scientific, MA, USA).

All plasmid transfections were performed using Nucleofactor Kit R with the Nucleofactor 2b Device (Lonza, Basel, Switzerland) using Y-001 program for human HMEC cells (high efficiency). To overexpress Eg5 protein, cells were transfected with 5 μg of mEmerald-Kinesin11-N-18 plasmid (Addgene number: 54137) 24 hours prior to imaging. For Kif18A overexpression, cells were transfected with 5 μm of EGFP-Kif18A plasmid that was a gift from Jason Stumpff

(University of Vermont, Burlington, VT, USA). To overexpress PRC1 protein, cells were transfected with 5 μg of mCherry-PRC1 plasmid that was a gift from Casper C. Hoogenraad (Utrecht University, Utrecht, Netherlands).

Metaphase arrest in RPE1 cells was performed with the proteasome inhibitor MG-132 (M7449, Sigma-Aldrich, MO, USA) added at least 2 hours prior to imaging at a final concentration of 20 μM.

All experiments were performed at least three times in both cell lines, except Kif18A overexpression that was preformed once. To prepare samples for microscopy, cells were seeded and cultured in DMEM medium with supplements at 37 °C and 5% CO2 on uncoated 35-mm glass coverslip dishes with 0.17-mm (1.5 coverglass) glass thickness (MatTek Corporation, Ashland, MA, USA).

3.3. Immunofluorescence

Human hTERT-RPE1 cells, permanently transfected and stabilized using CENP-A-GFP and centrin1-GFP, were grown on glass-bottomed dishes (as described above) and fixed in cold 100% methanol for 1 min on the ice block. After fixation, cells were washed in PBS 3 times for 5 min at room temperature. Next, cells were additionally permeabilized in 0.5% Triton-X-100 solution for 15 min at room temperature and then washed in PBS (as described above). To block unspecific binding of antibodies, cells were incubated in 1% NGS solution for 1 hour on 4 °C. After washing in PBS once, cells were incubated with primary antibodies (dilution 1:100 in 1% NGS) overnight on 4 °C. Next, cells were washed in PBS 3 times for 5 min at room temperature and incubated with secondary antibodies (dilution 1:250 in 2% NGS solution) for 1 hour at room temperature covered with aluminum foil. Before microscopy, cells were washed in PBS (as described above) and left in PBS during imaging. Cells were kept in the dark in PBS on 4 °C. Primary antibodies used: PRC1 (C-1) mouse monoclonal IgG1 (sc-376983, Santa Cruz Biotechnology, TX, USA), Rabbit anti-KIF18A Affinity Purified (A301-080A, Bethyl, TX, USA), Rb pAb to FAM29A (ab150806, Abcam, Cambridge, UK), HICE1 Polyclonal Antibody (PA5-21331, Invitrogen, MA, USA), KIFC1 (M-63) mouse monoclonal IgG2a (sc-100947, Santa Cruz Biotechnology, TX, USA), Rb pAb to MKLP1 (ab174304, Abcam, Cambridge, UK); secondary antibodies used: Dnk pAb to Ms

IgG (ab150112, Abcam, Cambridge, UK), Dnk pAb to Rb IgG (ab150064, Abcam, Cambridge, UK).

3.4. Spindle compression

Spindle compression method was optimized from (Dumont and Mitchison, 2009a). A solution of 2% ultra-pure agarose (15510 Invitrogen by Thermo Fisher Scientific, MA, USA) was prepared in PBS, brought to boil and put in a 35 mm petri dish to solidify at the final thickness of ∼0.5 cm. While in a process of solidifying, thin strings were put inside with one end while the other end was left free outside of a dish. This way, when fully solidified, areas of gel can be cut out around strings and strings can serve to easily manipulate gel while performing experiment. A 1 cm × 1 cm gel areas were cut out (with strings attached) and stored in PBS at 4 °C. Gels were warmed to 37 °C just before the use in experiments. Cells were plated on 14 or 20 mm glass microwell uncoated dishes before imaging. For the experiment, cells in metaphase were chosen among 80-100% confluent cells. After imaging of the metaphase cell before compression, the gel was deposited gently, centered on the cell. Note: it is important to do this step gently, with a help of strings, and with minimal moving of the dish so the position of the cell could stay intact. Compression was performed using an oil hydraulic fine manipulator (InjectMan 4, micromanipulator with dynamic movement control, 100–240 V/50–60 Hz) and a coarse manipulator attached to the confocal microscope. A metal rod (which is a part of micromanipulator where the needle for microinjection is inserted) was centered on the gel above the cell and lowered (z-axis) until weak contact was made with the gel (rod diameter ≫ cell diameter). The rod was lowered slowly (over ∼10 s) for several μm until the cell area expanded (visible by appearance of the blobs on a cell membrane, as well as expanding of a spindle) and its position kept constant as the cell and spindle responses were imaged. Cells were then, again, imaged for the third time as soon as the rod was removed and there was no pressure left on the cells. This way, we have 3 time points: images before compression, during compression, and soon after the compression. In some cases cells were left for a longer time to recuperate, so that we can determine whether they will divide, and then imaged once more. Cell health was monitored through the presence of the intact cell membrane and the ability of the cell to enter anaphase after the manipulation.

3.5. Confocal microscopy

Live RPE1 cells were imaged using Bruker Opterra Multipoint Scanning Confocal Microscope (Buđa et al., 2017) (Bruker Nano Surfaces, Middleton, WI, USA). The system is mounted on a Nikon Ti-E inverted microscope equipped with a Nikon CFI Plan Apo VC ×100/1.4 numerical aperture oil objective (Nikon, Tokyo, Japan). During imaging, cells were maintained at 37 °C in Okolab Cage Incubator (Okolab, Pozzuoli, NA, Italy). A 22 μm slit aperture was used. The xy-pixel size was 83 nm. For excitation of GFP and mCherry fluorescence, a 488 and a 561 nm diode laser line was used, respectively. For SiR-dyes, a 640 nm diode laser line was used. The excitation light was separated from the emitted fluorescence by using Opterra Dichroic and Barrier Filter Set 405/488/561/640. Images were captured with an Evolve 512 Delta EMCCD Camera (Photometrics, Tucson, AZ, USA) with no binning performed. To cover the whole metaphase spindle, z-stacks were acquired at 30–60 focal planes separated by 0.5 μm with unidirectional xyz scan mode. The system was controlled with the Prairie View Imaging Software (Bruker Nano Surfaces, Middleton, WI, USA).

3.6. Analysis of spindle twist

To calculate spindle twist, microscopy images of horizontal spindles were analyzed in Fiji Software (ImageJ, National Institutes of Health, Bethesda, MD, USA) (Schindelin et al., 2012). Only images with both spindle poles in the same plane before and during imaging of the z-stack were used in analysis to avoid unspecific spindle movements in the calculation of spindle twist. Horizontal spindles were transformed into vertical orientation (end-on) using a code written in R programming language in RStudio (Novak et al., 2018). In transformed stack microtubule bundles and poles appear as blobs.

Visual assessment. In this method, the spindle is observed end-on and the rotation of microtubule bundles around the pole-to-pole axis is estimated visually. If the bundles rotate clockwise when moving along the spindle axis in the direction towards the observer, the twist is left-handed, and vice versa (Figure 22A, left). The outcome of our visual assessment is a score of spindle twist, which describes whether the spindle has a left-handed, weak left-handed, right-handed, weak right-handed, or no visible twist. Weak left-handed or weak right-handed twists

correspond to a range of approximately -1 to -2 °/μm in the bundle tracing method. This is visible as a total rotation of 5-10° in the clockwise (left-handed) or counter-clockwise (right-handed) direction in the end-on view of the spindle when moving towards the observer along the bundle length, where bundles are typically 5 μm long. Left-handed or right-handed twists correspond to a rotation of more than 10° in the end-on view. The advantage of this method is its trustworthiness because coarse classification of spindles into 5 groups is reliable, whereas the main disadvantage is that the results are semi-quantitative rather than quantitative.

Optical flow. In the optical flow method, the movement of the signal coming from microtubule bundles is estimated automatically by comparing the signal from one z-plane to the next (Figure 22A, middle). This method yields a value for the average twist of all bundles in a spindle. It is the preferred choice for experiments on a large number of spindles because it is automated. Disadvantages are that it provides only the average twist value rather than the twist of each bundle, and that the results are sensitive to unspecific signal in the images, individual bundles with atypical behavior, and imperfect alignment of the spindle axis with the z-axis.

First, parts of the images containing the blobs were selected for analysis using Rectangle tool in ImageJ. In all transformed stacks only images between spindle poles were used for analysis. Transformed spindle images contained a lot of noise that was removed by using the Mexican hat filter and a threshold. The Mexican hat filter, also called the LoG (Laplacian of Gaussian) filter, was used for detection of blobs (Jin and Feng, 2014; Lowe, 2004). After applying the Mexican hat filter, a threshold was applied to the image. It removes all the pixels with intensity lower than the given threshold. Microtubule bundles of transformed spindles were detected and traced automatically using optical flow for calculating the movement of pixels between two consecutive images. Farnebäck's two-frame motion estimation algorithm (dense optical flow algorithm) was used (Farnebäck, 2003). The spindle poles were tracked manually using Multipoint tool in ImageJ. In CRISPR/Cas9 DYNC1H1 knockout RPE1 cell line, only spindles with splayed poles but bipolar shape were imaged, and the pole positions were determined visually as the outermost points of the spindle along the central spindle axis, which was defined as a line perpendicular to the metaphase plate passing through its center. Helicities of spindles were calculated using the algorithm called "All pixels weighted helicity algorithm". It calculates the total helicity as the average helicity of all pixels in the spindle, weighted by their normalized intensity. The tilt of the spindle with regard to the imaging plane was calculated from the tracked spindle poles, and the twist measurement

was corrected by this tilt angle. The code for tracing of bundles and helicity calculating was written in Python programming languange using PyCharm IDE. The external libraries used in image preprocessing, calculating helicity and visualisation are NumPy, scikit-image, Matplotib, PIL, OpenCV and SciPy. The code and instructions are available at https://gitlab.com/IBarisic/detecting-microtubules-helicity-in-microscopic-3d-images.

Bundle tracing. Bundles in images of amoeba spindles oriented end-on were traced manually using Multipoint tool in Fiji (Novak et al., 2018). If amoeba spindles were not already imaged in the end-on orientation, the imaging plane (z-plane) was converted to its corresponding z-coordinate by multiplying with the distance between successive planes set during image acquisition. Next, to describe the shape of a microtubule bundle, the oblique circle method (Ivec et al., 2021) was used. First, spindle is positioned so that the pole-to-pole axis is aligned with necessary coordinate system, i.e., the spindle is "untilted". Next, a plane is fitted to the points representing the bundle, and then a circle that lies in this plane is fitted to the same points. From these fits, the curvature and twist of the bundle are calculated as follows: (i) The curvature is calculated as one over the radius, and (ii) the twist is calculated as the angle between the plane and the z-axis divided by the mean distance of these points from the z-axis (Figure 22A, right). Contour length of the bundle was calculated as the length of the fitted circular arc plus the distance of bundle ends from the corresponding poles.

3.7. Analysis of spindle length and width

To measure spindle length and width, the Line tool in Fiji Software (ImageJ, National Institutes of Health, Bethesda, MD, USA) (Schindelin et al., 2012) was used. Length was measured by drawing a line from pole to pole of the spindle. In RPE1 cells expressing CENP-A-GFP and centrin1-GFP, length was measured by drawing a line from one centrosome to the other centrosome. In CRISPR/Cas9 DYNC1H1 knockout RPE1 cell line the pole positions were determined visually as the outermost points of the spindle along the central spindle axis, which was defined as a line perpendicular to the metaphase plate passing through its center. Width in RPE1 cells expressing CENP-A-GFP and centrin1-GFP was measured by drawing a line across the equatorial plane of the spindle, with the line ending at the outer kinetochore pairs. Width in CRISPR/Cas9 DYNC1H1

knockout RPE1 cell line was measured by drawing a line across the equatorial plane of the spindle, with the line ending at the outer edges of a spindle.

3.8. Analysis of spindle parameters in spindle compression experiments

In addition to spindle length and width measurements, as described in sub-chapter 3.7. "Analysis of spindle length and width" above, the height and curvature length of spindles were measured as well. Spindle height was calculated by multiplying the number of z-planes needed to encompass the entire spindle (from lower planes to upper planes following kinetochore signal) with 0.5 μm (z-distance between successive planes used during imaging). Curvature length was measured by using the Segmented Line tool in Fiji Software (ImageJ, National Institutes of Health, Bethesda, MD, USA) (Schindelin et al., 2012). Line was drawn in multiple short segments from one pole of the spindle to the other by following the outermost spindle contour. Poles of the spindles were determined in the same manner as described in the sub-chapter "3.7. Analysis of spindle length and width". Both contour sides of the spindle were measured and their average value was used for the further analysis.

3.9. Analysis of protein expression in spindles

To quantify protein expression, the fluorescence intensity signal of the protein of interest was measured on the whole spindle region using ImageJ Polygon Selection tool Software (ImageJ, National Institutes of Health, Bethesda, MD, USA) (Schindelin et al., 2012) on the sum-intensity projection of the whole z-stack. The mean background fluorescence intensity measured in the cytoplasm was subtracted from the mean value obtained on the spindle, and the resulting value was divided by the number of z-slices used in the sum projection.

3.10. Image processing and statistical analysis

Fiji was used to scale images and adjust brightness and contrast. Figures were assembled in Adobe Illustrator CS5 and CC (Adobe Systems, Mountain View, CA, USA). Graphs were plotted in MATLAB (MathWorks, Natick, MA, USA). For generation of univariate scatter plots, the open "UnivarScatter" Matlab extension was used (https://github.com/manulera/UnivarScatter). Data are given as mean ± SEM, unless otherwise stated. Significance of data was estimated by Student's t-test (two-tailed and two sample unequal-variance). $p < 0.05$ was considered statistically significant. Values of all significant differences are given with degree of significance indicated (*$0.01 < p < 0.05$, **$0.001 < p < 0.01$, ***$p < 0.001$). Statistically significant differences between groups of data were determined by one-way ANOVA and Tukey's HSD post hoc test, $p < 0.05$ was considered statistically significant. The number of analyzed cells and microtubule bundles is given in the respective figure panels.

4. RESULTS

4.1. Developed assays to measure spindle twist

In the rest of the text, I will refer to spindle chirality as spindle twist. Results shown in this dissertation were published in my paper (Trupinic et al., 2022), from which most figures, also, were taken and modified.

To estimate the twist of the spindle, the first step is to obtain end-on view images covering the whole spindle from pole to pole. If the spindle is standing vertically with respect to the imaging plane, a z-stack of images provides an end-of view of the spindle. If the spindle is lying horizontally, a z-stack provides a side view of the spindle and needs to be transformed into the end-on view. In the end-on view, if microtubule bundles look like flower petals, this is a signature of their twisted shape (Figure 21).

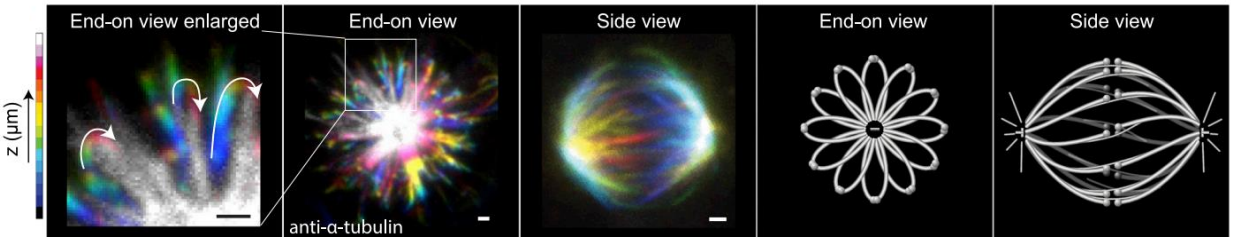

Figure 21. Point of view of the mitotic spindle. Images of spindles immunostained for α-tubulin in a HeLa-Kyoto BAC cell line stably expressing PRC1-GFP (PRC1-GFP signal is not shown). From left to right: enlarged section of the spindle imaged end-on showing microtubule bundles rotating in a clockwise direction (arrows) through z-planes when moving toward the observer, the end-on view and side view of a spindle, and the corresponding schemes. Images are color-coded for depth (see color bar).

We developed 3 approaches to estimate spindle twist: 1) Visual assessment, 2) Optical flow, 3) Bundle tracing (Figure 22). Here, I describe briefly the main concept underlying each approach together with its advantages and disadvantages, and technical details are given in the Methods section. As it is still an open question in the field what method is the most appropriate to measure spindle twist (Ivec et al., 2021; Neahring et al., 2021; Novak et al., 2018), visual

assessment is useful as a quick and rough estimate of the twist and as a control for automated or semi-automated methods. In the visual assessment method, the spindle is observed end-on and the rotation of microtubule bundles around the pole-to-pole axis is estimated visually. If the bundles rotate clockwise when moving along the spindle axis in the direction towards the observer, the twist is left-handed, and vice versa (Figure 22A, left). The result of our visual assessment is whether the spindle has a strong left-handed, weak left-handed, strong right-handed, weak right-handed, or no visible twist. Weak twists correspond to a range of approximately -1 to -2 °/μm in the bundle tracing method (Figure 22B). This is visible as a total rotation of 5-10° in the clockwise (left-handed) or counter-clockwise (right-handed) direction in the end-on view of the spindle when moving towards the observer along the bundle length, which is typically 5 μm. Accordingly, left and right twists correspond to a rotation of more than 10° in the end-on view (Figure 22B). The advantage of this method is its trustworthiness because such coarse classification of spindles into 5 groups is reliable, whereas the main disadvantage is that the results are semi-quantitative rather than quantitative.

In the optical flow method, the movement of the signal coming from microtubule bundles is estimated automatically by comparing the signal from one z-plane to the next (Figure 22A, middle). This method yields a value for the average twist of all bundles in a spindle. It is a preferred choice for high-throughput studies because it is automated. Disadvantages are that it provides only the average twist value instead of the twist of each bundle, and that the results are sensitive to individual bundles with atypical behavior and to imperfect alignment of the spindle axis with the z-axis. Visual assessment is always used as a control to optical flow method.

The bundle tracing method is an extension of the approach developed previously (Novak et al., 2018), where individual bundles are manually traced by following the bundle contour in the end-on view of the spindle to acquire their x, y, and z coordinates in each z-plane of the entire z-stack (Figure 22A, right). The main advantage of this method is that it yields a value of twist for each individual bundle in the spindle, whereas the main disadvantage is that it requires manual tracing, which makes it impractical for high-throughput studies. This method will be explained further in the text (Ivec et al., 2021.).

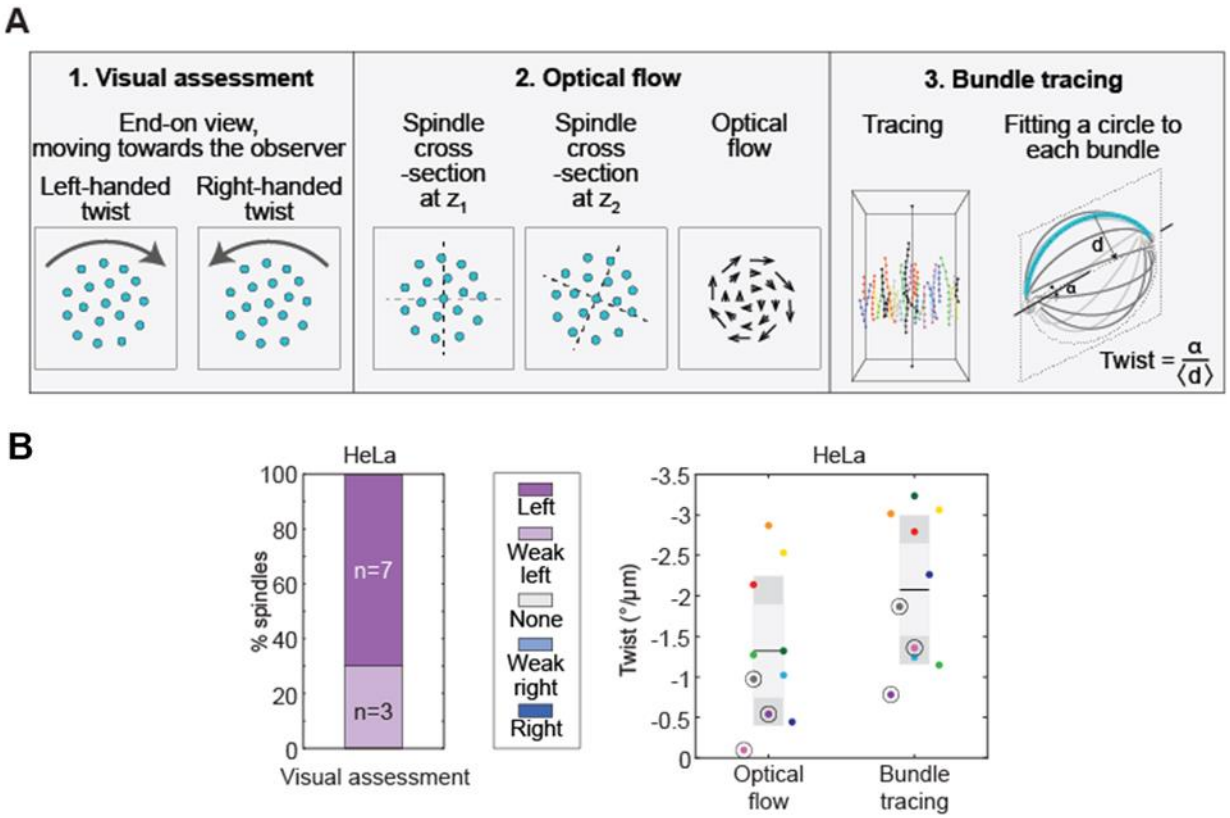

Figure 22. Methods for calculating spindle twist. A) Schemes of three methods used to measure spindle twist: visual assessment (1), optical flow (2) and bundle tracing (3). **B)** Comparison of the twist for 10 spindles calculated with three different methods. On the left, visual assessment graph represents percentages of spindles showing left, right, weak left, weak right or no twist as described in the legend. On the right, graph shows twist calculated with optical flow and bundle tracing methods; each color represents one cell; circled and un-circled data correspond to the 'weak left' and 'left' data from the visual assessment graph, respectively. Note that the weak left twist in the visual assessment graph corresponds to the range of approximately -1 to -2 °/μm in the bundle tracing method followed along the 5 μm of the bundle length, which corresponds to the rotation of 5-10° in the clockwise direction in the end-on view of the spindle. The black line shows the mean; the light and dark grey areas mark 95% confidence interval on the mean and standard deviation, respectively. Same cells were used to calculate the data for both methods. Experiments were performed on the HeLa-Kyoto BAC cells stably expressing PRC1-GFP (n=10; raw data taken and re-calculated from (Novak et al., 2018)).

As a label for microtubule bundles, we used SiR-tubulin or GFP-tubulin to observe all microtubule bundles, or PRC1-GFP to observe the bridging fibers. To compare the results of the three methods, we analyzed twist of 10 metaphase spindles in HeLa cells expressing PRC1-GFP (Figure 22B). All three methods yielded a left-handed twist, which is expressed by negative values, for all the 10 spindles. The spindles that were visually assessed as having a strong left twist had, on average, a higher left twist value also in the bundle tracing and optical flow method, than those with a weak left twist. The absolute values of twist of individual spindles obtained by bundle tracing and optical flow were similar, with optical flow yielding lower values (1.32°/μm ± 0.29°/μm, n = 10; all data are given as mean ± SEM) than bundle tracing (-2.07 °/μm ± 0.29°/μm, n = 10). This difference is likely due to the sensitivity of the optical flow method to all signals, including the background. Based on this cross-check between the three methods, we conclude that they provide a comparable value of spindle twist. Visual assessment method is always used and combined with optical flow for experiments in which I test changes in the overall twist of the spindle on a large number of cells, or with bundle tracing for experiments where high spatial precision is required.

4.2. Spindle twist is most pronounced at anaphase onset in a non-cancer RPE1 cells

Spindles in cancer cell lines are twisted in a left-handed manner in metaphase (Novak et al., 2018), but it is not known whether the twist is present already when the spindle assembles in prometaphase or whether it arises as the spindle matures. Furthermore, it is unknown how the twist changes during anaphase. To examine the development of spindle twist throughout mitosis, I measured the twist in the non-cancer immortalized epithelial cell line hTERT-RPE1 (from here on referred to as RPE1) (Figure 23A) and found that spindles in these cells showed a left-handed twist (Figure 23B), but the values were smaller than in HeLa cells (Trupinic et al., 2022). Moreover, the temporal pattern of twist in RPE1 cells was similar to that in HeLa cells. Twist was absent in prometaphase; it was very weak left-handed in metaphase and was at its peak value at anaphase onset; it decreased during anaphase and vanished in late anaphase (Figure 23B; Table 2). The value at anaphase onset was -0.53 °/μm ± 0.15 °/μm (n = 26), which indicates a weaker left-handed twist than in HeLa cells (Novak et al., 2018; Trupinic et al., 2022). Taken together, results show that spindles are born without a twist. The left-handed twist in cells arises as the spindle acquires its metaphase shape, peaks at the start of chromosome segregation, and declines afterward. In RPE1

cells the values are much less pronounced, and the twist is mostly noticeable only in early anaphase.

Table 2. Spindle twist, length and width in RPE1 cells in different phases of mitosis and after protein perturbations. All values are shown as mean ± SEM. Purple color denotes left-handed twist (mean value of twist < 0 and $p < 0.05$ for a difference from 0 in a t-test), blue color denotes right-handed twist (mean value of twist > 0 and $p < 0.05$ for a difference from 0 in a t-test), and grey denotes no twist ($p > 0.05$ for a difference from 0 in a t-test). The numbers in the brackets denote the number of cells; RPE1 cells used were hTERT-RPE1 cells permanently transfected and stabilized using CENP-A-GFP and centrin1-GFP and RPE1 inducible CRISPR/Cas9 DYNC1H1 knockout cells.

	RPE1		
	Twist (°/μm)	Length (μm)	Width (μm)
Prometaphase	0.004 ± 0.09 (20)	12.1 ± 0.2	8.7 ± 0.1
Metaphase	-0.21 ± 0.08 (34)	12.8 ± 0.3	9.0 ± 0.1
Anaphase onset	-0.53 ± 0.15 (26)	12.9 ± 0.2	8.7 ± 0.1
Early anaphase	-0.30 ± 0.15 (22)	13.8 ± 0.3	8.4 ± 0.2
Late anaphase	-0.20 ± 0.17 (16)	16.6 ± 0.4	7.5 ± 0.3
Eg5 inhibition (after < 5 min)	-0.06 ± 0.19 (11)	12.3 ± 0.4	8.8 ± 0.1
Eg5 inhibition (after 10-20 min)	0.06 ± 0.13 (12)	8.3 ± 0.2	7.7 ± 0.2
Eg5 overexpression	-0.25 ± 0.12 (11)	12.7 ± 0.4	9.0 ± 0.3
Kif18A siRNA	0.30 ± 0.11 (24)	15.0 ± 0.6	8.7 ± 0.2
Kif18A overexpression	-0.26 ± 0.20 (7)	10.3 ± 0.3	8.1 ± 0.2
MKLP1 siRNA	0.48 ± 0.10 (16)	13.6 ± 0.3	9.1 ± 0.3

HSET siRNA	-0.19 ± 0.12 (18)	13.9 ± 0.4	8.9 ± 0.1
Dynein inhibition	-0.18 ± 0.08 (16)	9.8 ± 0.3	8.4 ± 0.1
Dynein KO	-0.29 ± 0.13 (15)	15.8 ± 0.8	10.7 ± 0.5
PRC1 siRNA	0.22 ± 0.11 (22)	15.3 ± 0.4	9.6 ± 0.2
PRC1 overexpression	-0.08 ± 0.11 (10)	10.3 ± 0.4	8.0 ± 0.1
HAUS6 siRNA	0.49 ± 0.21 (16)	11.7 ± 0.3	9.0 ± 0.1
HAUS8 siRNA	0.85 ± 0.24 (13)	13.1 ± 0.4	9.0 ± 0.2
Mock siRNA	-0.22 ± 0.08 (39)	12.5 ± 0.2	8.6 ± 0.1
MG-132	0.51 ± 0.14	12.0 ± 0.4	8.8 ± 0.2

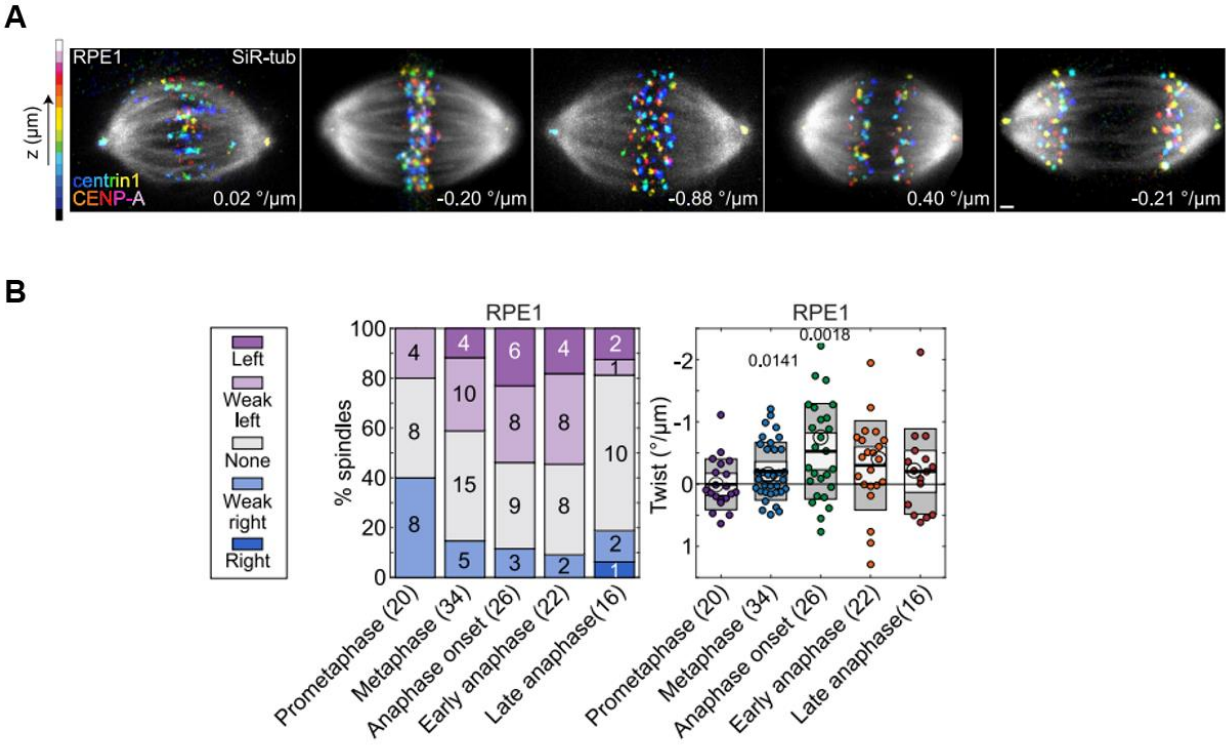

Figure 23. Spindle twist culminates at the beginning of the anaphase. A) Spindles in hTERT-RPE1 cells expressing CENP-A-GFP and centrin1-GFP in different phases of mitosis. Microtubules are shown in gray (SiR-tubulin), and kinetochores/centrosomes are color-coded for depth (color bar) and filtered with a Gaussian blur (radius 0.7). Twist values are given. **B)** Twist in different phases of mitosis in RPE1 cells. Left, visual assessment graph represents the percentages of spindles showing left, right, weak left, weak right, or no twist (see legend); numbers in the bars and in brackets show the number of cells. Right, the twist values calculated with the optical flow method. The black line shows the mean; the light and dark gray areas mark 95% confidence interval on the mean and standard deviation, respectively; numbers above the data show p-values (Student's t-test for the mean twist value different from 0). Non-significant differences are not shown. The circled dots represent the cells that are shown in the images above. Scale bar, 1 μm.

4.3. Proteins that regulate spindle twist

To explore the molecular origins of torques in the spindle and thus its twisted shape, I considered the following molecular activities. First, motors that exert torque on the microtubule may generate the twisted shape of the bundle by twisting the microtubules within the bundle around each other or by twisting the microtubules with respect to the spindle pole. Second, proteins that crosslink neighboring microtubules or link microtubules with the pole may prevent free rotation of the microtubules, thereby allowing for twisting of the bundles. Third, nucleation of new microtubules within the bundle may affect the bundle twist. To test the role of these activities in the regulation of spindle twist, I performed a candidate screen on RPE1 cells in which we perturbed motor proteins and other microtubule-associated proteins one by one using siRNA-mediated depletion, small-molecule inhibitors, or overexpression and measured the resulting spindle twist. As the candidates for this mini screen, I selected spindle-localized motor proteins for which it has been shown *in vitro* that they can rotate the microtubule (Eg5/kinesin-5, Kif18A/kinesin-8, MKLP1/kinesin-6, HSET/kinesin14, and dynein), the main crosslinker of antiparallel microtubules PRC1, and the augmin complex that is responsible for the nucleation of microtubules along existing microtubules (Figure 24). Spindle twist was measured during metaphase, rather than at the anaphase onset when the twist is most pronounced, because depletion or inhibition of some

of the candidate proteins, such as Eg5, Kif18A, and augmin, interferes with anaphase entry (Stumpff et al., 2008; Uehara et al., 2009; Zhu et al., 2005). Furthermore, the measurement of the twist in metaphase is more reproducible because spindles in metaphase are in a steady state, whereas anaphase spindles undergo extensive changes.

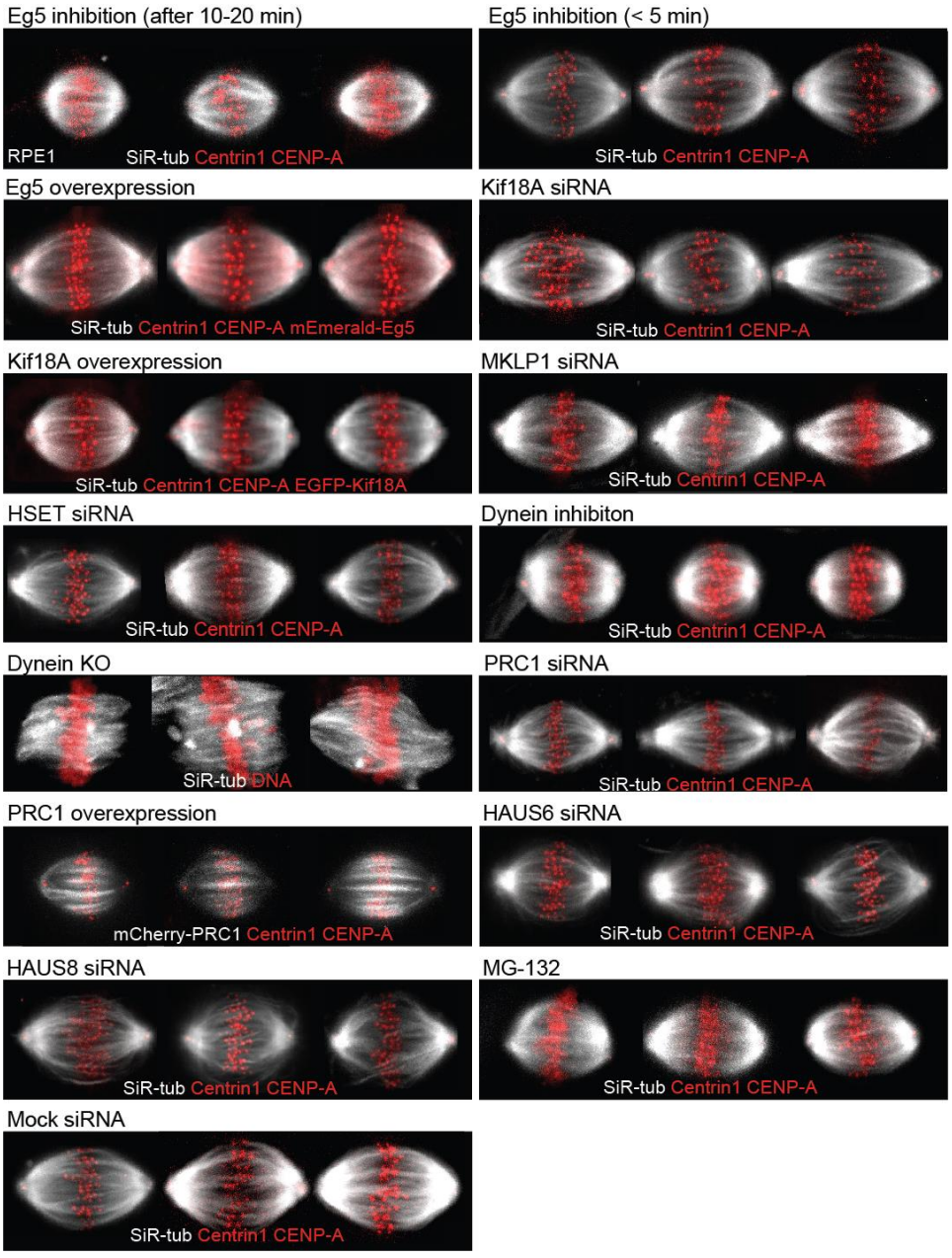

Figure 24. Spindles of RPE1 cells after perturbation of spindle-associated proteins. Examples of three spindles for every perturbation of spindle-associated proteins: Eg5 inhibition (after 10-20 min of STLC treatment), Eg5 inhibition (STLC treatment shorter than 5 min), Eg5 overexpression, Kif18A depletion, Kif18A overexpression, MKLP1 depletion, HSET depletion, dynein inhibition, dynein KO, PRC1 depletion, PRC1 overexpression, HAUS6 and HAUS8 depletion, MG-132 treatment, and mock control. Microtubule bundles are shown in grey (SiR-tubulin and, for PRC1 overexpression, mCherryPRC1) and kinetochores/centrosomes, DNA (NucBlue dye), Eg5 and KiF18A in red. Images are shown in maximum z-projections. Experiments were performed on hTERT-RPE1 cells, permanently transfected and stabilized using CENP-A-GFP and centrin1-GFP and RPE1 inducible CRISPR/Cas9 DYNC1H1 knockout cells.

All candidate proteins were depleted by siRNA, except Eg5 and dynein. Eg5 was inhibited with S-trityl-L-cysteine (STLC) (Skoufias et al., 2006) because siRNA depletion of Eg5 would not allow for spindles to properly assemble, resulting in monoasters (Zhu et al., 2005). For dynein inhibition, I used dynarrestin (Hoing et al., 2018), as well as CRISPR/Cas9-inducible DYNC1H1 (dynein heavy chain) knockout (KO) RPE1 cells (McKinley and Cheeseman, 2017). Depletion by siRNA of each protein was confirmed by measurements of the immunofluorescence signal of that protein on the spindle (Figure 25).

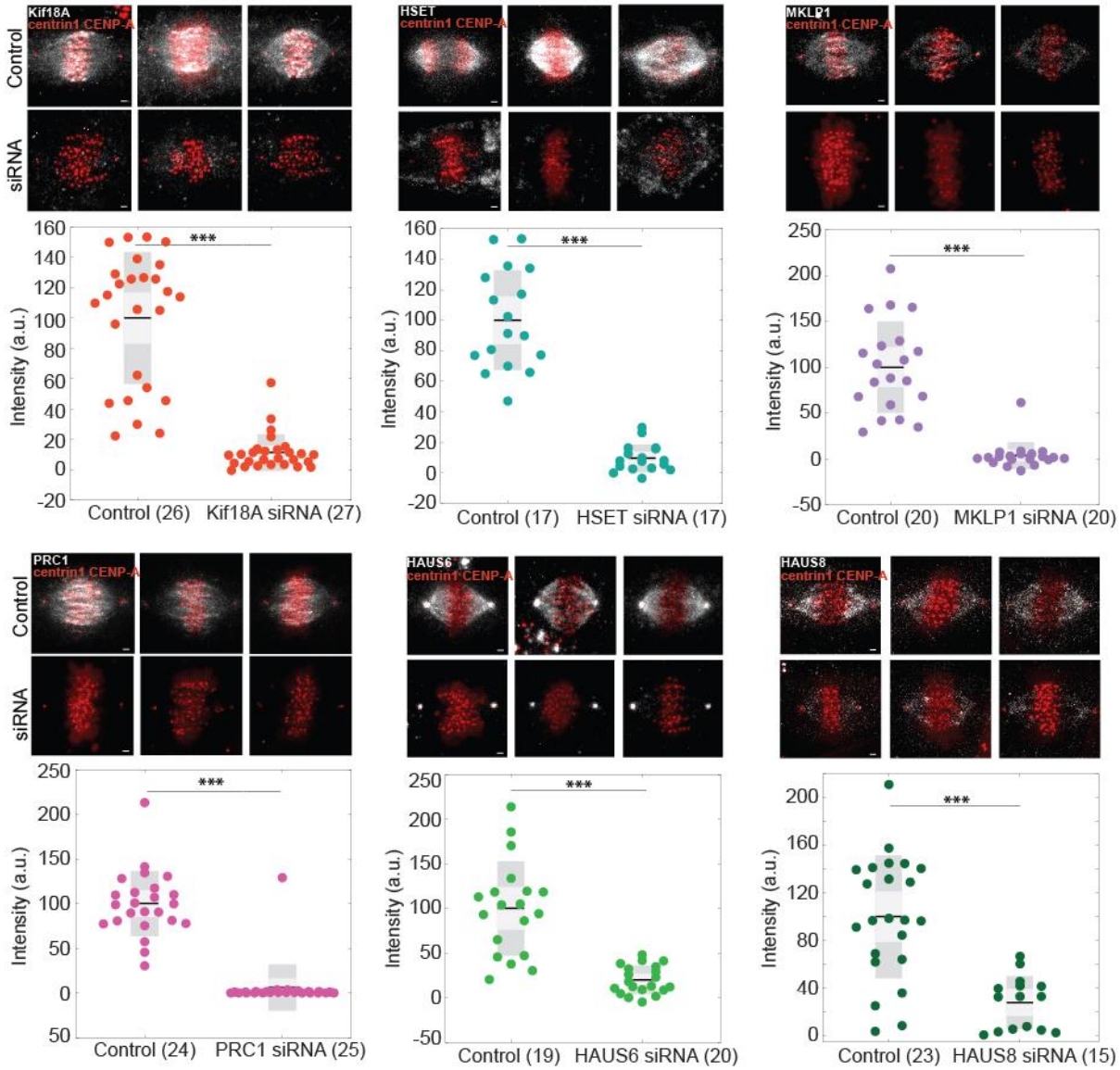

Figure 25. Immunofluorescence images of spindles in RPE1 cells after protein perturbations. Examples of three spindles for every perturbation of spindle-associated proteins and their controls: Kif18A depletion, HSET depletion, MKLP1 depletion, PRC1 depletion, HAUS6 and HAUS8 depletion, in that order. Microtubule bundles are shown in grey (proteins of interest) and kinetochores/centrosomes in red. Images are shown in maximum z-projections. Graphs show intensities of protein of interest in control cells and cells treated with siRNA. ***p<0.001 (Student's t-test). Numbers in bracket denote number of cells used in the experiments. Scale bar 1 μm.

4.3.1. Motor proteins Eg5/kinesin-5, Kif18A/kinesin-8, MKLP1/kinesin-6, and dynein regulate spindle twist

In agreement with our previous work on HeLa cells (Novak et al., 2018), I found that the acute inhibition of Eg5 with STLC decreased the left-handed spindle twist in RPE1 cells (Figure 26B; Table 2). The spindles had no twist 5 min after STLC addition, whereas the spindle length was the same as before the treatment and after 10–20 min when the spindles were shorter but still bipolar (Table 2). These results suggest that changes in the spindle twist due to Eg5 inhibition are independent of the changes in spindle length. Depletion of Kif18A, interestingly, resulted in a right-handed twist in RPE1 cells, causing ~71% of RPE1 spindles to twist in the right-handed fashion, with a mean twist of 0.30 °/μm ± 0.11°/μm ($n = 24$, $p = 0.0119$ for a difference from 0 in a Student's t-test; Figure 26B; Table 2). Overexpression of either Eg5 or Kif18A did not yield changes in the twist (Figure 26B; Table 2). Depletion of MKLP1 significantly changed the twist in RPE1 cells, where 94% of spindles were twisted in a right-handed direction (Figure 26B; Table 2). The mean twist was 0.48 °/μm ± 0.10 °/μm ($n = 16$, $p = 0.0003$ for a difference from 0 in a Student's t-test). Depletion of HSET/kinesin-14 did not change the twist (Figures 26B; Table 2). Dynarrestin treatment did not change the twist in RPE1 cells when measured with optical flow method, but effect was visible during visual assessment (Figure 26B; Table 2). In DYNC1H1 knockout RPE1 cells, the twist was absent, but it was challenging to measure the twist in these cells due to the unfocused spindle poles and altered spindle shape, but visually uniform twisting was absent (Figure 26B; Table 2). I can conclude that Eg5, Kif18A, MKLP1, and dynein regulate the torques within the spindle, which lead to the twisted shape of microtubule bundles, but their contribution differs in different cell lines (Trupinic et al., 2022).

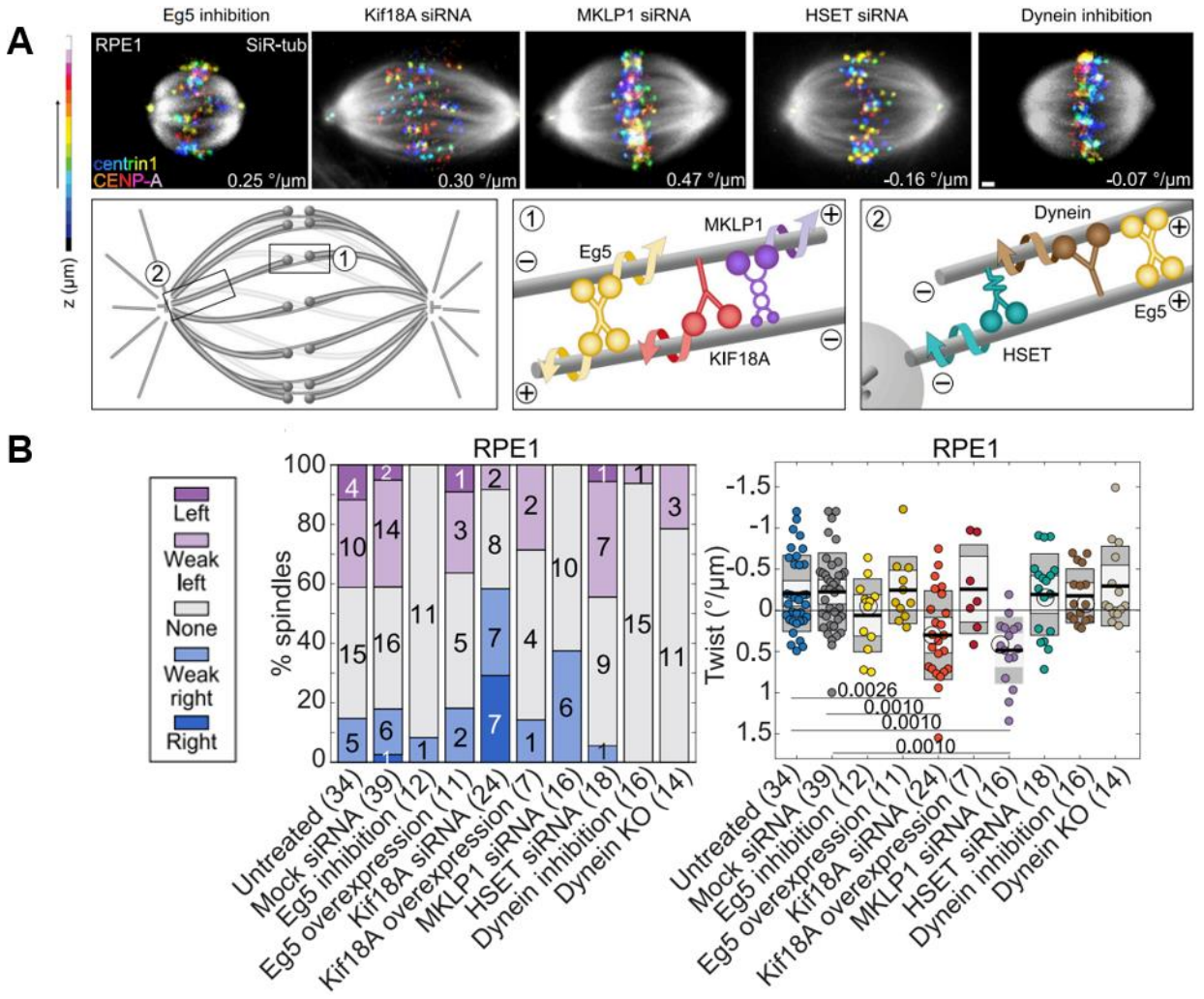

Figure 26. Motor proteins Eg5, Kif18A and MKLP1 control spindle twist in RPE1 cells. A) First row, spindles in hTERT-RPE1 cells expressing CENP-A-GFP and centrin1-GFP after the inhibitions/depletions of Eg5, Kif18A, MKLP1, HSET, and dynein, as indicated. Color-coding for depth as in Figure 24A. Second row, schemes showing localization and movement of the targeted motor proteins within the spindle. **B)** Spindle twist after perturbations of motor proteins in RPE1 cells expressing CENP-A-GFP and centrin1-GFP and RPE1 inducible CRISPR/Cas9 DYNC1H1 knockout cells. Left, visual assessment of twist; right, twist calculated with the optical flow method; legend as in Figure 24B. One-way ANOVA test showed a significant difference between group means ($p = 2.27 \times 10^{-7}$). Numbers below the data show p-values (Tukey's HSD post hoc test); non-significant differences are not shown; the encircled dots represent cells on the images above. Immunofluorescence after perturbations is shown in Figure 25. Data for Eg5 inhibition correspond to 10–20 min after STLC addition. Scale bar, 1 µm.

4.3.2. Depletion or overexpression of PRC1 in RPE1 spindles results in no twist

Without PRC1, bridging fibers are thinner and spindles have a less curved and more diamond-like shape (Jagric et al., 2021; Kajtez et al., 2016), which led me to hypothesize that the twist might also be affected. When I depleted PRC1 in RPE1 cells, the spindles had no twist on average, but certain percentage of spindles had a prominent right-handed twist (Figure 27B; Table 2). Overexpression of PRC1 in RPE1 cells also resulted in the abolishment of the spindle twist, as the microtubule bundles became almost straight (Figure 27B; Table 2). These data suggest that PRC1 regulates torques within the spindle in RPE1 cells, possibly by limiting the free rotation of microtubules within antiparallel bundles and by modulating the torsional rigidity of the bundle.

4.3.3. Depletion of augmin leads to right-handed twist in RPE1 cells

Augmin is important for the nucleation of the bridging fibers and, consequentially, the maintenance of the spindle shape (Stimac et al., 2022). When I depleted the augmin subunit HAUS6 (hDgt6/FAM29A), which binds to γTuRC through the adaptor protein NEDD1 (Uehara et al., 2009), the spindles in the RPE1 cells had a right-handed twist of 0.49 °/μm ± 0.21°/μm (n = 16, p = 0.0341 for a difference from 0 in a Student's t test; Figure 27B; Table 2). A similar result was observed after the depletion of the augmin subunit HAUS8 (hDgt4/Hice1), which binds to pre-existing microtubules (Song et al., 2018; Wu et al., 2008). This resulted in a strong right-handed twist in RPE1 cells of 0.85 °/μm ± 0.24 °/μm (n = 13, p = 0.0041 for a difference from 0 in a Student's t-test; Figure 27B; Table 2). The twist after the depletion of HAUS6 or after the depletion of HAUS8 was not significantly different (p = 0.27), as expected, given that they are part of the same complex. Thus, the augmin-mediated nucleation of microtubules along the wall of pre-existing microtubules is an important determinant of the direction and amount of spindle twist. As depletion of the augmin complex subunits prolongs metaphase (Uehara et al., 2009), I explored how the twist changes when cells are arrested in metaphase by adding the proteasome inhibitor MG132. Interestingly, the spindles in RPE1 cells that arrested in metaphase had a right-handed twist of 0.51 °/μm ± 0.14 °/μm (n = 15, Figure 27B; Table 2), suggesting that prolonging metaphase may cause a shift in the balance of torque-generating activities resulting in a right-handed twist.

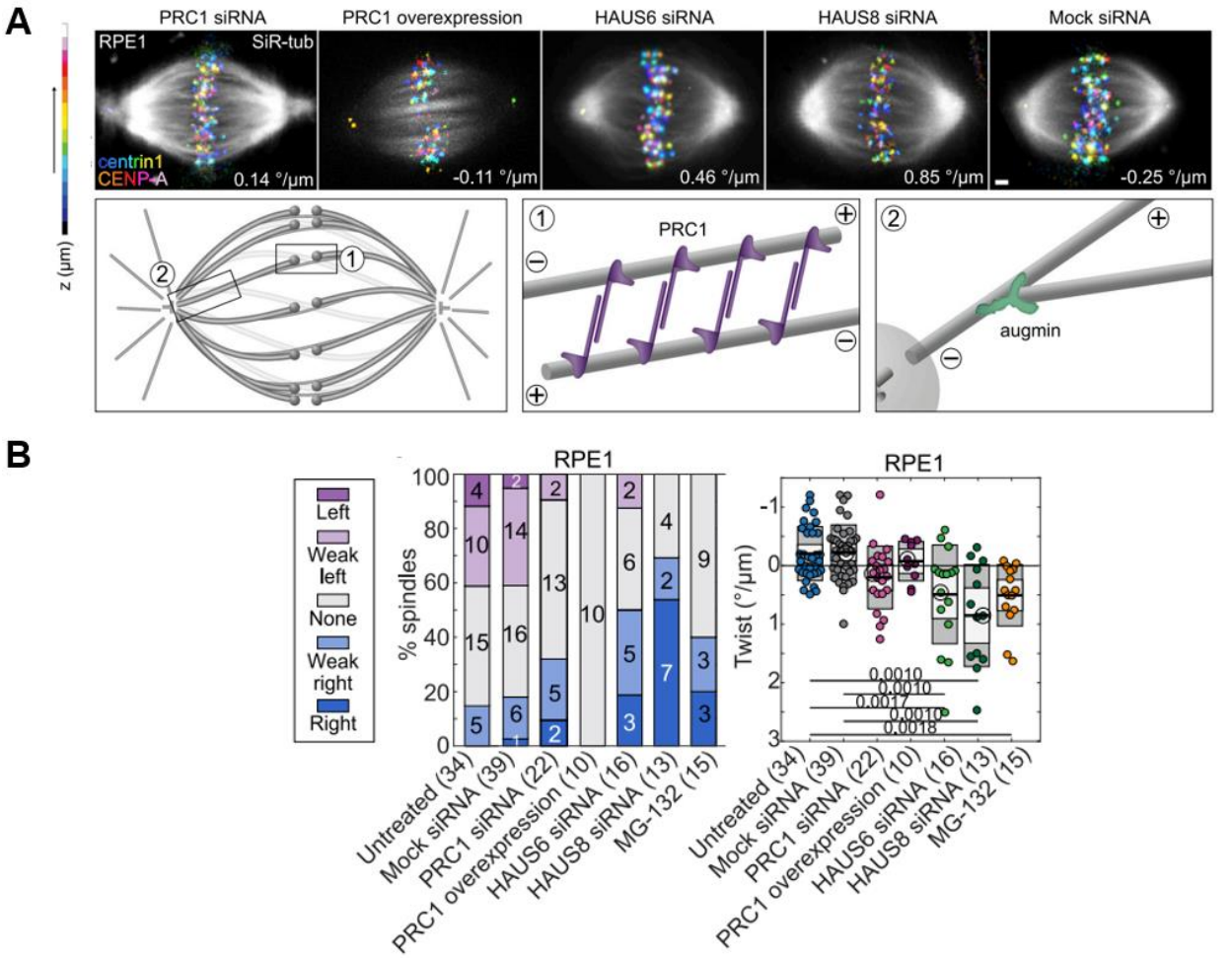

Figure 27. Microtubule crosslinker PRC1 and nucleator augmin regulate spindle twist. A) First row, images of spindles in hTERT-RPE1 cells expressing CENP-AGFP and centrin1-GFP after perturbations of PRC1 and depletions of HAUS6 or HAUS8, as indicated. Color-coding for depth as in Figure 24A. Gray represents SiR-tubulin, except in the cell with overexpressed PRC1 that shows PRC1-mCherry. Second row, the schemes showing the localization of PRC1 and augmin in the spindle. **B)** Spindle twist after perturbations of PRC1 and augmin in RPE1 cells expressing CENP-A-GFP and centrin1-GFP. Left, visual assessment of twist; right, twist calculated with the optical flow method; legend as Figure 24B. One-way ANOVA test showed a significant difference between group means ($p = 1.72 \times 10^{-9}$). Numbers below the data show p-values (Tukey's HSD post hoc test); non-significant differences are not shown; the encircled dots represent cells on the images above. Immunofluorescence is shown in Figure 25. Scale bar, 1 µm.

4.4. Round spindles are more twisted than elongated spindles

To explore the relationship between twisting and bending moments in the spindle, we tested the correlation between spindle twist and width/length ratio, as higher aspect ratios are a signature of stronger bending moments in the spindle (Novak et al., 2018). A plot of the twist as a function of the width/length ratio for various mitotic phases and treatments indicates that different combinations of twist and bending moments exist in spindles in different phases of mitosis or in which different molecular mechanisms are perturbed (Figures 28B and 28C). For comparison, data for the HeLa cell line, collected by my colleague, was taken from our study (Trupinic et al., 2022). In HeLa cells, prometaphase and late anaphase spindles are elongated with zero and small left-handed twist values, respectively (Figure 28B). Left-handed twist rises during metaphase when spindles are the roundest, and the highest twist values are at the beginning of anaphase when spindles are still rather round (Figure 28B). In contrast, in RPE1 cells, such a correlation between twist and roundness over mitotic phases was not observed (Figure 28B). When analyzing the twist of metaphase spindles across the treatments, we found that in HeLa cells, a strong left-handed twist was prevalent in spindles with high width/length ratios (higher than ~0.8; Figure 28C), whereas in RPE1 cells, a strong right-handed twist was found in a subset of treatments with lower width/length ratios (lower than ~0.8, Figure 28C). Taken together, these results suggest a link between bending moments and left-handed twisting moments in HeLa cells, whereas in RPE1 cells, this relationship is less clear.

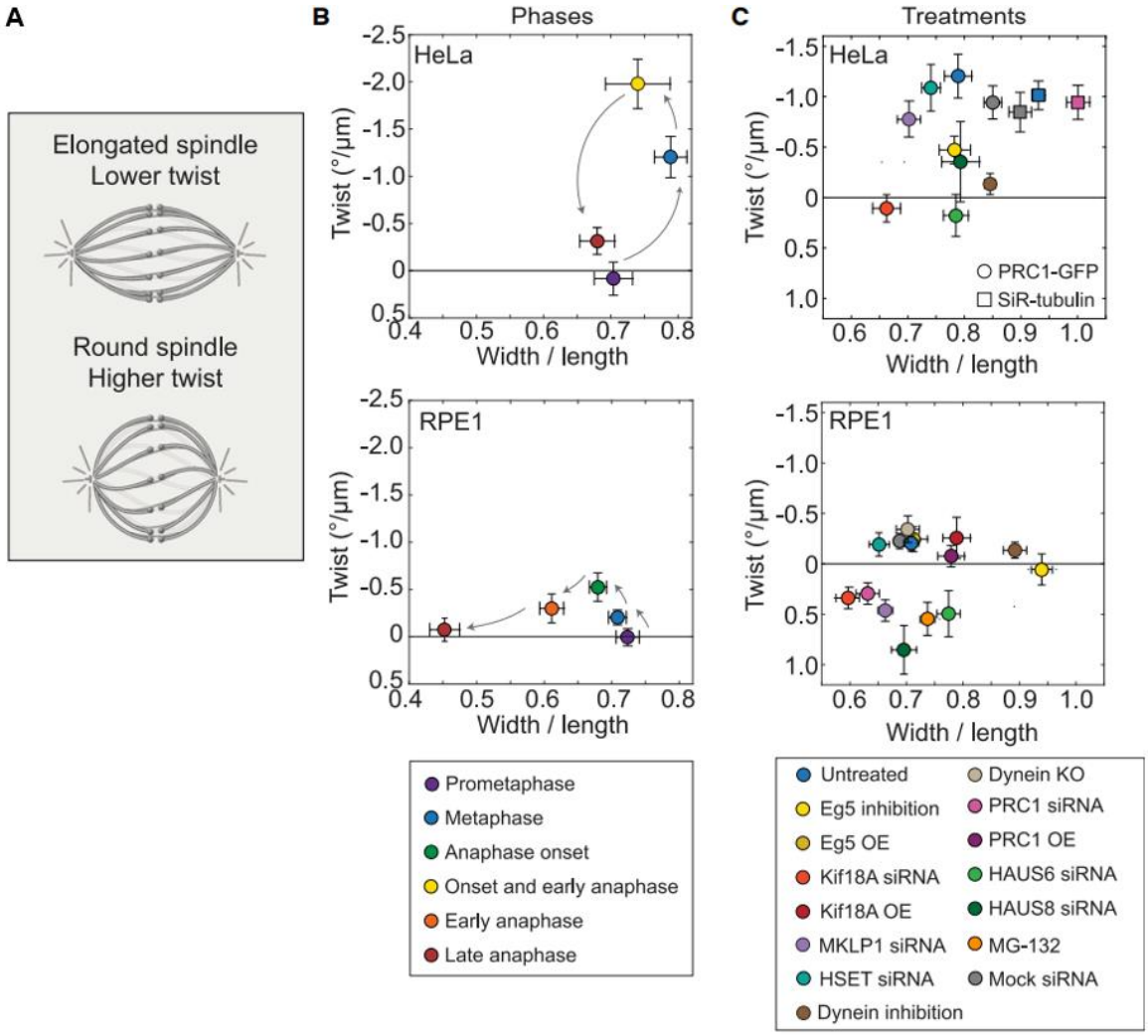

Figure 28. Round spindles have a stronger twist than elongated spindles. A) The scheme depicts the relationship between spindle twist and roundness. **B)** Spindle twist versus width/length ratio in HeLa-Kyoto BAC cells expressing PRC1-GFP (top) and hTERT-RPE1 cells expressing CENP-A-GFP and centrin1-GFP (bottom) over different phases of mitosis, as indicated in the legend; the error bars represent SEM; the arrows indicate progression of mitosis. The same data were used in Figure 23. **C)** Spindle twist versus width/length ratio after perturbations of spindle-associated proteins, as indicated in the legend, the error bars represent SEM. The same data were used in Figures 26 and 27. For HeLa cells, the experiments were performed on HeLa-Kyoto BAC cells expressing PRC1-GFP (circles) and non-transfected HeLa cells stained with SiR-tubulin (rectangles); data was obtained with the help of Barbara Kokanović. For RPE1 cells, hTERT-RPE1 cells expressing CENP-A-GFP and centrin1-GFP were used, with the exception of RPE1 inducible CRISPR/Cas9 DYNC1H1 knockout cells in the case of ‘‘Dynein KO.’’

4.5. Spindle compression of RPE1 cells in horizontal orientation causes spindle midzone widening

The biological role of spindle chirality is still unknown. Although chirality may be simply a side effect of the activity of torque generating motors, the twisted shapes of microtubule bundles may contribute to spindle physiology by allowing changes of spindle shape as a mechanical response to external forces. To test this idea, in our recent study (Trupinic et al., 2022) we gently compressed vertically oriented HeLa cell spindles in metaphase along the pole-to-pole axis for 1.5 min (Figure S1A). We used the bundle tracing method to measure spindle twist (Ivec et al., 2021), which allowed us to graphically reconstruct spindles from the end-on view and side view (Figure S1B). Traces of the microtubule bundles in the end-on view after 1 min of compression were more rounded than before compression, indicating an increase in twist, and the mitotic spindle shortened (Figures S1B and S1C). Spindle shortening was used as a measure to confirm successful compression. Spindle width increased after compression in some cases, but overall, this change was not significant (Figure S1D). Interestingly, compression resulted in a 2.3-fold increase of the left-handed spindle twist (Figure S1E). We were unable to detect changes in microtubule bundle curvature after compression (Figures S1G), which is consistent with the non-significant change in spindle width. Thus, as the spindle was compressed end-on by an external force, which resulted in spindle shortening, the microtubule bundles did not shorten substantially but instead became more twisted. These results support the idea that the twist within the bundles allows for a mechanical response to external forces.

Unlike in HeLa cells, in RPE1 cells spindles do not often exist in the naturally vertical orientation (end-on view). For this reason, I could not perform experiments with the spindle compression along the pole-to-pole axis, as we did on HeLa cells (Trupinic et al., 2022). Nevertheless, I compressed horizontal spindles in RPE1 with the idea to measure spindle parameters, e.g. spindle length, width, height, curvature length and twist (Figure 29). In compressed spindles, in this manner, it was not possible to measure twist as spindles were flattened from height 10.64 ± 0.35 μm to 5.89 ± 0.45 μm (spindle height is measured in the z-axis of a horizontal spindle; Figure 29B). This caused undistinguishable signal of microtubule bundles which was not suitable to measure twist with either optical flow or bundle tracing method. I still measured spindle length which did not change (from 13.62 ± 0.43 μm to 13.78 ± 0.50 μm; Figure

29C) during compression that lasted ~2 min. On the other hand, during that time spindle midzones widened from 9.25 ± 0.19 to 12.50 ± 0.43 μm (Figure 29D), which means that the width expansion of spindle is a passive mechanical process. These results perfectly correlate with the study which showed spindles' reaction after the mechanical compression, done in Dumont lab (Dumont and Mitchison, 2009a). Expectedly, curvature length (lengths of outermost bundles in the spindle, measured from pole to pole) was also larger when spindles were compressed (from 17.38 ± 0.46 to 19.62 ± 0.54 μm; Figure 29E). All changes were reversible, meaning that right after the compression (~1 min after the ending of manipulation) all spindle parameters mostly returned close to their original state (Figures 29A-E). Analyzed data were taken only for the healthy cells that were able to enter anaphase after the manipulation. Next step in this research will question whether spindle width expands purely because of the properties of microtubule bundles, or if and how much condensed chromosomes play a role in this process by crowding the space inside the spindle. Also, it will be interesting to investigate about the role of centrosomes at the poles in this process.

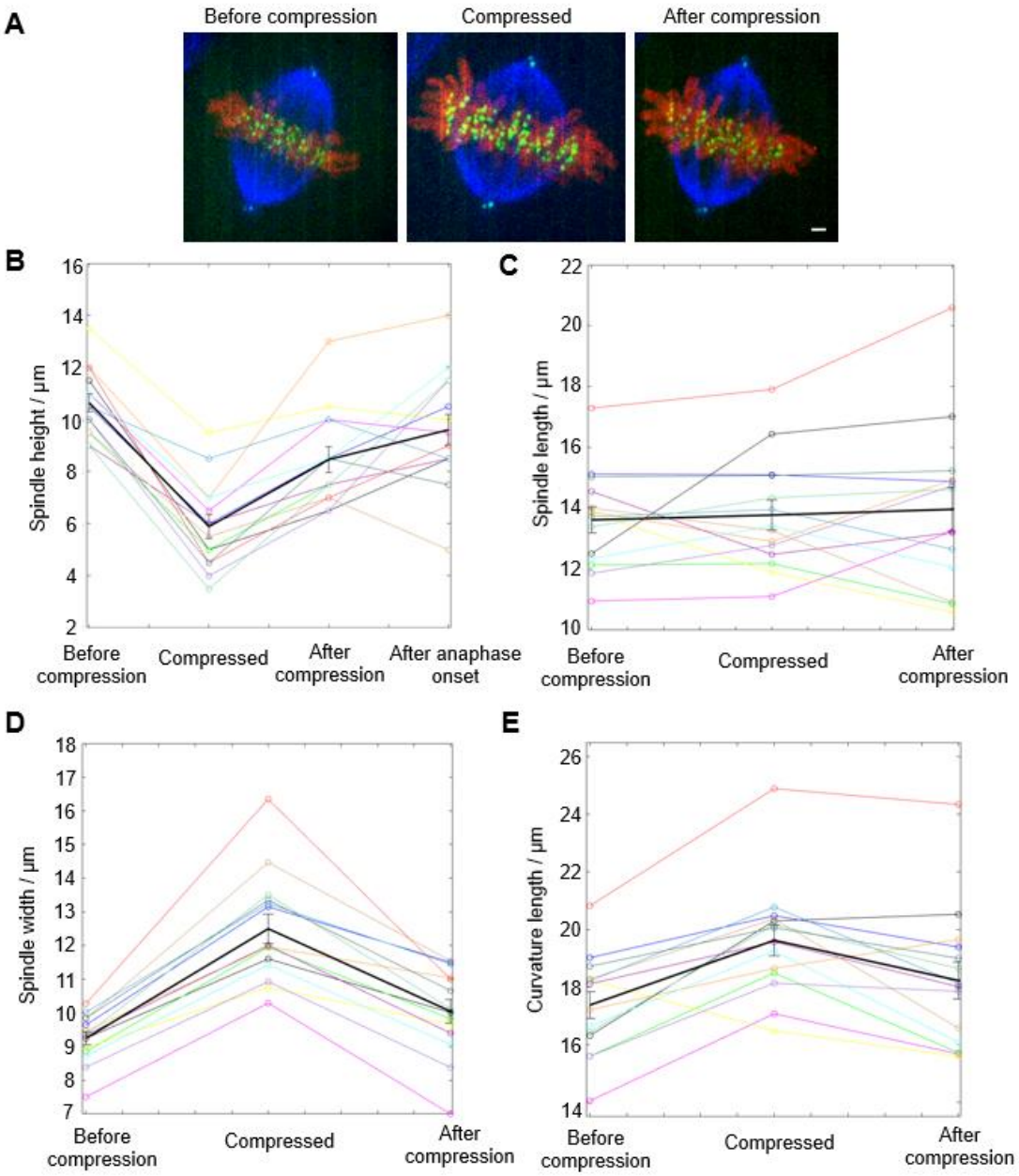

Figure 29. Spindle height, length, width and curvature length measured after the spindle compression by an external force in RPE1 cells. A) Images of spindles in hTERT-RPE1 cells expressing CENP-AGFP and centrin1-GFP before compression (left), during compression (middle) and after compression (right); SiR-tub is shown in blue, kinetochores and centrosomes in green and chromosomes in red. Scale bar 1 µm. **B)-E)** Geometry of spindles in cells described in A) before, during and after compression, with the exception in B) where additional time point is shown after cells entered anaphase. Each color represents one cell. Thick black line represents

average value. Error bars represent SEM. **B)** Spindle height. **C)** Spindle length. **D)** Spindle width. **E)** Curvature length of outermost microtubule bundles in the spindle.

4.6. The *Naegleria* spindle is twisted in a right-handed fashion

In order to explore whether other species have twisted mitotic spindles, or if it is only a human characteristic, we used an opportunity to work on amoeba's spindles. The single-celled eukaryote *Naegleria gruberi*, which diverged from the "yeast-to-human" lineage over a billion years ago, has the peculiar capacity to distinguish between a crawling amoeba and a swimming flagellate (Fulton, 1970). While some organisms disassemble the nuclear envelope to allow for microtubule-chromosome interaction (open mitosis), other organisms nucleate microtubules in the cytoplasm that pass through openings in the nuclear envelope to interact with chromosomes (semi-open mitosis), or, like *Naegleria*, assemble microtubules inside an intact nuclear envelope (closed mitosis) (Walsh, 2012). The *Naegleria* spindle's architecture is quite unusual; it is barrel-shaped, lacks clear microtubule-organizing centers, and homologs of numerous proteins seen in typical kinetochores (Fulton and Dingle, 1971; Schuster, 1975). Interphase *Naegleria* amoebae do not exhibit detectable microtubules or tubulin transcripts, in contrast to other eukaryotes, as shown by immunofluorescence or electron microscopy. However, the nucleus of *Naegleria* does build microtubules for closed mitosis (Fulton and Dingle, 1971; Schuster, 1975; Walsh, 2012).

In a collaboration with our colleagues from the University of Massachusetts, Amherst, USA and theoretical physicist from the Faculty of Science, University of Zagreb, we analyzed microscope images of mitotic spindles in this amoeba. The 3D reconstructions of vertically oriented amoeba spindles revealed that the microtubule bundles curved and appeared to twist from one end of the spindle to the other (Figure 30A). To quantify the degree of twist in the *Naegleria* spindle, I used bundle tracing method to trace individual metaphase bundles (Figure 30A) and then their curvature and twist was measured by oblique circle method. The resulting data show that microtubule bundles in the *Naegleria* spindle are curved ($0.146 \pm 0.009/\mu m$, Figures 30B and 30E) and twisted ($0.873° \pm 0.316°/\mu m$; Figures 30C and 30F), with shorter bundles having more curve and twist than longer bundles (Figures 30E and 30F). I corroborated this result by visual assessment of the handedness of the spindle twist and found a mixture of left- and right-handed twist, with the majority of spindles showing a strong right-handed twist (Figure 30G). Analyzing

early metaphase (Stage II, defined for this analysis as cells with <20 bundles) separate from late metaphase (Stage III, cells with >20 bundles) suggests that bundles increase in length and decrease in curvature during metaphase (Figures 30B and 30D). Right-handed twist was more often found in both vertically and horizontally oriented spindles and for cells in early and late metaphase (Figure 30G), suggesting that the handedness of spindle twist does not depend on mitotic stage or spindle orientation during imaging. The microtubule bundles of the *Naegleria* spindle are less curved than those of HeLa cells, as the radius of curvature is larger for *Naegleria*, 6.9 ± 0.4 μm, than for the outermost bundles in HeLa cells, 5.1 ± 0.3 μm (Stimac et al., 2022). Moreover, the radius of curvature normalized to the spindle half-length, which is equal to 1 for bundles shaped as a semicircle, is 1.26 ± 0.05 for *Naegleria* and 0.90 ± 0.05 for HeLa cells (Stimac et al., 2022), also indicating a smaller curvature of *Naegleria* spindles. In line with the smaller curvature, the absolute value of the average spindle twist in *Naegleria* is smaller than in HeLa cells, 0.9° ± 0.3°/μm in *Naegleria* versus 2°/μm in HeLa (Novak et al., 2018). The twist of *Naegleria* spindles is visually more obvious than in HeLa cells due to the smaller number of microtubule bundles, which are well defined and have a uniform shape, in contrast to the less ordered distribution and shapes of bundles in HeLa cells. Together, these data indicate that the microtubule bundles that comprise the *Naegleria* spindle are physically linked and under rotational forces.

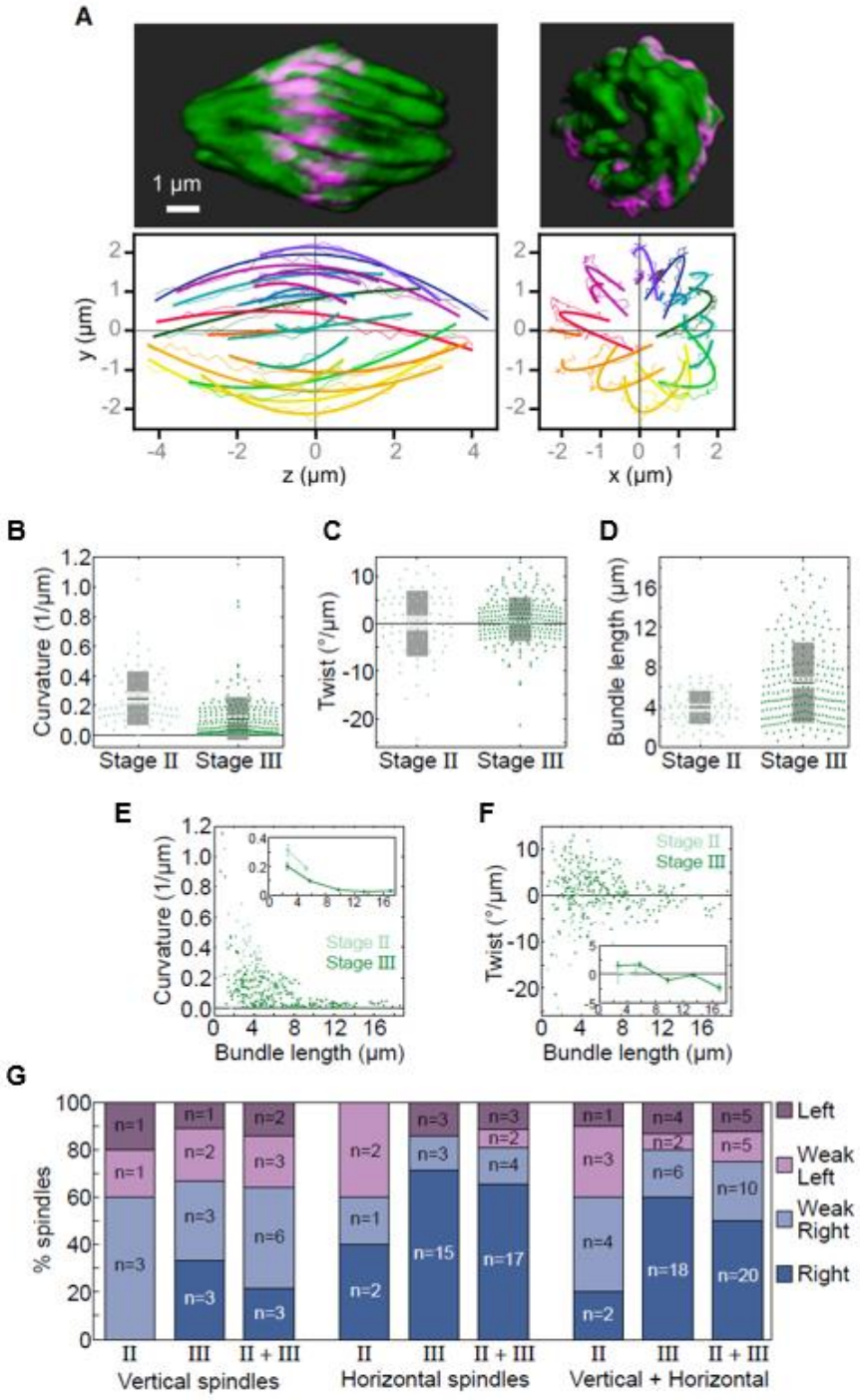

Figure 30. ***Naegleria*** **mitotic spindles are curved and twisted in a right-handed fashion. A)** 3D reconstructed spindle is shown from side and end-on view. Microtubules are shown in green, and DNA is in magenta. Microtubule bundles were quantified from the side view (left graph) and end-on view (right graph). Each bundle is represented by a different color, thin lines mark the manually traced points along the bundle, and thick lines show circular arcs of the fitted circles. **B-**

F) Geometry of microtubule bundles from vertically oriented spindles (standing perpendicular to the coverslip) in Stage II (light green) and Stage III (dark green) of mitosis, analyzed as shown in A). **B)** Curvatures of microtubule bundles. **C)** Twists of microtubule bundles. The mean twist is different from 0 at stage III (p=0.0003), but not so at Stage II (p=0.94). **D)** Microtubule bundle length. **E)** Curvature of microtubule bundles as a function of bundle length. **F)** Twist of microtubule bundles as a function of bundle length. In B-F, the black line shows the mean; the light and dark grey areas mark 95% confidence interval on the mean and standard deviation, respectively. In E) and F), insets show mean of the binned data, with error bars representing SEM. n = 75 bundles (light green dots) from 5 spindles in Stage II and 226 bundles (dark green dots) from 9 spindles in Stage III. **G)** Percentage of spindles showing left, right, weak left or weak right twist. Spindles are grouped according to the stage of mitosis (II, early metaphase or III, late metaphase) and their orientation (vertical or horizontal), as indicated. Adapted from (Velle et al., 2022).

4.6.1. Oblique circle method for measuring the curvature and twist of mitotic spindle

For our recent studies on ameoba, we introduced an oblique circle method developed by the theoretical physicist from the Department of Physics, Faculty of Science, University of Zagreb (Ivec et al., 2021). In order to precisely measure spindle twist in amoeba, we had to modify or re-develop our method, as compared to the one used in previous study from our group published in (Novak et al., 2018). Like mentioned above, amoeba spindles greatly differentiate from human spindles so new approach in spindle twist measurement was necessary.

To extract the information about the shape of a microtubule bundles from traced experimental data, we consider the bundle as a part of a circular arc. This description allows us to faithfully represent the microtubule bundle and extract the relevant geometrical information, i.e., the curvature and the twist, but it is also simple enough to be done systematically on a wide variety of microtubule bundles by fitting a plane to the points representing the bundle and a circle that lies in this plane to the same points. From these fits, the curvature of the bundle is calculated as one over the radius, and the twist is calculated as the angle between the fitted plane and the z-axis divided by the mean distance of the points from the z-axis (Figure 22A, right).

Each bundle is traced through all z-planes in the direction from left centrosome toward the right centrosome (the left centrosome represents the bottom z-plane, and the right centrosome represents the highest tracked z-plane in the stack). The positions of the centrosomes are the starting and end points of the spindle with the left centrosome as the starting data point, and the right centrosome as the ending data point. The z-plane refers to the imaging plane, which is converted to its corresponding z-coordinate by multiplying with the distance between successive planes set during microscope imaging.

During imaging, spindles have an arbitrary orientation with the respect to the laboratory coordinate system. To make traces of microtubule bundles suitable for analysis, the laboratory coordinate system is transformed in a way that the left centrosome is positioned at the origin of the new coordinate system and the right centrosome is positioned on the z-axis (Figure 31A); we can now referee to it as the spindle coordinate system. In this method, curvature and twist, which measure the extent the bundles extend along curved paths in three dimensions, are the geometrical quantities that represent the information about the bundle shapes. To obtain these quantities from the experimental traces, a circular arc extending through three dimensions is fitted to these data. A circle is fitted to the data by choosing only from those circles that lie in the bundle plane. The projection of the traced bundle points onto the bundle plane is calculated and a circular arc is fitted to them (Figure 31B). The fitting parameters are the radius of the circle, and the position of the circle center. These parameters, together with the normal vector of the bundle plane, determine the geometry of our traced bundles. Based on the fitting parameters, we can determine the curvature and twist of the microtubule bundles.

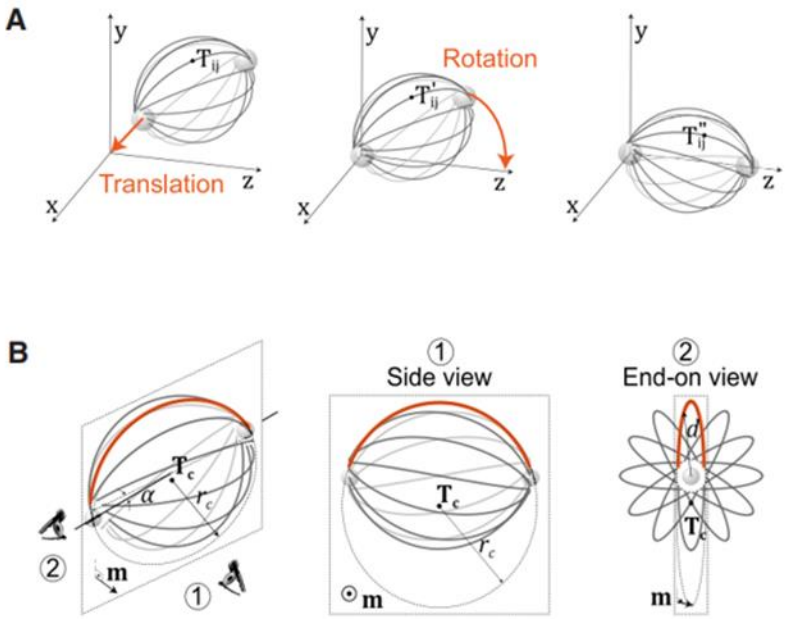

Figure 31. **Overview of method**. **A)** The spindle, along with the centrosomes and the marked traced bundle point Tij, is positioned at an arbitrary position from the origin of the coordinate system (left). The spindle is translated so that the left centrosome is located at the origin of the coordinate system (middle). The spindle is rotated so that the pole-to-pole axis, along with the right centrosome, aligns with the z-axis of the coordinate system (right). **B)** A view of the spindle from an arbitrary angle (left) where the eyes show the viewing angle for the side view (1) and the end-on view (2), which are shown in the middle and on the right, respectively. A microtubule bundle (orange curved line) is fitted by a circle of radius rc. The angle between the central spindle axis (solid line) and the plane in which the fitted circle lies (dashed parallelogram) is denoted. Adapted from (Ivec et al., 2021).

5. DISCUSSION

Given that chirality is present in everything around us, it is not too hard to imagine that some cell structures could also be chiral, as we now know to be true for the mitotic spindle (Novak et al., 2018). The human mitotic spindle's chiral form, which is seen in the left-handed twist of microtubule bundles, suggests that torques act inside the spindle. The torques within microtubule bundles, which are reflected in the spindle twist, are regulated by biomechanical and molecular mechanisms that were shown in this thesis. Here, it was demonstrated that spindle twist is controlled by forces inside or outside the spindle from a biomechanical perspective (Figure 32A, box 1).

Work done for this thesis includes the discovery of numerous molecular players involved in the control of spindle chirality by conducting a candidate screen in which motor proteins that step in a chiral fashion were disrupted, along with the other microtubule-associated proteins. In line with earlier discoveries from my group on HeLa cells (Novak et al., 2018), Eg5 inactivation produced no twist in RPE1 cells. Kif18A depletion resulted in a change from left-handed to right-handed twist in RPE1 cells. When these proteins were overexpressed, the twist remained the same. A change to a right-handed twist was also produced by the depletion of MKLP1 in RPE1 cells. All three motors are known to produce torques on microtubules *in vitro* (Bormuth et al., 2012; Maruyama et al., 2021; Mitra et al., 2018; Yajima et al., 2008), and are found within the antiparallel overlaps of bridging microtubules in the spindle (Jagric et al., 2021; Kajtez et al., 2016; Mann and Wadsworth, 2018). Therefore, the proposition is that they produce the twisted shape of the bundle by rotating the bundle's antiparallel microtubules around one another (Figure 32A, box 2). Given that Eg5 is most prominently localized in the spindle pole region (Kajtez et al., 2016; Mann and Wadsworth, 2018) (Figure 32A, box 3), it is possible that it can also contribute to spindle twist by acting there. In this situation, Eg5 might crosslink parallel microtubules (Valentine et al., 2006; Walczak et al., 1998), preventing them from freely rotating inside the bundle and promoting the buildup of torsional tensions, but it might also actively produce torques. Additionally, dynein acts through microtubule rotation close to the spindle pole. In HeLa cells, inhibition of dynein abolished the spindle twist (Trupinic et al., 2022). Cytoplasmic dynein shows a bidirectional helical motility that can generate torque in either direction, but prefers right-directed movement (Can et al., 2014). Thus, its net torque generation may also influence spindle twist (Figure 32A,

box 3). Also, other motors localized at the pole, like the kinesin-13 family members Kif2a (Jang et al., 2008) and Kif2c/MCAK (Ganguly et al., 2008), may cause spindle twist by rotating the microtubules in relation to the spindle pole (Figure 32A, box 3).

Interestingly, depletion of the HAUS6 and HAUS8 subunits of the augmin complex, which promotes nucleation of new microtubules from the wall of existing microtubules (David et al., 2019; Goshima et al., 2008; Uehara et al., 2009), resulted in the biggest effect on spindle twist. In RPE1 cells, spindles acquired a right-handed twist as a result of these depletions. The proposition is that the changed twist is connected to the diminished antiparallel overlaps (Stimac et al., 2022), where torque-generating motors like Eg5, Kif18A, and MKLP1 bind, because augmin depletion decreases the microtubule quantity within bridging fibers (Figure 32A, box 2). In addition, because augmin initiates new microtubules at an angle to the old microtubule's wall (Kamasaki et al., 2013; Petry et al., 2013), it is tempting to hypothesize that if the new microtubules spiral around the old microtubules, this might cause the entire microtubule bundle to twist.

RPE1 cells' spindles changed twist direction or did not twist when PRC1, the crosslinker of antiparallel microtubules, was depleted or overexpressed. Despite the fact that the effects were confusing, the hypothesis would be that in a metaphase spindle, the microtubules crosslinked by PRC1 cannot rotate freely within the bundle (Figure 32A, box 2), leading to the accumulation of torsional stresses, even though the overall bundle's torsional rigidity is low enough to permit twisting. In contrast, the increased quantity of PRC1-bundled microtubules in late anaphase, when PRC1 is relatively abundant on midzone microtubules, or upon PRC1 overexpression in metaphase, may enhance the torsional rigidity of the entire bundle and make it more difficult to twist.

The spindle twist is also influenced by metaphase duration. Right-handed twist was produced when RPE1 cells were arrested during metaphase, which was comparable to Kif18A or the augmin complex depletion. It's interesting to note that these depletions also extend metaphase (Stumpff et al., 2008; Uehara et al., 2009), which would explain the observed influence on twist.

The change from left-handed to right-handed twisting suggests that there are conflicting mechanisms that encourage twist in the two opposite directions. The equilibrium could be tipped one way or the other by different protein perturbations. In contrast to metaphase, twist is largely absent in spindles during anaphase. A recent study demonstrated that coupled Eg5 inhibition and NuMa depletion caused substantial left-handed twist during anaphase in RPE1 cells (Neahring et

al., 2021), indicating that opposing motors are necessary to prevent twisting in the anaphase spindle. It is possible that the mentioned molecular players encourage left-handed twist because all of the several molecular perturbations utilized in this thesis modified the twist in the same direction, toward larger positive values. As a result, the assumption was made that the right-handed twist may result from the activity of microtubule-associated proteins that preformed candidate screen did not include. The twist of a microtubule bundles may also be influenced by the helical structure of the microtubule lattice itself (Amos and Hirose, 2007).

Round spindles are more twisted than elongated ones during metaphase in HeLa cells (Trupinic et al., 2022). This is supported by the fact that HeLa cell spindles are rounder and more twisted during metaphase and the early stages of anaphase than they are during prometaphase and late anaphase, when the spindles are elongated and twist is entirely gone. The twist is weaker and unrelated to the width/length ratio in RPE1 spindles, which are generally more elongated than HeLa spindles. Therefore, the same molecular processes that result in rounder spindles and larger bending moments may also result in stronger twists of the microtubule bundles. It's intriguing to note that spindles, which are intricate and dynamic structures, exhibit a relationship between twisting and bending that is comparable to those of straightforward systems from classical beam mechanics (Landau et al., 1986).

In order to explore whether other species have twisted mitotic spindles, or if it is only a human characteristic, we used an opportunity to work on amoeba's spindles. Spindles in the amoeba *Naegleria gruberi* are twisted in a right-handed manner as opposed to the left-handed twist of human spindles, which may be because kinesins and other microtubule-associated proteins differ between *Naegleria* and humans. The lack of augmin complex subunit homologs in *Naegleria* (Fritz-Laylin et al., 2010) is consistent with the right-handed twist of spindles in this amoeba and in augmin-depleted RPE1 cells. It is possible that mitotic motor-generated torque also contributes to *Naegleria* spindle twist. The previous transcriptional analyses of *Naegleria* differentiation (Fritz-Laylin and Cande, 2010) was examined, in support of this hypothesis, and discovered a number of kinesins whose expression was up to 8-fold enriched in asynchronously dividing amoebae compared to non-dividing flagellates, including homologs of spindle-associated kinesin-5 and kinesin-14 (Velle et al., 2022). Future research will be interesting in determining what factors affect the direction and degree of twist in microtubules of various organisms and whether there are any common factors.

In order to precisely calculate the twist of *Naegleria* spindles, a new oblique circle method was developed (Ivec et al., 2021) that has the advantage of being more robust and applicable to a greater variety of microtubule bundles, as compared to method used in the previous work from my group (Novak et al., 2018). Previously, twist was calculated for short bundles, calculating twist for finite segments using only the starting and ending points of the bundle, whereas bundle data points close to the poles and entire bundles close to the pole-to-pole axis were excluded. With new oblique circle method, twist is calculated by utilizing all data points, including those with longer bundle segments and bundles closer to the pole-to-pole axis. Fitting the simple shape of a circular arc is a straightforward approach to extract the most important geometrical parameters from the data obtained from confocal microscopy, namely from microtubule bundles that have a low number of data points and make less than one helical turn.

Although spindle twist may be simply a side-effect of the action of motors that generate torque, the twisted shapes of microtubule bundles may contribute to spindle function. In contrast to metaphase, during late anaphase, the spindle is not twisted as the bundles lose their twist and become straight. This straightening is likely due to the accumulation of PRC1 and also other midzone proteins within these bundles. Here it is tempting to hypothesize that the spindle in late anaphase benefits from the straight bundles to enable force transfer from the central overlap region to the poles, move the chromosomes apart, and maintain their separation (Figure 32B, bottom). Spindle twist may also encourage the physical separation of neighboring bundles during prometaphase or aid in the beginning of spindle elongation at the beginning of anaphase by releasing elastic energy from the twisted bundles. It's interesting to note that chromosome segregation faults can be linked to variations in twist, according to a recent study (Neahring et al., 2021). Thus, it is yet unknown how crucial twist regulation may be for the accuracy of chromosome segregation.

Additionally, recently we showed that the built-in twist helps the spindle to respond to external forces and reduces the risk of spindle breakage under high load (Trupinic et al., 2022). In that study, we performed experiments in which we compressed the spindle along the pole-to-pole axis and noticed an increase in twist as the spindle shortened, while the contour length of microtubule bundles remained largely unchanged. This means that a twisted spindle can swiftly shrink when subjected to compressive forces by tightening it up like an elastic spring would by increasing the twist (Figure 32B, top). In contrast to non-twisted spindles, this response does not

necessitate depolymerization of microtubules during spindle shortening. On the other hand, compression of horizontal spindles can also give us an insight in how spindles maintain their shape. For example, round spindles in this thesis were shown to have larger twists. The hypothesis is that if spindle has more chromosomes, for example in tumor cells, spindles are rounder and have larger twists, which was seen in examples of HeLa cells versus RPE1 cells. To confirm this, additional experiments are needed in which more types of spindles with different number of chromosomes would be analyzed.

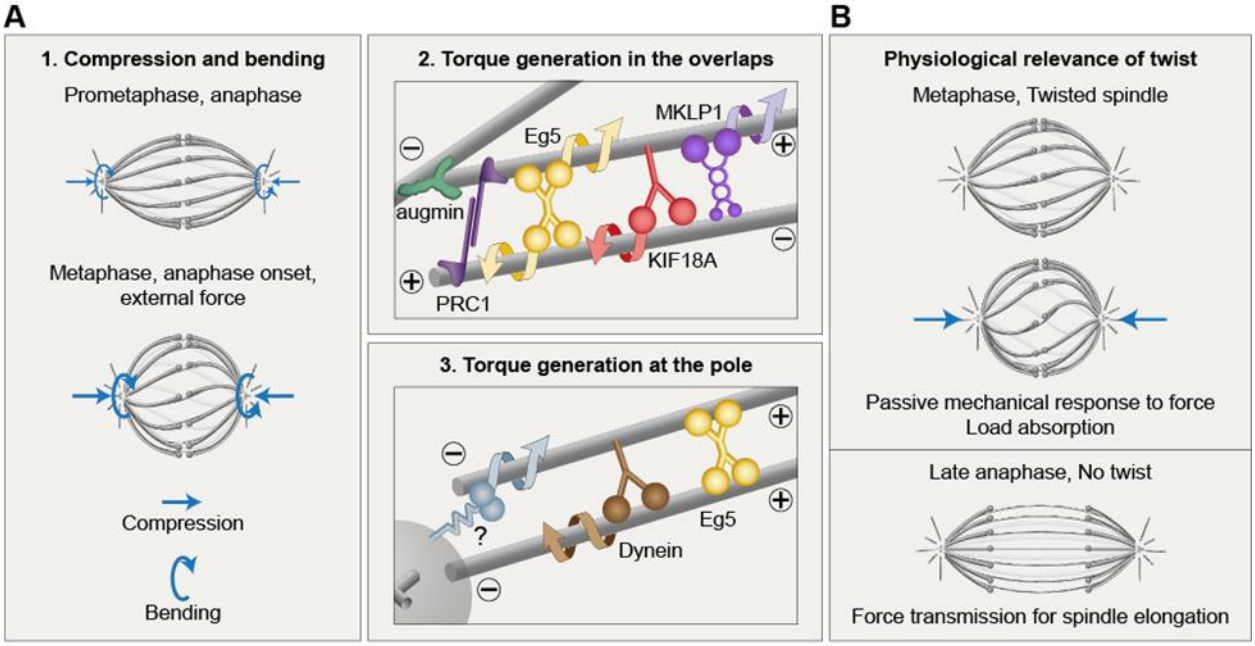

Figure 32. Biomechanical and molecular origins of spindle twist and its biological role. A) Forces regulate twist (box 1). Round spindles or those compressed by external forces (blue straight arrows) are more twisted than elongated ones, suggesting that larger bending moments (blue curved arrows) are correlated with larger twist. Within the antiparallel overlaps of bridging microtubules (box 2), Eg5, Kif18A, and MKLP1 rotate the microtubules around one another, whereas crosslinking by PRC1 constrains the free rotation of microtubules within the bundle, allowing for accumulation of torsional stresses. Augmin contributes to the twist by nucleating bridging microtubules. At the spindle pole (box 3), Eg5 crosslinks parallel microtubules, which may prevent their free rotation. Eg5 and other motors (question mark) may rotate the microtubules around the pole. Dynein contributes to torque generation by moving in a minus-end directed helical manner. **B)** Spindle twist allows for a mechanical response to external forces by absorbing load during metaphase (top). In contrast, in late anaphase twist is absent, which promotes force transmission for spindle elongation and maintenance of chromosome separation (bottom).

6. CONCLUSION

Mitotic spindle is an irreplaceable cell structure responsible for the most important process during mitosis – division of genetic material. Therefore, mitotic spindle must function perfectly in order to equally divide the identical copies of chromosomes in both daughter cells. Spindles in human somatic cells have a complex architecture in which numerous microtubule bundles are organized in a recognizable spindle-shaped structure. Shape of the spindle is generated by forces within.

Relevant to this thesis, the most interesting discovery was the chirality of the mitotic spindle, i.e. microtubule bundles in the spindle have a left-handed helical rotation, or twist (Novak et al., 2018). It was also shown that motor protein Eg5, due to rotational forces, generates twist of the spindle, but it was not clear whether it is solely responsible for this architecture. Other motor proteins present at the spindle are known to also exert rotational forces – these proteins were candidates for this thesis. Here, it was shown that, in addition to Eg5, motor proteins Kif18A, MKLP1 and dynein regulate spindle twist in RPE1 cells. Interestingly, depletion of Kif18A, or MKLP1, caused spindles to switch from left-handed twist to right-handed twist in RPE1 cells. We speculate that mechanism by which these proteins produce twist is by rotating the bundle's antiparallel microtubules around one another. Additionally, Eg5 and dynein, localized mostly at spindle poles, may contribute in bundle twisting by crosslinking parallel microtubules and preventing them from freely rotating inside the bundle and promoting the buildup of torsional tensions, or by actively producing torques, respectively. Augmin complex and PRC1 also have a role in generating spindle twist, as their depletions cause switch in the twist direction, or loss of twist, respectively. Depletion of augmin or PRC1 leads to the weaker bridging fibers which, consequently, lead to the change in spindle architecture and twist. On the other hand, overexpression of PRC1 causes thick, rigid bridging fibers and leads to the loss of spindle twist. The observed switch of the direction of twist from left-handed to right-handed indicates the existence of competing mechanisms promoting a twist in the opposite directions. HeLa spindles have a stronger left-handed twist than RPE1 spindles have, and protein depletions that led to zero twist in HeLa cells largely resulted in a right-handed twist in RPE1 cells (Trupinic et al., 2022); thus, the twist changed in both cell lines by a similar amount. This implies that torques are regulated by similar mechanisms in both cell lines, but the torque balance is shifted more toward the formation of left-handed twist in HeLa than in RPE1 spindles. All the diverse molecular

perturbations used here tuned the twist toward more positive values, suggesting that the corresponding molecular players promote a left-handed twist.

Rounder spindles have more pronounced twist, as it is the case for round spindles in HeLa cells, while more elongated spindles in RPE1 cells have lower twist values. This shows a clear relationship between twisting and bending. Hypothesis for the biological role of spindle twist is that it protects the spindle from breaking under the external forces, which was seen in larger twists when spindles were compressed in pole-to-pole direction (Trupinic et al., 2022).

Other than human cells, another organisms' spindles showed a tendency to twist. As compared to human cells, spindles of amoeba *Naegleria gruberi* predominately twist in a right-handed fashion. Speculation is that this is because of the evolutionary differences between proteomes in these two species, e.g. *Naegleria* does not have a homologue to augmin complex.

Overall, I anticipate that the findings presented here will spur innovative new research into the molecular causes of rotational forces in the spindle and their biological functions.

7. REFERENCES

Quantum Diaries, 19 June 2016. Helicity, chirality, mass, and the Higgs. *Quantum Diaries*. Retrieved 4 January 2023.

Akhmanova, A., and M.O. Steinmetz. 2008. Tracking the ends: a dynamic protein network controls the fate of microtubule tips. *Nat Rev Mol Cell Biol*. 9:309-322.

Al-Bassam, J., and F. Chang. 2011. Regulation of microtubule dynamics by TOG-domain proteins XMAP215/Dis1 and CLASP. *Trends Cell Biol*. 21:604-614.

Alberts, B., A. Johnson, J. Lewis, D. Morgan, M.C. Raff, K. Roberts, P. Walter, J.H. Wilson, and T. Hunt. 2014. Molecular biology of the cell. *W.W Norton & Company, New York*. 6th Edition.

Alfaro-Aco, R., and S. Petry. 2015. Building the Microtubule Cytoskeleton Piece by Piece. *J Biol Chem*. 290:17154-17162.

Amos, L.A., and K. Hirose. 2007. Studying the structure of microtubules by electron microscopy. *Methods Mol Med*. 137:65-91.

Asbury, C.L. 2017. Anaphase A: Disassembling Microtubules Move Chromosomes toward Spindle Poles. *Biology (Basel)*. 6.

Barisic, M., R. Silva e Sousa, S.K. Tripathy, M.M. Magiera, A.V. Zaytsev, A.L. Pereira, C. Janke, E.L. Grishchuk, and H. Maiato. 2015. Mitosis. Microtubule detyrosination guides chromosomes during mitosis. *Science*. 348:799-803.

Barton, N.R., and L.S. Goldstein. 1996. Going mobile: microtubule motors and chromosome segregation. *Proc Natl Acad Sci U S A*. 93:1735-1742.

Bechstedt, S., and G.J. Brouhard. 2013. Motors and MAPs collaborate to size up microtubules. *Dev Cell*. 26:118-120.

Bormuth, V., B. Nitzsche, F. Ruhnow, A. Mitra, M. Storch, B. Rammner, J. Howard, and S. Diez. 2012. The highly processive kinesin-8, Kip3, switches microtubule protofilaments with a bias toward the left. *Biophys J*. 103:L4-6.

Brinkley, B.R., and J. Cartwright, Jr. 1971. Ultrastructural analysis of mitotic spindle elongation in mammalian cells in vitro. Direct microtubule counts. *J Cell Biol*. 50:416-431.

Brouhard, G.J., and L.M. Rice. 2014. The contribution of alphabeta-tubulin curvature to microtubule dynamics. *J Cell Biol*. 207:323-334.

Brouhard, G.J., J.H. Stear, T.L. Noetzel, J. Al-Bassam, K. Kinoshita, S.C. Harrison, J. Howard, and A.A. Hyman. 2008. XMAP215 is a processive microtubule polymerase. *Cell*. 132:79-88.

Brunnbauer, M., R. Dombi, T.H. Ho, M. Schliwa, M. Rief, and Z. Okten. 2012. Torque generation of kinesin motors is governed by the stability of the neck domain. *Mol Cell*. 46:147-158.

Buđa, R., K. Vukusic, and I.M. Tolic. 2017. Dissection and characterization of microtubule bundles in the mitotic spindle using femtosecond laser ablation. *Method Cell Biol*. 139:81-101.

Bugiel, M., E. Bohl, and E. Schaffer. 2015. The Kinesin-8 Kip3 switches protofilaments in a sideward random walk asymmetrically biased by force. *Biophys J*. 108:2019-2027.

Burnham, R.J., W.H.d. Almeida, R.S. Carpanedo, C.M.d. Cruz, A.C.S. Dresch, M. Machiner, L.P. Pinto, R.C.A.d. Oliveira, E.F.d. Santos, and B. Spilka. 2019. Asymmetry in Plants. *CRC Press*. 1st edition.

Can, S., M.A. Dewitt, and A. Yildiz. 2014. Bidirectional helical motility of cytoplasmic dynein around microtubules. *Elife*. 3:e03205.

Cheeseman, I.M., and A. Desai. 2008. Molecular architecture of the kinetochore-microtubule interface. *Nat Rev Mol Cell Biol*. 9:33-46.

Civelekoglu-Scholey, G., and J.M. Scholey. 2010. Mitotic force generators and chromosome segregation. *Cell Mol Life Sci*. 67:2231-2250.

Cooper, G.M., and R.E. Hausman. 2003. The Cell : A Molecular Approach. *Sunderland: Sinauer Associates*. 3rd Edition.

Cross, R.A., and A. McAinsh. 2014. Prime movers: the mechanochemistry of mitotic kinesins. *Nat Rev Mol Cell Biol*. 15:257-271.

David, A.F., P. Roudot, W.R. Legant, E. Betzig, G. Danuser, and D.W. Gerlich. 2019. Augmin accumulation on long-lived microtubules drives amplification and kinetochore-directed growth. *J Cell Biol*. 218:2150-2168.

Dogterom, M., and B. Yurke. 1997. Measurement of the force-velocity relation for growing microtubules. *Science*. 278:856-860.

Downing, K.H., and E. Nogales. 1998. Tubulin and microtubule structure. *Curr Opin Cell Biol*. 10:16-22.

Dumont, S., and T.J. Mitchison. 2009a. Compression regulates mitotic spindle length by a mechanochemical switch at the poles. *Curr Biol*. 19:1086-1095.

Dumont, S., and T.J. Mitchison. 2009b. Force and length in the mitotic spindle. *Curr Biol*. 19:R749-761.

Dumont, S., E.D. Salmon, and T.J. Mitchison. 2012. Deformations within moving kinetochores reveal different sites of active and passive force generation. *Science*. 337:355-358.

Farnebäck, G. 2003. Two-Frame Motion Estimation Based on Polynomial Expansion. Springer Berlin Heidelberg, Berlin, Heidelberg. 363-370.

Fededa, J.P., and D.W. Gerlich. 2012. Molecular control of animal cell cytokinesis. *Nat Cell Biol*. 14:440-447.

Fink, G., L. Hajdo, K.J. Skowronek, C. Reuther, A.A. Kasprzak, and S. Diez. 2009. The mitotic kinesin-14 Ncd drives directional microtubule-microtubule sliding. *Nat Cell Biol*. 11:717-723.

Fritz-Laylin, L.K., and W.Z. Cande. 2010. Ancestral centriole and flagella proteins identified by analysis of Naegleria differentiation. *J Cell Sci*. 123:4024-4031.

Fritz-Laylin, L.K., S.E. Prochnik, M.L. Ginger, J.B. Dacks, M.L. Carpenter, M.C. Field, A. Kuo, A. Paredez, J. Chapman, J. Pham, S. Shu, R. Neupane, M. Cipriano, J. Mancuso, H. Tu, A. Salamov, E. Lindquist, H. Shapiro, S. Lucas, I.V. Grigoriev, W.Z. Cande, C. Fulton, D.S. Rokhsar, and S.C. Dawson. 2010. The genome of Naegleria gruberi illuminates early eukaryotic versatility. *Cell*. 140:631-642.

Fu, J., I.M. Hagan, and D.M. Glover. 2015. The centrosome and its duplication cycle. *Cold Spring Harb Perspect Biol*. 7:a015800.

Fulton, C. 1970. Chapter 13 Amebo-flagellates as research partners: the laboratory biology of Naegleria and Tetramitus. *In Methods in Cell Biology*:341–476.

Fulton, C., and A.D. Dingle. 1971. Basal bodies, but not centrioles, in Naegleria. *J Cell Biol*. 51:826-836.

Furutani, I., Y. Watanabe, R. Prieto, M. Masukawa, K. Suzuki, K. Naoi, S. Thitamadee, T. Shikanai, and T. Hashimoto. 2000. The SPIRAL genes are required for directional control of cell elongation in Aarabidopsis thaliana. *Development*. 127:4443-4453.

Ganguly, A., R. Bhattacharya, and F. Cabral. 2008. Cell cycle dependent degradation of MCAK Evidence against a role in anaphase chromosome movement. *Cell Cycle*. 7:3187-3193.

Gatlin, J.C., and K. Bloom. 2010. Microtubule motors in eukaryotic spindle assembly and maintenance. *Semin Cell Dev Biol*. 21:248-254.

Gittes, F., B. Mickey, J. Nettleton, and J. Howard. 1993. Flexural rigidity of microtubules and actin filaments measured from thermal fluctuations in shape. *J Cell Biol*. 120:923-934.

Glotzer, M. 2009. The 3Ms of central spindle assembly: microtubules, motors and MAPs. *Nat Rev Mol Cell Biol*. 10:9-20.

Godinho, S.A., and D. Pellman. 2014. Causes and consequences of centrosome abnormalities in cancer. *Philos Trans R Soc Lond B Biol Sci*. 369.

Goshima, G., M. Mayer, N. Zhang, N. Stuurman, and R.D. Vale. 2008. Augmin: a protein complex required for centrosome-independent microtubule generation within the spindle. *J Cell Biol*. 181:421-429.

Goshima, G., R. Wollman, S.S. Goodwin, N. Zhang, J.M. Scholey, R.D. Vale, and N. Stuurman. 2007. Genes required for mitotic spindle assembly in Drosophila S2 cells. *Science*. 316:417-421.

Helme, N.E., and H.P. Linder. 1992. Morphology, evolution and taxonomy of *Wachendorfia* (Haemodoraceae). *Bothalia*. 22:a826.

Hochegger, H., S. Takeda, and T. Hunt. 2008. Cyclin-dependent kinases and cell-cycle transitions: does one fit all? *Nat Rev Mol Cell Biol*. 9:910-916.

Hoing, S., T.Y. Yeh, M. Baumann, N.E. Martinez, P. Habenberger, L. Kremer, H.C.A. Drexler, P. Kuchler, P. Reinhardt, A. Choidas, M.L. Zischinsky, G. Zischinsky, S. Nandini, A.P. Ledray, S.A. Ketcham, L. Reinhardt, M. Abo-Rady, M. Glatza, S.J. King, P. Nussbaumer, S. Ziegler, B. Klebl, T.A. Schroer, H.R. Scholer, H. Waldmann, and J. Sterneckert. 2018. Dynarrestin, a Novel Inhibitor of Cytoplasmic Dynein. *Cell Chem Biol*. 25:357-369 e356.

Howard, J. 2001. Mechanics of motor proteins and the cytoskeleton. Sinauer Associates, Sunderland, Mass. xvi, 367 p. pp.

Howard, J., and A.A. Hyman. 2009. Growth, fluctuation and switching at microtubule plus ends. *Nat Rev Mol Cell Biol*. 10:569-574.

Hsia, K.C., E.M. Wilson-Kubalek, A. Dottore, Q. Hao, K.L. Tsai, S. Forth, Y. Shimamoto, R.A. Milligan, and T.M. Kapoor. 2014. Reconstitution of the augmin complex provides insights into its architecture and function. *Nat Cell Biol*. 16:852-863.

Ivec, A., M. Trupinic, I.M. Tolic, and N. Pavin. 2021. Oblique circle method for measuring the curvature and twist of mitotic spindle microtubule bundles. *Biophys J*. 120:3641-3648.

Jagric, M., P. Risteski, J. Martincic, A. Milas, and I.M. Tolic. 2021. Optogenetic control of PRC1 reveals its role in chromosome alignment on the spindle by overlap length-dependent forces. *Elife*. 10:e61170.

Jang, C.Y., J. Wong, J.A. Coppinger, A. Seki, J.R. Yates, 3rd, and G. Fang. 2008. DDA3 recruits microtubule depolymerase Kif2a to spindle poles and controls spindle dynamics and mitotic chromosome movement. *J Cell Biol*. 181:255-267.

Jiang, W., G. Jimenez, N.J. Wells, T.J. Hope, G.M. Wahl, T. Hunter, and R. Fukunaga. 1998. PRC1: a human mitotic spindle-associated CDK substrate protein required for cytokinesis. *Mol Cell*. 2:877-885.

Jin, F., and D.Z. Feng. 2014. Image Registration Algorithm Using Mexican Hat Function-Based Operator and Grouped Feature Matching Strategy. *Plos One*. 9.

Kajtez, J., A. Solomatina, M. Novak, B. Polak, K. Vukusic, J. Rudiger, G. Cojoc, A. Milas, I. Sumanovac Sestak, P. Risteski, F. Tavano, A.H. Klemm, E. Roscioli, J. Welburn, D. Cimini, M. Gluncic, N. Pavin, and I.M. Tolic. 2016. Overlap microtubules link sister k-fibres and balance the forces on bi-oriented kinetochores. *Nat Commun*. 7:10298.

Kamasaki, T., E. O'Toole, S. Kita, M. Osumi, J. Usukura, J.R. McIntosh, and G. Goshima. 2013. Augmin-dependent microtubule nucleation at microtubule walls in the spindle. *J Cell Biol*. 202:25-33.

Kaseda, K., A.D. McAinsh, and R.A. Cross. 2012. Dual pathway spindle assembly increases both the speed and the fidelity of mitosis. *Biol Open*. 1:12-18.

Kelvin, W.T. 1894. The molecular tactics of a crystal. Clarendon Press, Oxford. 59, 51 p. pp.

Kirschner, M., and T. Mitchison. 1986. Beyond self-assembly: from microtubules to morphogenesis. *Cell*. 45:329-342.

Kline-Smith, S.L., and C.E. Walczak. 2002. The microtubule-destabilizing kinesin XKCM1 regulates microtubule dynamic instability in cells. *Mol Biol Cell*. 13:2718-2731.

Knouse, K.A., T. Davoli, S.J. Elledge, and A. Amon. 2017. Aneuploidy in Cancer: Seq-ing Answers to Old Questions. *Annu Rev Canc Biol*. 1:335-354.

Landau, L.D., E.M. Lifshitz, A.M. Kosevich, J.B. Sykes, L.P. Pitaevskii, and W.H. Reid. 1986. Theory of Elasticity: Volume 7. Elsevier Science.

Lawo, S., M. Bashkurov, M. Mullin, M.G. Ferreria, R. Kittler, B. Habermann, A. Tagliaferro, I. Poser, J.R. Hutchins, B. Hegemann, D. Pinchev, F. Buchholz, J.M. Peters, A.A. Hyman, A.C. Gingras, and L. Pelletier. 2009. HAUS, the 8-subunit human Augmin complex, regulates centrosome and spindle integrity. *Curr Biol*. 19:816-826.

Lodish, H., C.A. Kaiser, A. Bretscher, A. Amon, A. Berk, M. Krieger, H. Ploegh, and M.P. Scott. 2014. Molecular cell biology. *W. H. Freeman and Company, New York*. 7th Edition.

Lowe, D.G. 2004. Distinctive image features from scale-invariant keypoints. *Int J Comput Vision*. 60:91-110.

Luders, J., and T. Stearns. 2007. Microtubule-organizing centres: a re-evaluation. *Nat Rev Mol Cell Biol*. 8:161-167.

Magidson, V., C.B. O'Connell, J. Loncarek, R. Paul, A. Mogilner, and A. Khodjakov. 2011. The spatial arrangement of chromosomes during prometaphase facilitates spindle assembly. *Cell*. 146:555-567.

Maiato, H., A.M. Gomes, F. Sousa, and M. Barisic. 2017. Mechanisms of Chromosome Congression during Mitosis. *Biology (Basel)*. 6.

Maney, T., M. Wagenbach, and L. Wordeman. 2001. Molecular dissection of the microtubule depolymerizing activity of mitotic centromere-associated kinesin. *J Biol Chem*. 276:34753-34758.

Mann, B.J., and P. Wadsworth. 2018. Distribution of Eg5 and TPX2 in mitosis: Insight from CRISPR tagged cells. *Cytoskeleton (Hoboken)*. 75:508-521.

Marques, S., J. Fonseca, P.M. Silva, and H. Bousbaa. 2015. Targeting the spindle assembly checkpoint for breast cancer treatment. *Curr Cancer Drug Targets*. 15:272-281.

Maruyama, Y., M. Sugawa, S. Yamaguchi, T. Davies, T. Osaki, T. Kobayashi, M. Yamagishi, S. Takeuchi, M. Mishima, and J. Yajima. 2021. CYK4 relaxes the bias in the off-axis motion by MKLP1 kinesin-6. *Commun Biol*. 4:180.

Mastronarde, D.N., K.L. McDonald, R. Ding, and J.R. McIntosh. 1993. Interpolar spindle microtubules in PTK cells. *J Cell Biol*. 123:1475-1489.

Mayr, M.I., S. Hummer, J. Bormann, T. Gruner, S. Adio, G. Woehlke, and T.U. Mayer. 2007. The human kinesin Kif18A is a motile microtubule depolymerase essential for chromosome congression. *Curr Biol*. 17:488-498.

Mazumdar, M., and T. Misteli. 2005. Chromokinesins: multitalented players in mitosis. *Trends Cell Biol*. 15:349-355.

McIntosh, J.R., and S.C. Landis. 1971. The distribution of spindle microtubules during mitosis in cultured human cells. *J Cell Biol*. 49:468-497.

McIntosh, J.R., M.I. Molodtsov, and F.I. Ataullakhanov. 2012. Biophysics of mitosis. *Q Rev Biophys*. 45:147-207.

McKinley, K.L., and I.M. Cheeseman. 2017. Large-Scale Analysis of CRISPR/Cas9 Cell-Cycle Knockouts Reveals the Diversity of p53-Dependent Responses to Cell-Cycle Defects. *Dev Cell*. 40:405-420 e402.

Meraldi, P., V.M. Draviam, and P.K. Sorger. 2004. Timing and checkpoints in the regulation of mitotic progression. *Dev Cell*. 7:45-60.

Miki, H., Y. Okada, and N. Hirokawa. 2005. Analysis of the kinesin superfamily: insights into structure and function. *Trends Cell Biol*. 15:467-476.

Mishima, M. 2016. Centralspindlin in Rappaport's cleavage signaling. *Semin Cell Dev Biol*. 53:45-56.

Mishima, M., S. Kaitna, and M. Glotzer. 2002. Central spindle assembly and cytokinesis require a kinesin-like protein/RhoGAP complex with microtubule bundling activity. *Dev Cell*. 2:41-54.

Mitchison, T., and M. Kirschner. 1984. Dynamic instability of microtubule growth. *Nature*. 312:237-242.

Mitra, A., L. Meissner, R. Gandhimathi, R. Renger, F. Ruhnow, and S. Diez. 2020. Kinesin-14 motors drive a right-handed helical motion of antiparallel microtubules around each other. *Nat Commun*. 11:2565.

Mitra, A., F. Ruhnow, S. Girardo, and S. Diez. 2018. Directionally biased sidestepping of Kip3/kinesin-8 is regulated by ATP waiting time and motor-microtubule interaction strength. *Proc Natl Acad Sci U S A*. 115:E7950-E7959.

Mogilner, A., and E. Craig. 2010. Towards a quantitative understanding of mitotic spindle assembly and mechanics. *J Cell Sci*. 123:3435-3445.

Musacchio, A., and A. Desai. 2017. A Molecular View of Kinetochore Assembly and Function. *Biology (Basel)*. 6.

Musacchio, A., and E.D. Salmon. 2007. The spindle-assembly checkpoint in space and time. *Nat Rev Mol Cell Biol*. 8:379-393.

Neahring, L., N.H. Cho, and S. Dumont. 2021. Opposing motors provide mechanical and functional robustness in the human spindle. *Dev Cell*. 56:3006-3018 e3005.

Nezi, L., and A. Musacchio. 2009. Sister chromatid tension and the spindle assembly checkpoint. *Curr Opin Cell Biol*. 21:785-795.

Nicklas, R.B. 1983. Measurements of the force produced by the mitotic spindle in anaphase. *J Cell Biol*. 97:542-548.

Niethammer, P., I. Kronja, S. Kandels-Lewis, S. Rybina, P. Bastiaens, and E. Karsenti. 2007. Discrete states of a protein interaction network govern interphase and mitotic microtubule dynamics. *PLoS Biol*. 5:e29.

Novak, M., B. Polak, J. Simunic, Z. Boban, B. Kuzmic, A.W. Thomae, I.M. Tolic, and N. Pavin. 2018. The mitotic spindle is chiral due to torques within microtubule bundles. *Nat Commun*. 9:3571.

Panda, S.K., S. Ray, S.R. Nayak, S. Behera, S.S. Bhanja, and V. Acharya. 2019. A Review on Cell Cycle Checkpoints in Relation to Cancer. *J Med Sci*. 5:88–95.

Pavin, N., and I.M. Tolic. 2016. Self-Organization and Forces in the Mitotic Spindle. *Annu Rev Biophys*. 45:279-298.

Pavin, N., and I.M. Tolic. 2021. Mechanobiology of the Mitotic Spindle. *Dev Cell*. 56:192-201.

Petry, S., A.C. Groen, K. Ishihara, T.J. Mitchison, and R.D. Vale. 2013. Branching microtubule nucleation in Xenopus egg extracts mediated by augmin and TPX2. *Cell*. 152:768-777.

Polak, B., P. Risteski, S. Lesjak, and I.M. Tolic. 2017. PRC1-labeled microtubule bundles and kinetochore pairs show one-to-one association in metaphase. *EMBO Rep*. 18:217-230.

Prelog, V. 1976. Chirality in chemistry. *Science*. 193:17-24.

Prosser, S.L., and L. Pelletier. 2017. Mitotic spindle assembly in animal cells: a fine balancing act. *Nat Rev Mol Cell Biol*. 18:187-201.

Ramaiya, A., B. Roy, M. Bugiel, and E. Schaffer. 2017. Kinesin rotates unidirectionally and generates torque while walking on microtubules. *Proc Natl Acad Sci U S A*. 114:10894-10899.

Rieder, C.L., and E.D. Salmon. 1994. Motile kinetochores and polar ejection forces dictate chromosome position on the vertebrate mitotic spindle. *J Cell Biol*. 124:223-233.

Risteski, P., M. Jagric, N. Pavin, and I.M. Tolic. 2021. Biomechanics of chromosome alignment at the spindle midplane. *Curr Biol*. 31:R574-R585.

Rogers, G.C., S.L. Rogers, T.A. Schwimmer, S.C. Ems-McClung, C.E. Walczak, R.D. Vale, J.M. Scholey, and D.J. Sharp. 2004. Two mitotic kinesins cooperate to drive sister chromatid separation during anaphase. *Nature*. 427:364-370.

Rubinstein, B., K. Larripa, P. Sommi, and A. Mogilner. 2009. The elasticity of motor-microtubule bundles and shape of the mitotic spindle. *Phys Biol*. 6:016005.

Sandblad, L., K.E. Busch, P. Tittmann, H. Gross, D. Brunner, and A. Hoenger. 2006. The Schizosaccharomyces pombe EB1 homolog Mal3p binds and stabilizes the microtubule lattice seam. *Cell*. 127:1415-1424.

Sanganyado, E., Z. Lu, Q. Fu, D. Schlenk, and J. Gan. 2017. Chiral pharmaceuticals: A review on their environmental occurrence and fate processes. *Water Res*. 124:527-542.

Santaguida, S., and A. Amon. 2015. Short- and long-term effects of chromosome mis-segregation and aneuploidy. *Nat Rev Mol Cell Biol*. 16:473-485.

Sawin, K.E., K. LeGuellec, M. Philippe, and T.J. Mitchison. 1992. Mitotic spindle organization by a plus-end-directed microtubule motor. *Nature*. 359:540-543.

Schilthuizen, M., and A. Davison. 2005. The convoluted evolution of snail chirality. *Naturwissenschaften*. 92:504-515.

Schindelin, J., I. Arganda-Carreras, E. Frise, V. Kaynig, M. Longair, T. Pietzsch, S. Preibisch, C. Rueden, S. Saalfeld, B. Schmid, J.Y. Tinevez, D.J. White, V. Hartenstein, K. Eliceiri, P. Tomancak, and A. Cardona. 2012. Fiji: an open-source platform for biological-image analysis. *Nat Methods*. 9:676-682.

Scholey, J.M., G. Civelekoglu-Scholey, and I. Brust-Mascher. 2016. Anaphase B. *Biology (Basel)*. 5.

Schuster, F.L. 1975. Ultrastructure of mitosis in the amoeboflagellate Naegleria gruberi. *Tissue Cell*. 7:1-11.

Shim, A., G. Tezuka, L. Kupcha, and L. Tao. 2017. Gliding Assay to Analyze Microtubule-based Motor Protein Dynamics. *Bio Protoc*. 7:e2210.

Simunic, J., and I.M. Tolic. 2016. Mitotic Spindle Assembly: Building the Bridge between Sister K-Fibers. *Trends Biochem Sci*. 41:824-833.

Solomons, T.W.G., and C.B. Fryhle. 2003. Organic Chemistry. *Wiley*. 8th edition.

Song, J.G., M.R. King, R. Zhang, R.S. Kadzik, A. Thawani, and S. Petry. 2018. Mechanism of how augmin directly targets the gamma-tubulin ring complex to microtubules. *J Cell Biol*. 217:2417-2428.

Stearns, T. 2004. The centrosome yields its secrets. *Nature Cell Biology*. 6:14.

Stimac, V., I. Koprivec, M. Manenica, J. Simunic, and I.M. Tolic. 2022. Augmin prevents merotelic attachments by promoting proper arrangement of bridging and kinetochore fibers. *Elife*. 11.

Stumpff, J., G. von Dassow, M. Wagenbach, C. Asbury, and L. Wordeman. 2008. The kinesin-8 motor Kif18A suppresses kinetochore movements to control mitotic chromosome alignment. *Dev Cell*. 14:252-262.

Subramanian, R., S.C. Ti, L. Tan, S.A. Darst, and T.M. Kapoor. 2013. Marking and measuring single microtubules by PRC1 and kinesin-4. *Cell*. 154:377-390.

Thitamadee, S., K. Tuchihara, and T. Hashimoto. 2002. Microtubule basis for left-handed helical growth in Arabidopsis. *Nature*. 417:193-196.

Tirnauer, J.S., and B.E. Bierer. 2000. EB1 proteins regulate microtubule dynamics, cell polarity, and chromosome stability. *J Cell Biol*. 149:761-766.

Tolic-Norrelykke, I.M. 2008. Push-me-pull-you: how microtubules organize the cell interior. *Eur Biophys J*. 37:1271-1278.

Tolic, I.M. 2018. Mitotic spindle: kinetochore fibers hold on tight to interpolar bundles. *Eur Biophys J*. 47:191-203.

Tolic, I.M., M. Novak, and N. Pavin. 2019. Helical Twist and Rotational Forces in the Mitotic Spindle. *Biomolecules*. 9:132.

Trupinic, M., B. Kokanovic, I. Ponjavic, I. Barisic, S. Segvic, A. Ivec, and I.M. Tolic. 2022. The chirality of the mitotic spindle provides a mechanical response to forces and depends on microtubule motors and augmin. *Curr Biol*. 32:2480-2493 e2486.

Uehara, R., R.S. Nozawa, A. Tomioka, S. Petry, R.D. Vale, C. Obuse, and G. Goshima. 2009. The augmin complex plays a critical role in spindle microtubule generation for mitotic progression and cytokinesis in human cells. *Proc Natl Acad Sci U S A*. 106:6998-7003.

Vale, R.D. 1987. Intracellular transport using microtubule-based motors. *Annu Rev Cell Biol*. 3:347-378.

Vale, R.D., and Y.Y. Toyoshima. 1988. Rotation and translocation of microtubules in vitro induced by dyneins from Tetrahymena cilia. *Cell*. 52:459-469.

Valentine, M.T., P.M. Fordyce, and S.M. Block. 2006. Eg5 steps it up! *Cell Div*. 1:31.

Velle, K.B., A.S. Kennard, M. Trupinic, A. Ivec, A.J.M. Swafford, E. Nolton, L.M. Rice, I.M. Tolic, L.K. Fritz-Laylin, and P. Wadsworth. 2022. Naegleria's mitotic spindles are built from unique tubulins and highlight core spindle features. *Curr Biol*. 32:1-15.

Vukusic, K., R. Buda, A. Bosilj, A. Milas, N. Pavin, and I.M. Tolic. 2017. Microtubule Sliding within the Bridging Fiber Pushes Kinetochore Fibers Apart to Segregate Chromosomes. *Dev Cell*. 43:11-23 e16.

Vukusic, K., R. Buda, and I.M. Tolic. 2019. Force-generating mechanisms of anaphase in human cells. *J Cell Sci*. 132:jcs231985.

Vukusic, K., I. Ponjavic, R. Buda, P. Risteski, and I.M. Tolic. 2021. Microtubule-sliding modules based on kinesins EG5 and PRC1-dependent KIF4A drive human spindle elongation. *Dev Cell*. 56:1253-1267 e1210.

Vukusic, K., and I.M. Tolic. 2021. Anaphase B: Long-standing models meet new concepts. *Semin Cell Dev Biol*. 117:127-139.

Waitzman, J.S., and S.E. Rice. 2014. Mechanism and regulation of kinesin-5, an essential motor for the mitotic spindle. *Biol Cell*. 106:1-12.

Walczak, C.E., I. Vernos, T.J. Mitchison, E. Karsenti, and R. Heald. 1998. A model for the proposed roles of different microtubule-based motor proteins in establishing spindle bipolarity. *Curr Biol*. 8:903-913.

Walker, R.A., E.D. Salmon, and S.A. Endow. 1990. The Drosophila claret segregation protein is a minus-end directed motor molecule. *Nature*. 347:780-782.

Walsh, C.J. 2012. The structure of the mitotic spindle and nucleolus during mitosis in the amebo-flagellate Naegleria. *Plos One*. 7:e34763.

Webster, A., and M. Schuh. 2017. Mechanisms of Aneuploidy in Human Eggs. *Trends Cell Biol*. 27:55-68.

Wieczorek, M., L. Urnavicius, S.C. Ti, K.R. Molloy, B.T. Chait, and T.M. Kapoor. 2020. Asymmetric Molecular Architecture of the Human gamma-Tubulin Ring Complex. *Cell*. 180:165-175 e116.

Wiese, C., and Y. Zheng. 2006. Microtubule nucleation: gamma-tubulin and beyond. *J Cell Sci*. 119:4143-4153.

Wu, G., Y.T. Lin, R. Wei, Y. Chen, Z. Shan, and W.H. Lee. 2008. Hice1, a novel microtubule-associated protein required for maintenance of spindle integrity and chromosomal stability in human cells. *Mol Cell Biol*. 28:3652-3662.

Yajima, J., and R.A. Cross. 2005. A torque component in the kinesin-1 power stroke. *Nat Chem Biol*. 1:338-341.

Yajima, J., K. Mizutani, and T. Nishizaka. 2008. A torque component present in mitotic kinesin Eg5 revealed by three-dimensional tracking. *Nat Struct Mol Biol*. 15:1119-1121.

Yokokawa, R., T. Murakami, T. Sugie, and T. Kon. 2008. Polarity orientation of microtubules utilizing a dynein-based gliding assay. *Nanotechnology*. 19:125505.

Yu, H. 2007. Cdc20: a WD40 activator for a cell cycle degradation machine. *Mol Cell*. 27:3-16.

8. SUPPLEMENT

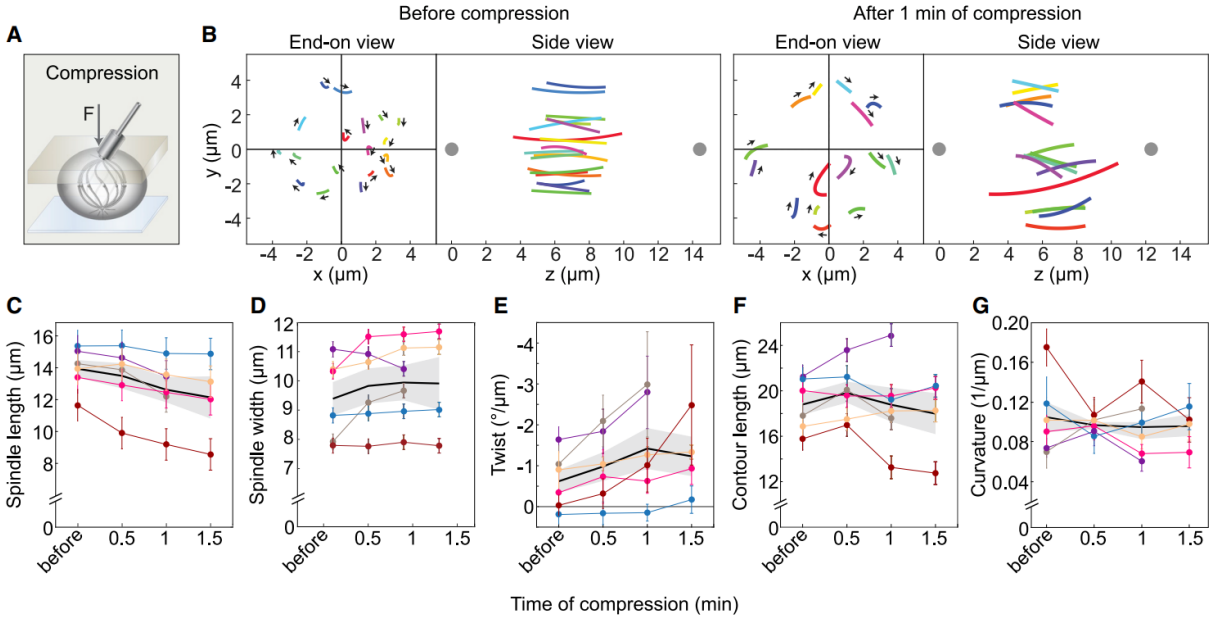

Figure S1. The spindles compressed by an external force have a stronger twist. A) Setup for spindle compression. The blue layer represents the dish and the gray layer the gel with a metal rod on top; arrow shows the direction of force, F. **B)** Microtubule bundles in a spindle shown from the end-on and side view before compression and after 1 min of compression, as indicated. In the end-on and side view, the individual bundles are colored with the same color, but colors before and after compression do not represent the same bundles; the lines show circular arcs of the fitted circles and arrows represent the rotation direction; the gray dots are spindle poles. **C–G)** Spindle parameters from before compression up to 1.5 min of compression are as follows: spindle length (C), spindle width (D), twist of microtubule bundles (E), length of the bundle contours (F), and bundle curvature (G). Each color represents one cell; the dots represent mean values; the error bars in (C) and (D) show the estimated errors in the determination of spindle length and width, 1 and 0.25 mm, respectively; the error bars in other graphs represent SEM. The black line and gray area represent mean ± SEM. Successful compression was performed on six spindles from five independent experiments on HeLa-Kyoto BAC cells expressing PRC1-GFP. Taken from (Trupinic et al., 2022).

9. AUTHOR BIOGRAFY

Monika Trupinić was born on July 13, 1994 in Požega, Croatia. She finished her elementary education and high school in Zagreb. In 2013 she became a student at the Faculty of Science, University of Zagreb, where she finished her undergraduate and graduate studies in molecular biology. She graduated in 2018 on a double-master graduate program (*Techniques-Bioindustrielles,* TBI) and received her diplomas from Faculty of Science, University of Zagreb, and Collegium Sciences et Techniques, University of Orléans, France. Her master thesis, titled "Role of miRNA-486 in cisplatin-treated non-small cell lung carcinoma A549 cells", was done at the Center for Molecular Biophysics (CNRS-CBM), in the group of prof. PhD Chantal Pichon, in Orléans, France. In that period of 6 months, she worked under the guidance of a mentor, PhD Patrick Baril on the "RILES project" where she investigated the role of miRNA-486 in lung cancer cells after treatment with the chemotherapeutic agent cisplatin. She continued her education at the Faculty of Science, University of Zagreb, where she enrolled in the Postgraduate Study of Biology. Since then, she has been working in the group of prof. PhD Iva Tolić at the Ruđer Bošković Institute. As part of Tolić group she combined molecular biology tools including cell culture, confocal microscopy, molecular genetics, biophysical tools including laser ablations and mechanical manipulations, computer quantifications and statistical analysis. Her current research interests focus on spindle chirality, mechanisms that generate spindle twist and role of the same during mitosis. She is the author on 3 papers published in journals *Current Biology* and *Biophysical Journal*, among which is a collaboration with the American scientists from the University of Massachusetts, Amherst. She participated in 7 international conferences, including EMBO/EMBL Symposium: Microtubules: From Atoms to Complex Systems, ASCB/EMBO Meeting: The American Society for Cell Biology, Cell Cycle Meeting/Salk Institute, Mitotic spindle: From living and synthetic systems to theory, and 9th World Congress of Biomechanics/2022 Taipei, where she had presentations in the form of posters or oral presentations. During her study she received "Scholarship of excellence" from University of Zagreb and Erasmus+ (SMP) scholarship. She participated at the events to promote science, such as "Night of Biology" at the Faculty of Science, "Women in science" in Zagreb, "PhD café" etc. She was also one of the main organizers of student symposium of biology "SymBioSe" in 2018 in Zagreb.

Publications:

1. Ivec, Arian; **Trupinić, Monika**; Tolić, Iva M.; Pavin, Nenad. Oblique circle method for measuring the curvature and twist of mitotic spindle microtubule bundles. *Biophys J*, 120(7): 3641-3648 (2021)

2. Velle, Katrina B.; Kennard, Andrew S.; **Trupinić, Monika**; Ivec, Arian; Swafford, Andrew J.M.; Nolton, Emily; Rice, Luke; Tolić, Iva M.; Fritz-Laylin, Lillian K.; Wadsworth, Patricia. Naegleria's mitotic spindles are built from unique tubulins and highlight core spindle features. *Curr Biol*, 32(6): 1247–1261 (2022)

3. **Trupinić, Monika;** Kokanović, Barbara; Ponjavić, Ivana; Barišić, Ivan; Šegvić, Siniša; Ivec, Arian; Tolić, Iva M. The chirality of the mitotic spindle provides a mechanical response to forces and depends on microtubule motors and augmin. *Curr Biol*, 32: 2480-2493. (2022)

Conferences:

1. First author on **poster** on EMBO / EMBL Symposium: Microtubules: From Atoms to Complex Systems Heidelberg, Germany, 2020.: **Trupinić, Monika**; Ivec, Arian; Wadsworth, Patricia; Fritz-Laylin, Lillian; Simunić, Juraj; Pavin, Nenad; Tolić, Iva M. Spindle chirality dynamics during mitosis

2. First author on **poster** on Cell Bio Virtual 2020 | An Online ASCB|EMBO Meeting USA, 2020.: **Trupinić, Monika**; Kokanović, Barbara; Ponjavić, Ivana; Ivec, Arian; Wadsworth, Patricia; Fritz-Laylin, Lillian; Pavin, Nenad; Tolić, Iva.M. Spindle twist culminates at anaphase onset and depends on microtubule-associated proteins along with external forces

3. First author on **poster** on Mitotic spindle: From living and synthetic systems to theory Split, Croatia, 2021.: **Trupinić, Monika**; Kokanović, Barbara; Ponjavić, Ivana; Wadsworth, Patricia; Fritz-Laylin, Lillian; Tolić, Iva M. Twist of the mitotic spindle culminates at anaphase onset and depends on microtubule-associated proteins along with external forces

4. First author on **poster** on Virtual 2021 Cell Cycle Meeting, USA, 2021.: **Trupinić, Monika**; Kokanović, Barbara; Ponjavić, Ivana; Wadsworth, Patricia; Fritz-Laylin, Lillian; Tolić, Iva M. Twist of the Mitotic Spindle Culminates at Anaphase Onset and Depends on Microtubule-associated Proteins along with External Forces

5. **Oral presentation** on Cell Bio Virtual 2021 | An Online ASCB|EMBO Meeting, USA, 2021.: **Trupinić, Monika** Mitotic Spindle Chirality Provides a Passive Mechanical Response to Forces and Depends on Microtubule Motors and Crosslinkers

6. First author on **poster** on Cell Bio Virtual 2021 | An Online ASCB|EMBO Meeting, USA, 2021.: **Trupinić, Monika**; Kokanović, Barbara; Ponjavić, Ivana; Tolić, Iva M. Mitotic Spindle Chirality Provides a Passive Mechanical Response to Forces and Depends on Microtubule Motors and Crosslinkers

7. **Oral presentation (Flash talk)** on EMBO / EMBL Symposium: Microtubules: From Atoms to Complex Systems Heidelberg, Germany, 2022.: **Trupinić, Monika** The chirality of the mitotic spindle provides a mechanical response to forces and depends on microtubule motors and augmin

8. First author on **poster** on EMBO / EMBL Symposium: Microtubules: From Atoms to Complex Systems Heidelberg, Germany, 2022.: **Trupinić, Monika**; Kokanović, Barbara; Ponjavić, Ivana; Ivec, Arian; Tolić, Iva M. The chirality of the mitotic spindle provides a mechanical response to forces and depends on microtubule motors and augmin

9. **Oral presentation** on 9th World Congress of Biomechanics / 2022 Taipei Taipei, Taiwan, 2022.: **Trupinić, Monika** The chirality of the mitotic spindle provides a mechanical response to forces and depends on microtubule motors and crosslinkers